Budker Institute of Nuclear Physics

Conceptual Design Report on Superconducting Dipole Magnet Designed for the CBM detector

Novosibirsk
February, 2018

THIS WORK HAS BEEN DONE UNDER SPECIFIC CONSULTANCY AGREEMENT BETWEEN FAIR FROM ONE SIDE AND BINP FROM THE OTHER SIDE FOR A FEASABILITY STUDY AND A CONCEPTUAL DESIGN OF A SUPERCONDUCTING DIPOLE MAGNET FOR THE CBM DETECTOR

Authors of the report are:

Mezentsev N.	e-mail: N.A.Mezentsev@inp.nsk.su
Bragin A.	e-mail: A.V.Bragin@inp.nsk.su
Pivovarov S.	e-mail: S.G.Pivovarov@inp.nsk.su
Shkaruba V.	e-mail: V.A.Shkaruba@inp.nsk.su
Erokhin A.	e-mail: A.I.Erokhin@inp.nsk.su
Khrushchev S.	e-mail: S.V.Khrushchev@inp.nsk.su
Tsukanov V.	e-mail: V.M.Tsukanov@inp.nsk.su
Volkov A.	e-mail: A.A.Volkov@inp.nsk.su
Tarasenko O.	e-mail: O.A.Tarasenko@inp.nsk.su
Syrovatin V	e-mail: V.M.Syrovatin@inp.nsk.su
Kholopov M.	e-mail: M.A.Kholopov@inp.nsk.su

Head of Laboratory,
Budker Institute of Nuclear Physics,
SB RAS, Novosibirsk, Russia

Mezentsev N.A.

CONTENT

1. Introduction

1.1 Content of the conceptual design

The scope of the contract is to design, manufacture, measure, deliver, install and commission the superconducting dipole magnet for CBM experiment at FAIR.

The Budker INP agrees to satisfy to the main parameters of the superconducting magnet for the CBM presented in "Collaboration Contract CBM Magnet BINP Annex3 specifications", design, prototyping, production, delivery, assembly and testing of the complete Dipole Magnet for the CBM experiment and tools necessary for its transport, storage and assembly Acceptance Test at the Customer's Site and Commissioning of the CBM superconducting magnet for the FAIR including extent of delivery, general conditions of the Contract, General mechanical requirements, general manufacturing standards, instrumentation and, documentation.

The conceptual design report should present the following items:

- Magnetic field calculations;
- Design of superconducting cable and coil;
- Quench calculations;
- Stress calculations, including all mechanical structures;
- Design of cryogenics including the cryostat, brunch box, feed box and cryogenic lines.

1.2 Preamble

The superconducting dipole magnet will be installed in the CBM detector at FAIR. The magnet provides vertical magnetic field with a magnetic field integral of 1 T*m which is needed to obtain a momentum resolution of $\Delta p/p=1$ % for track reconstruction at FAIR beam energies.

The magnet gap has a height of 144 cm and a width of 300 cm in order to accommodate the STS detector system with a polar angle acceptance of 25° and a horizontal acceptance of 30°. The magnet is of the H-type with a warm iron yoke/pole and cylindrical superconducting coils. The coil winding has 1749 turns. The wire has Nb-Ti filaments embedded into a copper matrix with a total Cu/SC ratio of about 7.1. The operating current and the maximal magnetic field in the coils are 686 A and 3.9 T, respectively. The coil case is made of stainless steel. The vertical force in the coils is about 250 tons. The cold mass is suspended from the room temperature vacuum vessel by six suspension links. Six cylindrical support struts compensate the vertical forces. The energy stored in the magnet is about 5 MJ.

1.3 General requirements

The scope of delivery includes the following, see Fig. 1:

- Magnetic and engineering design of the magnet including all necessary tools, dimensioning calculations for stands and lifting units, etc;
- Engineering design of the Feed Box and the Branch Box incl. the cryogenic connection line;
- Production and delivery of the magnet (consisting of yoke, cold masses and cryostats, alignment components, Feed box and stand), the Branch Box, the cryogenic connection line and all tools;
- Engineering design, production and delivery of the Power Converter;
- Transportation of all components to site, complete assembly and the preparation of installation;
- Documentation.

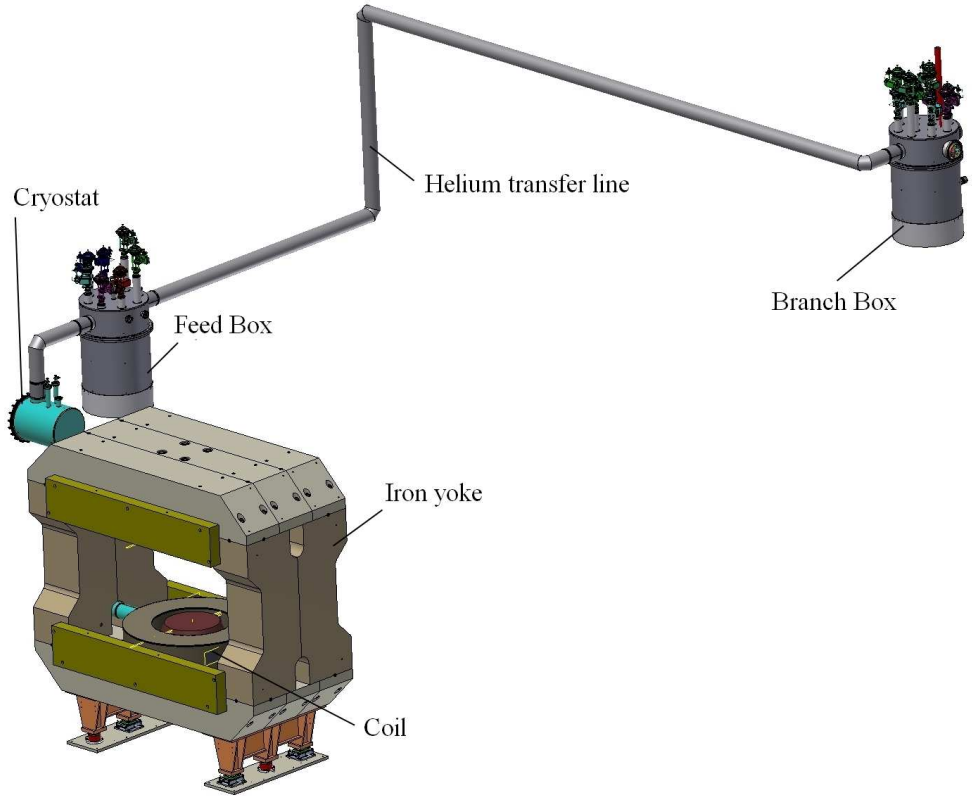

Fig. 1. General view of the CBM magnet and cryogenics supplied by BINP.

1.4 General parameters

The following list contains the mandatory required parameters of the CBM dipole magnet:

Geometry

- Opening angle: ±25° vertically, ± 30° horizontally from the target
- Free aperture: 1.44 m vertically x 3.0 m horizontally, no conical geometry.

The Silicon Tracking System (STS) and its services will occupy all available space in the aperture, from left to right vertical yoke. It requires also space between lower coil and the vertical yoke bar. Distance target- magnet core end: 1m (STS detector must fit in).

- Total length: 1.5 m
- Free space upstream of the magnet: >2 m
- Field integral within STS detector (along straight lines): 1 T*m along ± 0.5 m line around the center, and maximal field ≈ 1 T, depending on the magnet length
- Field integral variation over the whole opening angle along straight lines: ≤ 20% (± 10%)
- Fringe field downstream < reasonable value of the order of 50 to 100 Gauss at a distance of 1.6 m from the target at the position of the first RICH box (RICH only).

Operating conditions

- Operates at both polarities
- 100% duty cycle, 3 months/year, 20 years
- No real time restriction on the ramp: 1 hour up ramp
- Radiation damage (<10MG for organics): no problem
- Radiation Energy deposit in the cryogenic system: max. 1 W

Assembly

- Field clamps dismountable for MUCH
- Assembly in situ
- Weight restriction: crane 30 tons (including lifting jacks)

- Maximum floor load: 100 tons/m^2
- Beam height over magnet base: 2.7 m

Alignment
- Position accuracy: ± 0.2 mm
- Orientation accuracy (roll): ± 0.5 mrad

The requirements given above are mandatory.

1.5 The schedule

The realization of the CBM magnet is discussed here. Two conditions are important:

1. The CBM magnet should be assembled and tested on BINP site. Only iron yoke and the magnet itself will be tested. The cryogenics of the CBM magnet may be tested only in GSI site. The BINP tests may/will be performed with another equipment of cryogenics. The radiation shields will be cooled with liquid nitrogen. In case of using the HTS current leads then a cryocooler will be installed during the tests on the BINP site.

2. The GSI will be able to install the CBM magnet and the cryogenics not earlier than during 2022 and make the cooling down test of the CBM cryogenics not earlier than in March 2023.

So, the current conceptual study is mainly aimed on the magnet and iron yoke designs. It is desired to accomplish the CDR and following stages during the 2018 year.

Now, January 2018, the contract for the cable manufacturing is signed. First part of the cable should be delivered to BINP in November 2018. It will be supplied 6 pieces of the cable each of 5 km length. One spare coil may be manufactured.

Preliminary agreement with Novosibirsk plant about iron yoke manufacturing is obtained.

2. General design

2.1 The magnet design

The rough sketch of the CBM magnet showing only principal elements is presented in the Fig. 2. It consists of the iron yoke, the superconducting magnet and the cryostat.

The iron yoke serves as a construction frame for the magnet and systems of the detector. Total mass of the iron yoke is about 140 tons. It has special tools for adjusting its position in all directions. The yoke is assembled of iron blocks having masses in the range between 3 and 13.6 tons. The material of the blocks is a kind of *steel 20* in Russian specification. The yoke blocks may have different magnet permeability, so they can be made of different steels, it will be discussed in the chapter of the magnetic field calculations. Particularly, the cylindrical parts of the iron yoke representing the poles will be made of technically pure iron – Armco. The Armco iron has similar properties as for the Russian steel *08kp*.

The superconducting magnet is designed of two separated superconducting coils symmetrically placed in the detector close to the top and bottom blocks of the iron yoke, as shown in Fig. 3. Such configuration represents a dipole magnet. The coils are placed around the cylindrical blocks of the iron yoke (poles). The distance between the poles is 1440 mm. The total view of the lower coil is shown on the Fig. 4.

The superconducting coil consists of the superconducting winding, copper case and stainless steel case, Fig. 5, Fig. 6. The coil is surrounded by copper radiation shield cooled by 50 -55 K helium. This stainless steel case of the coil will be covered by aluminum foils (aluminized Mylar) in order to reduce its thermal emissivity. The radiation shields will be covered by multilayer insulation up to 20 layers. The coil is suspended inside the vacuum vessel on three titanium rods. Six cylinder support struts withstand attracting vertical force of the charged coils towards the iron poles.

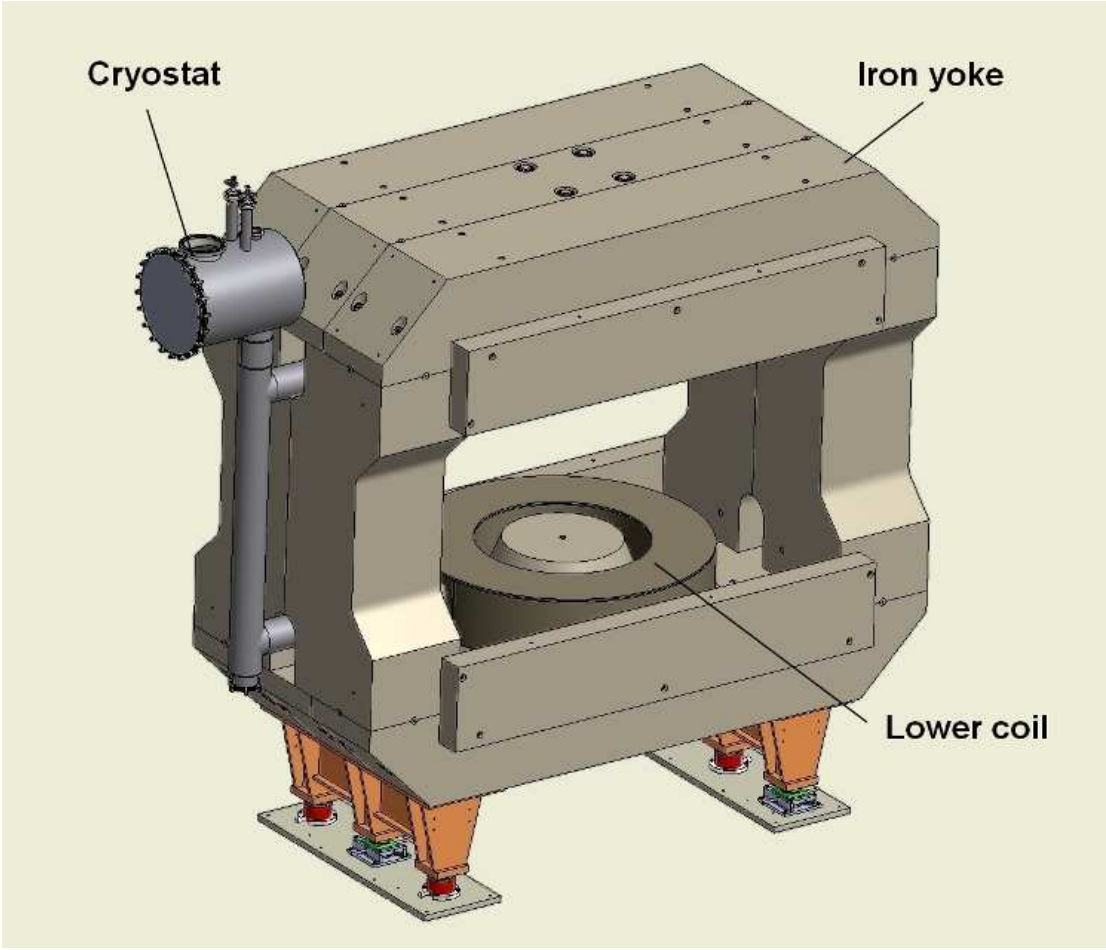

Fig. 2. The sketch of the CBM magnet of May 2017. The magnet consists of upper and lower coils.

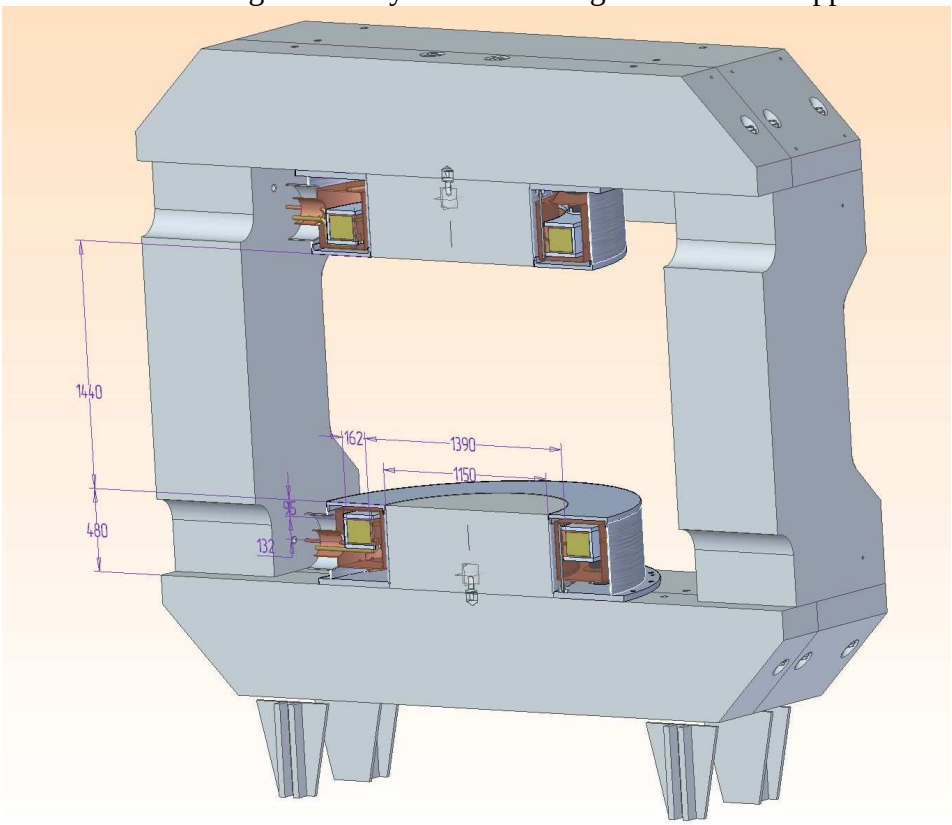

Fig. 3. The cross-section of the iron yoke and the magnet. The design of the yoke and coils is by January 2018.

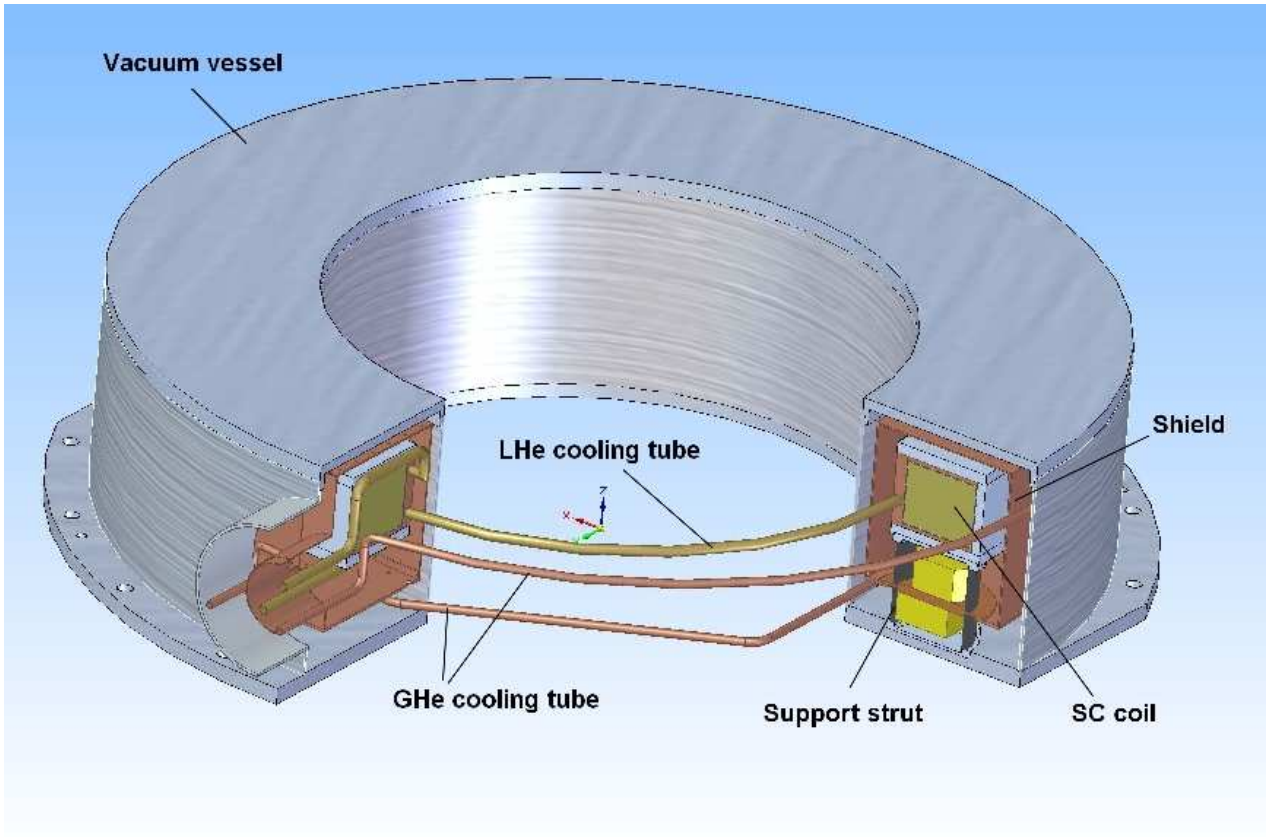

Fig. 4 Total view of the lower coil of the CBM magnet.

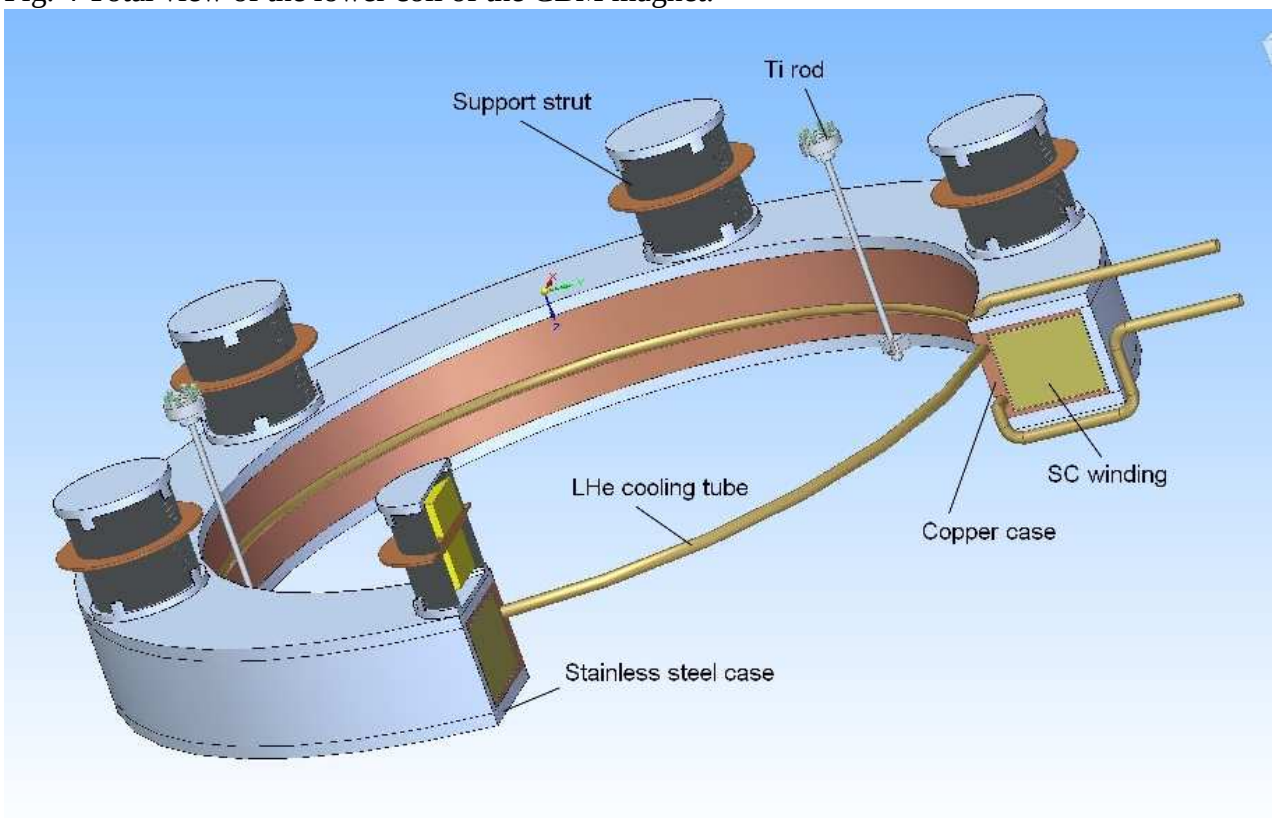

Fig. 5. The superconducting upper coil, radiation shield and support struts.

The support struts design is shown on the Fig. 6. Each support should withstand vertical compressive force up to 55 tons. They are consisted of large number of the stainless steel thin plates. It is considered that large amount of the plates will affect significant thermal resistance for

vertical thermal conductivity of the support structure. These struts will give major part of the heat loads on the cold mass of the magnet. The hot spots on the LHe case should be taken into account in the design. It will be also important to reduce emissivity of the stainless steel plates by gluing aluminized Mylar foils on outer surfaces of the struts.

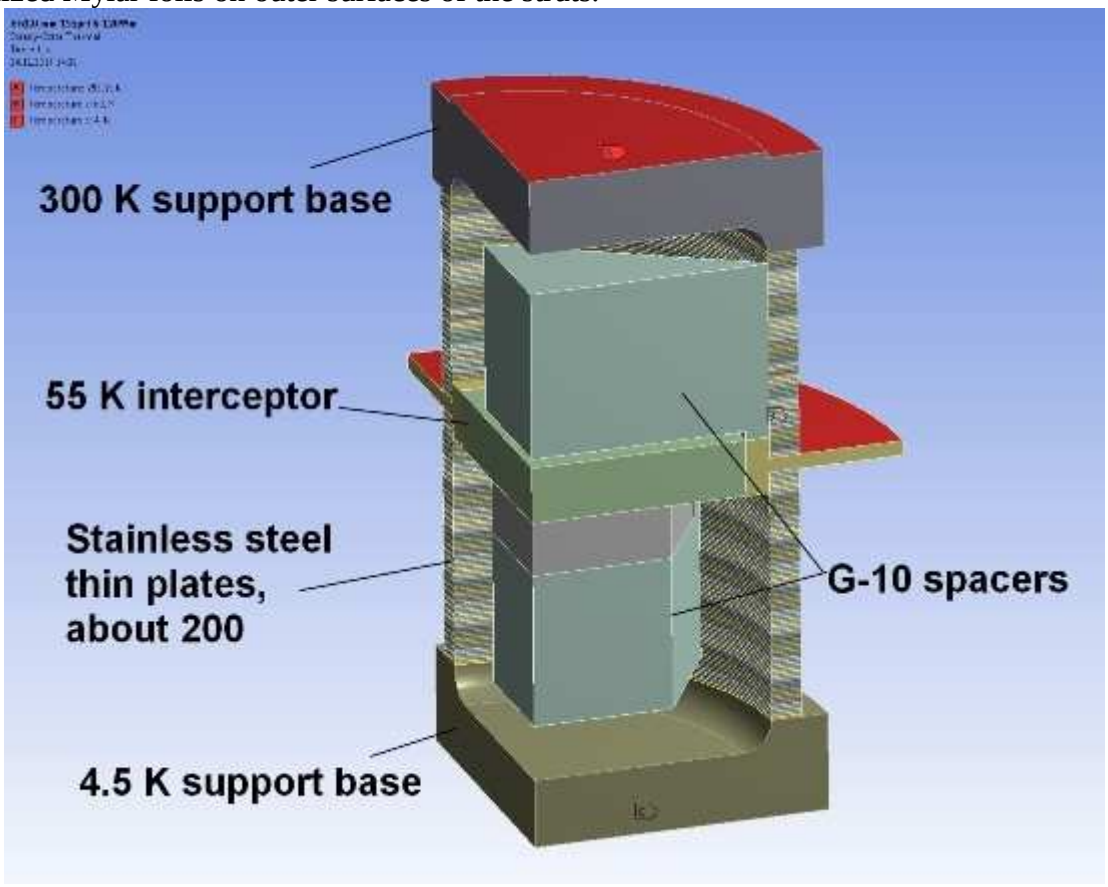

Fig. 6. View of the support struts. It consists of stainless steel plates of about 200 pieces. Inner G-10 block spacers fix position of the stainless steel plates fixing the plates position from horizontal movements.

2.2 Superconducting coil design

The total view of the superconducting coil as a cold mass at 4.5 K is shown on the Fig. 7. The main components of the coils are superconducting winding, the copper and the stainless steel cases. The copper case has a U-shape profile, the material for it will be 99.9% technical copper (M1 as Russian standard), see Fig. 8. It will serve as a bobbin during a winding procedure. The LHe cooling tube will be soldered and fixed in the groove of the copper case before winding procedure. The thickness of the side walls of the copper case is 8 mm, the thickness of the inner wall is 25 mm.

The stainless steel case will be assembled around the copper case after finishing of the winding procedure. The parts of the stainless steel case will be bolted together. So its cross section has a U profile shape.

The parameters of the superconducting winding are listed in the Table 1. The winding will be made of two pieces of the superconducting cable having length of about 4.5÷5 km. One splicing will be made during a winding procedure of one coil using soft soldering on a base of Sn-Ag alloy. The splicing place will be positioned inside the wall of the copper case as shown in Fig. 9. This wall is faced towards the center of the magnet. The length of the splicing will be not less than 10 cm.

It is planned to make dry winding in special winding tools. During the winding procedure the copper case will look as shown in Fig. 8. Glass-fiber insulation having thickness 0.3 mm will be

placed between the layers. After this the coil winding will be impregnated by epoxy resin. Special tools will be manufactured for the vacuum impregnation procedure. Fine powder of Al_2O_3 is often added to epoxy resin that improves thermal parameters of epoxy compound. Typical grain size of such powder is 3-5 μm and the volume content of the powder is ~ 50%. Such technology is widely used in BINP.

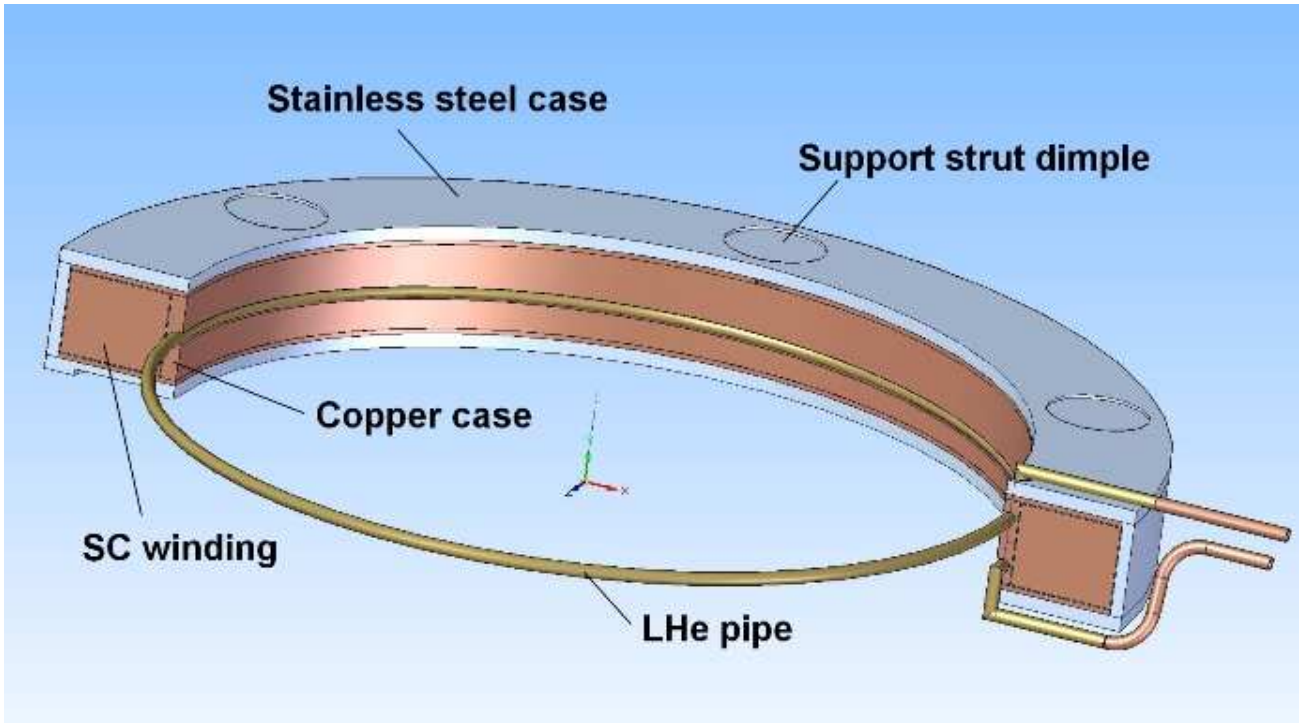

Fig. 7 The superconducting coil assembled with the stainless steel case.

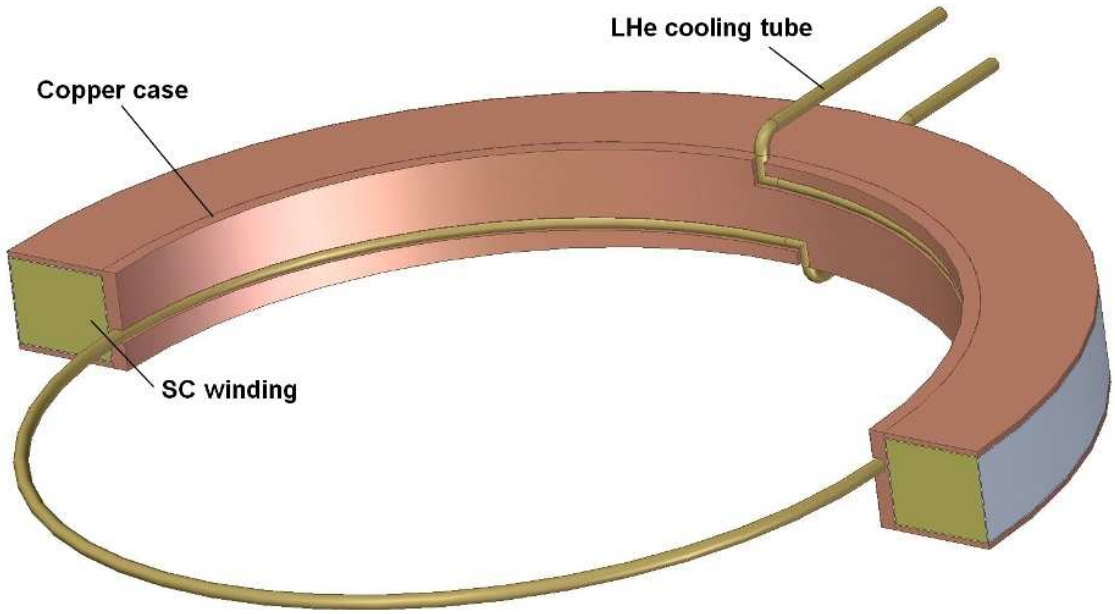

Fig. 8. The superconducting winding inside the copper case. The view after impregnation of the winding.

The stainless steel case made of 316LN stainless steel serves as a structural frame for supports connections and for rigidity of the whole coil structure. The thickness of the walls of this stainless steel case is from 20 to 30 mm. The yield strength of 316LN at 77 K is 1400 MPa [Iwasa, p. 638]. As far the there are no needs to test this case for the tightness of welded seams, as a proposal, BINP

may use other stainless steel material provided by Russian manufacturers.

The view of the superconducting coil after assembling is shown on the Fig. 10. The bolts will be used for this purpose. The holes of the copper case will have thread inserts a kind of Helicoil®. The copper case is fixed at one circumference to the stainless steel case that will allow its sliding during cooling down due to different contraction coefficients.

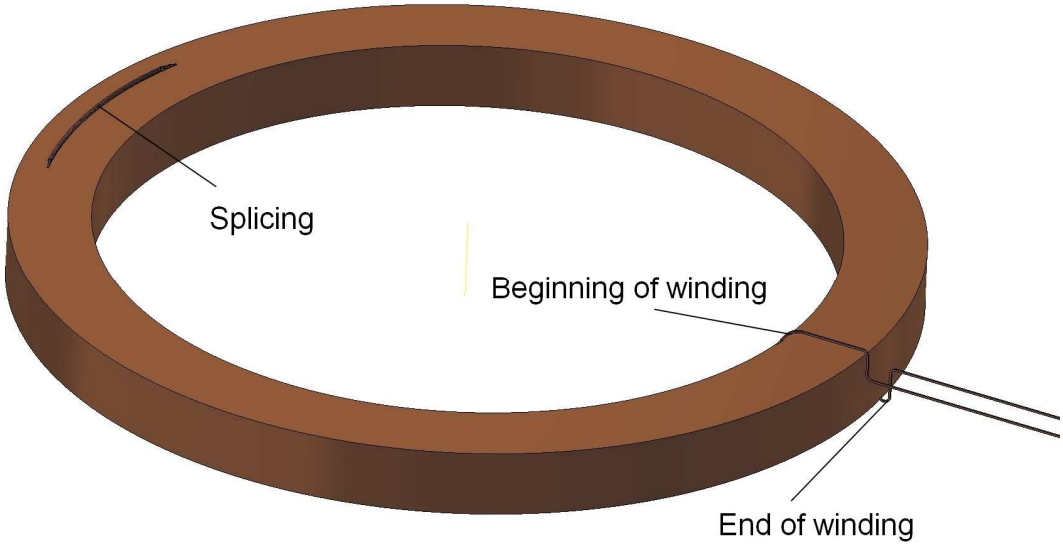

Fig. 9. The superconducting winding inside the copper case – the splicing is shown inside the copper wall.

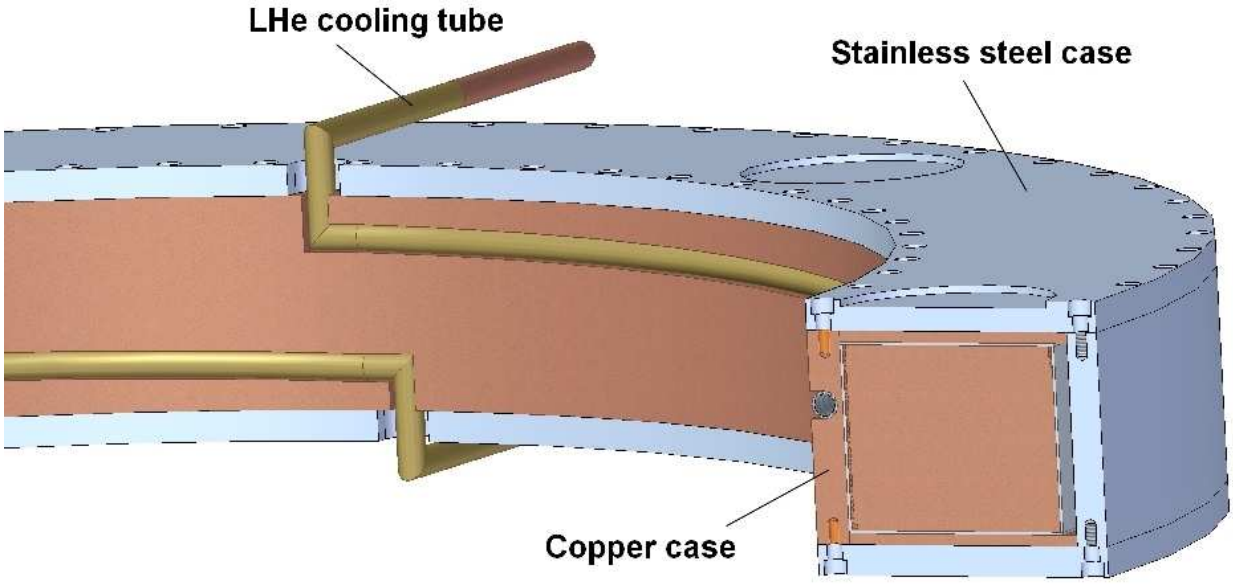

Fig. 10. The stainless steel case and the copper case assembled by using bolts.

Table 1 Superconducting coil parameters

Coils parameters	**Values**
Inner diameter of the winding, mm	1390
Cross section sizes of the winding:	
height, mm	131
radial thickness, mm	160
Number of turns in one coil	1749
Number of layers in one coil	53

Interlayer insulation, mm	0.3
Operating current Io, A	686[1]
Test current, Io*1.05, A	720
Magnetic field on the coil Bmax, T	3.9
Io/Ic ratio along the load line, %	52
Io/Ic at fixed B, %	25
Operating temperature, K	4.5
Temperature of current sharing, K	6.8
Stored energy of the magnet, MJ	5.1
Cold mass of one coil, kg	1800
Cold mass of one coil winding, kg	790
Inductance of the magnet at full current, H	21.2
E/M ratio for two windings, kJ/kg	3.2
Mutual inductance between the coils, H	0.21
Vertical force on one coil toward the yoke, MN	2.6

The thermal stabilization of the coil will be realized by flow of liquid helium at 4.5 K through the tube, see Fig. 8. The tube has an internal diameter 16 mm and wall thickness 2 mm. These tubes will be placed differently for upper and lower coils of the magnet in such a way that the exit end of the tube should be placed at highest position than the inlet end of the tube. In this case the helium bubbles will accelerate the total helium flow along the tubes. Accumulation of gaseous helium especially in the lower coil is very undesirable because it may produce local hot spots and restrict the helium flow.

The main parameters of the superconducting cable are almost the same which were specified in the TDR except the cable length, see Table 2. BINP proposes to make superconducting winding of two pieces as stated above. It will give more convenience as in producing the cable for BINP subcontractors as in manufacturing of the superconducting coil.

The superconducting cable will be produced of Cu/NbTi wire of ∅1.2 mm by co-extrusion into a copper matrix to have high Cu/NbTi ratio as it is shown on the Fig. 11. Working point is shown on the load line of the CBM magnet, it corresponds to 3.9 T of magnetic field, see Fig. 12. The I_o/I_c ratio and other critical parameters of the wire are almost the same that were proposed in the TDR.

Table 2 Superconducting cable parameters approved by manufacturers in November 2017

SC wire parameters	**Values**
Rectangular bare/insulated sizes:	
a, mm	2.02/2.62
b, mm	3.25/3.85
facets radius, mm	0.45
Cable total length per one coil, km	8.6
One piece of the cable length, km	5
Cu/NbTi ratio	≥7.4
RRR	>100
Filament diameter, μm	39±1
Number of filaments	651
Filament twist pitch, mm	<45
Cu+NbTi cross section area, mm^2	6.342

[1] The 686 A current is the main value. Some calculations (quench magnetic field) were also done for 700 A current to be sure that the needed field integral will be obtained.

NbTi cross section area, mm^2	0.755
I_c (5 T, 4.2 K), min A/	2270
I_c (4.5 K, 3.9 T), min A	2700

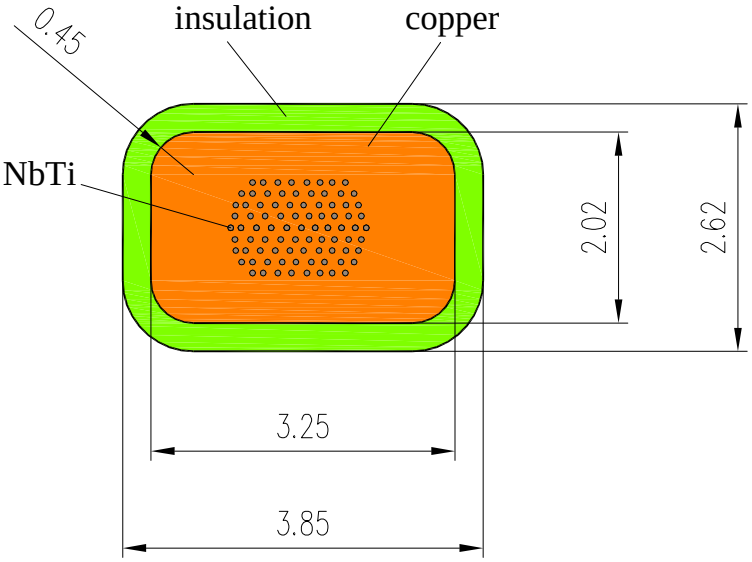

Fig. 11 Cross section of the proposed SC cable for the CBM magnet. The cable will be covered by insulation of total thickness 0.3 mm. It will include Kevlar insulation with thickness 0.1 mm, the rest will be fiber glass cloth.

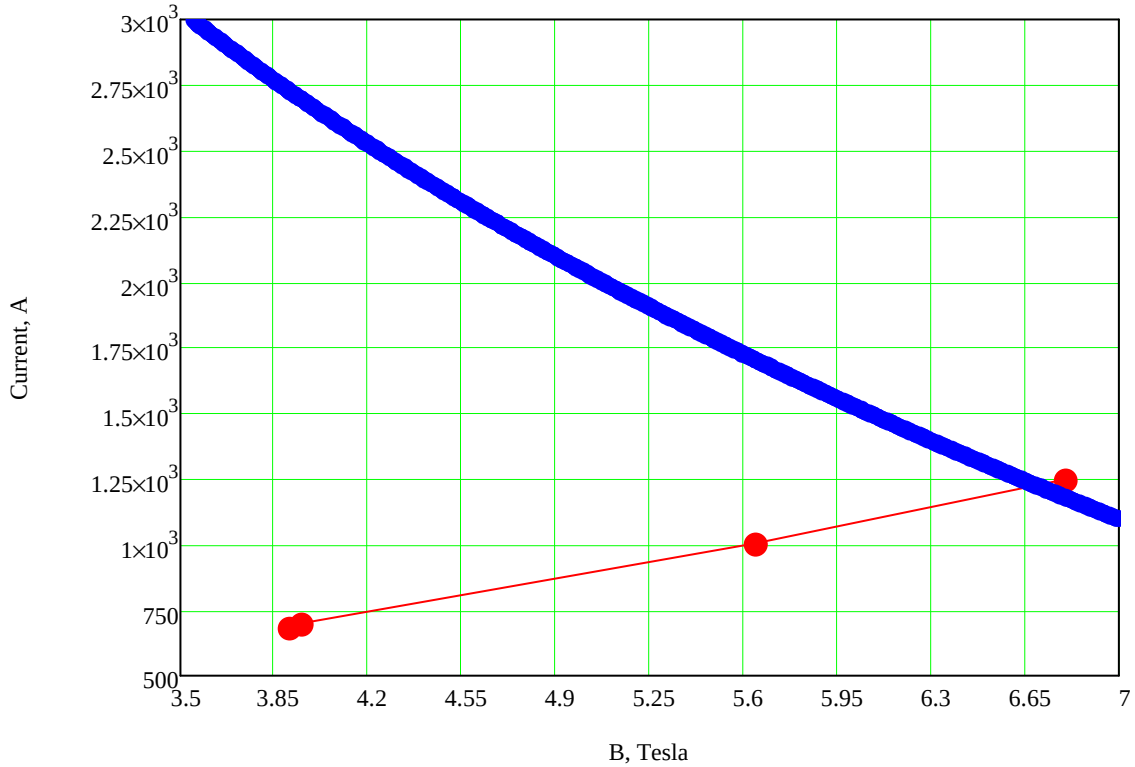

Fig. 12. Load line of the CBM magnet at 4.5 K. The blue line is the NbTi superconductor properties. The two left dots are for 686 A and 700 A currents.

2.3 Cryostat design

The CBM magnet will be supplied from the external cryogenic station with *gaseous* helium of

4.6 K at 3 bar and helium of 50 K at 18 bar. The cryostat itself will be filled with 4.5 K liquid helium due to expansion after the J-T valve. The magnet will be supplied with liquid helium from the cryostat placed on the top of the iron yoke as shown on the Fig. 2. The preliminary design of the cryostat is shown on the Fig. 13. The volume of the liquid helium will be about 40 l. The level of liquid helium will be controlled to contain about 20 l of liquid helium. The LHe volume will be filled from the Feed Box via the phase separator.

The LHe volume of the cryostat will supply the coils of the magnet with liquid helium. The cooling of the coil in ordinary operation is considered as thermosyphon cooling. The liquid helium goes from the LHe volume down to the lower coil, then it makes on turn around this coil inside copper pipe, shown in Fig. 8. After this helium goes up to upper coil and goes one turn around this coil in the same manner as for the lower coil. After this, helium goes to the top part of the LHe volume. The gaseous helium returns from the LHe volume to the cryogenic station.

The cryostat also has ports for vacuum measurement and initial pumping of the magnet and the Feed Box.

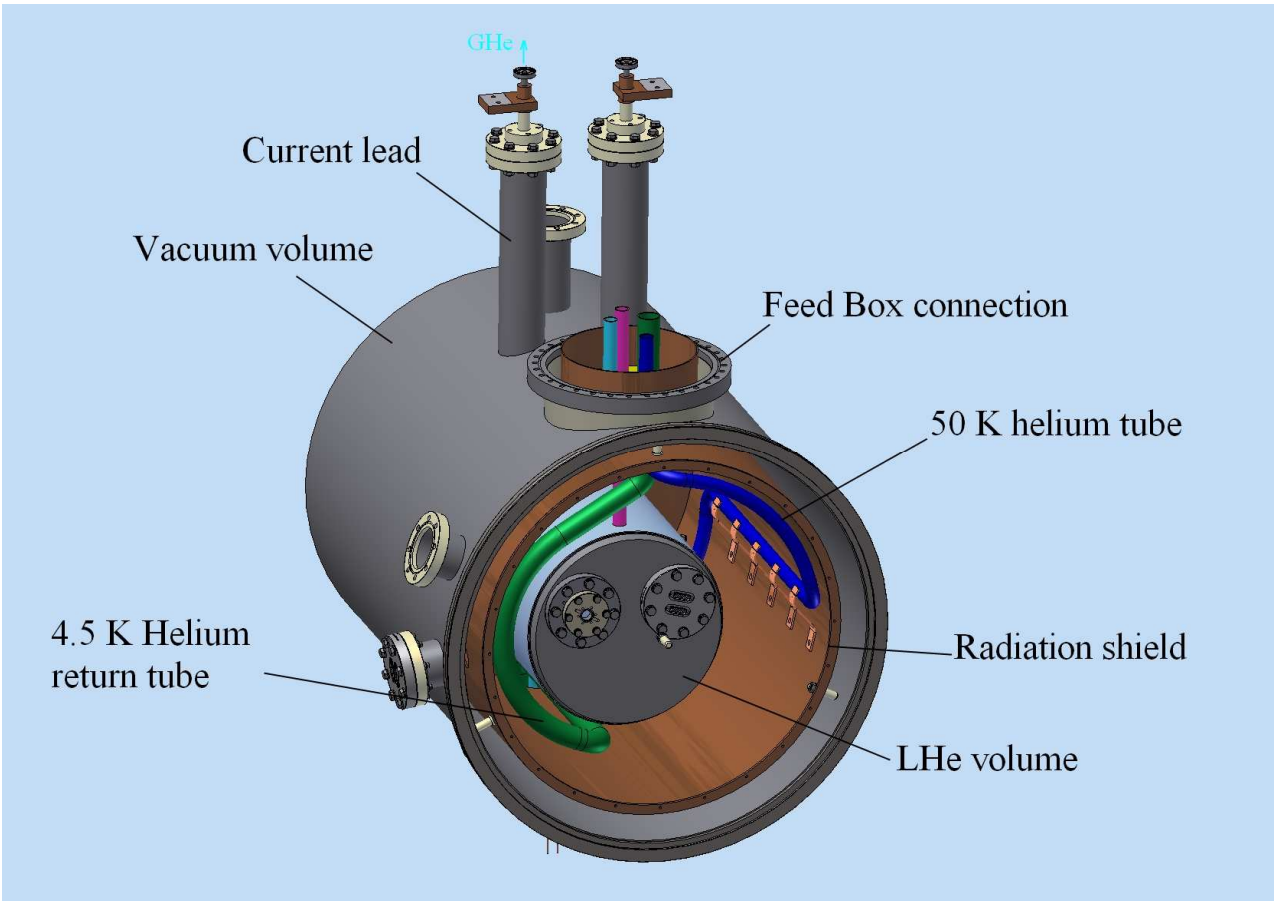

Fig. 13. View of the cryostat top of the CBM magnet.

The current leads will be designed for the current up to 800 A. Some part of the gaseous helium entering the cryostat will cool these current leads. If additional gas will be needed then a heater may be installed. Another design of the current leads with HTS insertions will be proposed and discussed on later stages. This current leads will not use 4.5 K gaseous helium for internal cooling, so the design of the cryostat and control process will be simplified.

The neck of the cryostat serves for various purposes. On the warm part of a rapture diaphragm, valves for connection with multipurpose line, connections for measurements and filling of liquid helium in the BINP tests will be placed. The rapture diaphragm should not let helium go to atmosphere; it should be led to specific manifold.

The radiation shield of the cryostat will be cooled by return line of the gaseous helium at about 55 K of temperature. The direct line of 50 K helium should directly go to the magnet for cooling its

supports and the radiation shields.

The radiation shield of the cryostat will be suspended on ball supports made of a kind of G-10 composite. The outer surfaces of the shield will be covered by multilayer superinsulation. .

The cryogenic valves in the cryostat are not shown.

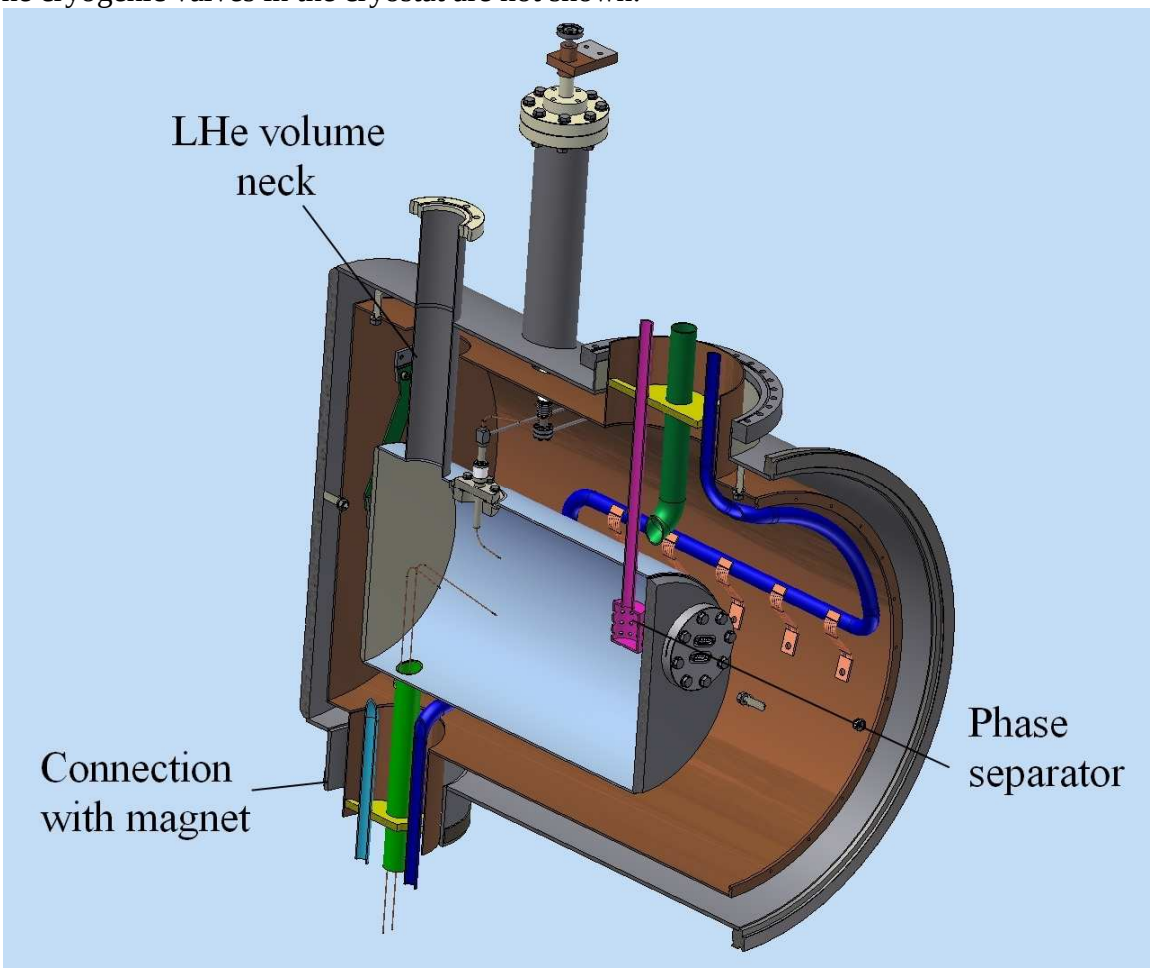

Fig. 14. Cross section of the cryostat.

3. Design calculations

3.1 Magnetic field calculations

The magnetic field calculations should present that the general design of the magnet gives the desired parameters of the magnetic field listed in the specifications, and also the results of forces acting on the yoke blocks and the magnet. The design of the iron yoke was changed with respect to the TDR. The changes are the height and the shape of the poles. Now they have a cylindrical shape and the height is decreased by 2 cm. The field clamps became of simple bar shape. The vertical side supports of the iron yoke are also simplified.

The 3D calculations were made in Mermaid code. Some calculations were modeled in ANSYS 2D model, see Fig. 15. The iron yoke steel was chosen as Steel 1010 (as Russian specification, that corresponds to Steel 1020 of USA and Steel 1.0402 of Germany). The poles of the yoke are a kind of ARMCO Steel or Steel 08kp (as of Russian specification, which corresponds to Steel 1008 of USA and Steel 1.0322 of Germany).

The magnetic properties of the steels taken into the calculations are presented on the Table 3.

The magnetic field values inside the SC winding are presented in the Fig. 16 as results of

Mermaid 3D calculations. The magnetic field values in the SC winding were compared with ANSYS 2D model, the details of such comparison were presented in specific report. The magnetic field differences between these two models are less than 10%.

The magnetic field distribution along the central line of the detector is shown on the Fig. 17.

The forces on the coils and the poles were calculated in the ANSYS 2 D model. The accuracy of the values of the forces is about 5% that is according to calculations in the TDR.

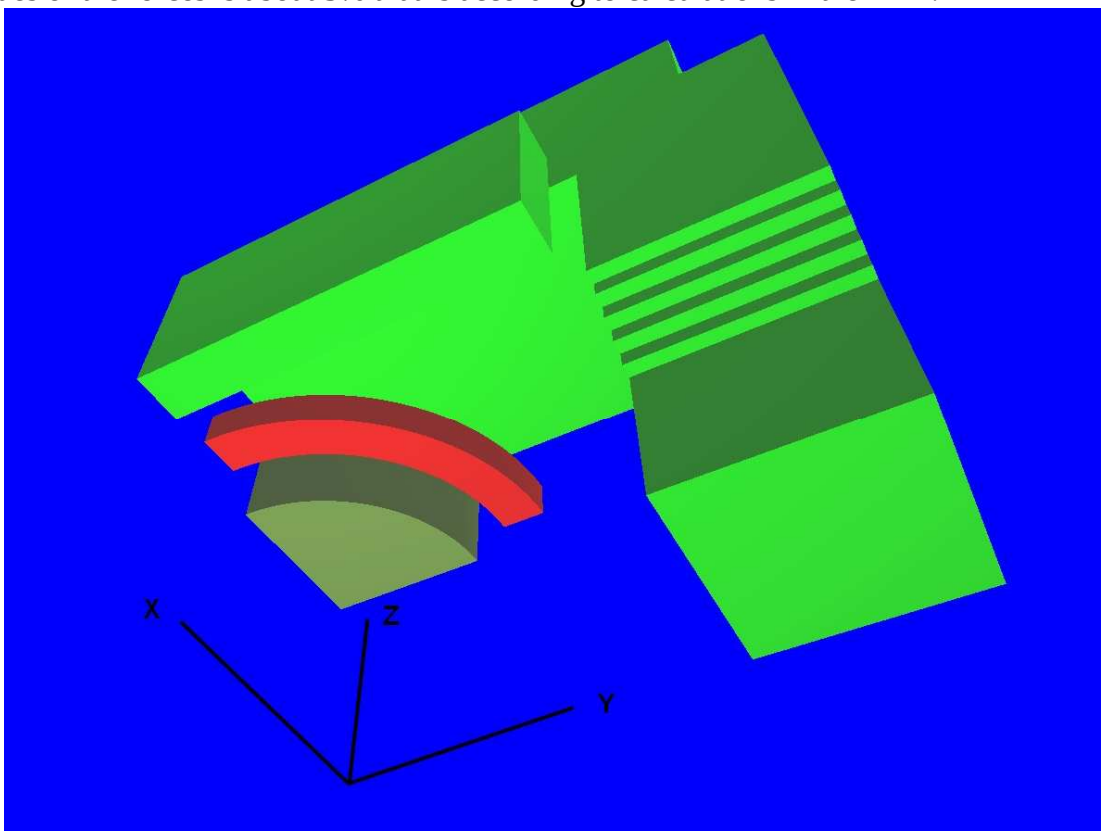

Fig. 15. The 3D model in the Mermaid code.

Fig. 16. The magnetic field values inside the SC winding as Mermaid result. The magnetic filed

values are in kG, the distances are in cm. The coordinate axis corresponds to the Fig. 15. These filed values are highest in the coil as this winding part is closest to the iron field clamps.

The map of the magnetic field around the RICH detector is shown in the Table 4. The axis directions are shown on the Fig. 15. In this table the Y = 0 that gives largest values of the magnetic field. The filed clamp of the iron yoke is limited by X = 119 cm. That is the widest size of the iron yoke along X direction. The presented values of the magnetic field around the RICH detector are very close to the corresponding values of the TDR report.

Table 3 The magnetic properties of the Mermaid code steels.

Armco		**Steel 1010**	
B, kGs	**μ**	**B, kGs**	**μ**
0.000	2500.00	0.000	700.00
1.000	2500.00	1.000	840.00
2.000	3333.00	2.000	990.00
3.000	3846.00	3.000	1120.00
4.000	4347.00	4.000	1320.00
5.000	4672.00	5.000	1500.00
6.000	4800.00	6.000	1520.00
7.000	4730.00	7.000	1500.00
8.000	4651.00	8.000	1450.00
9.000	4456.00	9.000	1370.00
10.000	4201.00	10.000	1270.00
11.000	3767.00	11.000	1175.00
12.000	3154.00	12.000	990.00
13.000	2551.00	13.000	830.00
14.000	1919.00	14.000	660.00
15.000	1153.00	15.000	530.00
16.000	615.00	16.000	400.00
17.000	303.00	17.000	270.00
18.000	146.00	18.000	180.00
19.000	89.00	19.000	120.00
20.000	61.00	20.000	80.00
21.000	43.00	21.000	43.00
22.000	30.00	22.000	24.00
23.000	19.00	23.000	15.00
24.000	12.00	24.000	10.00
25.000	8.00	25.000	7.00

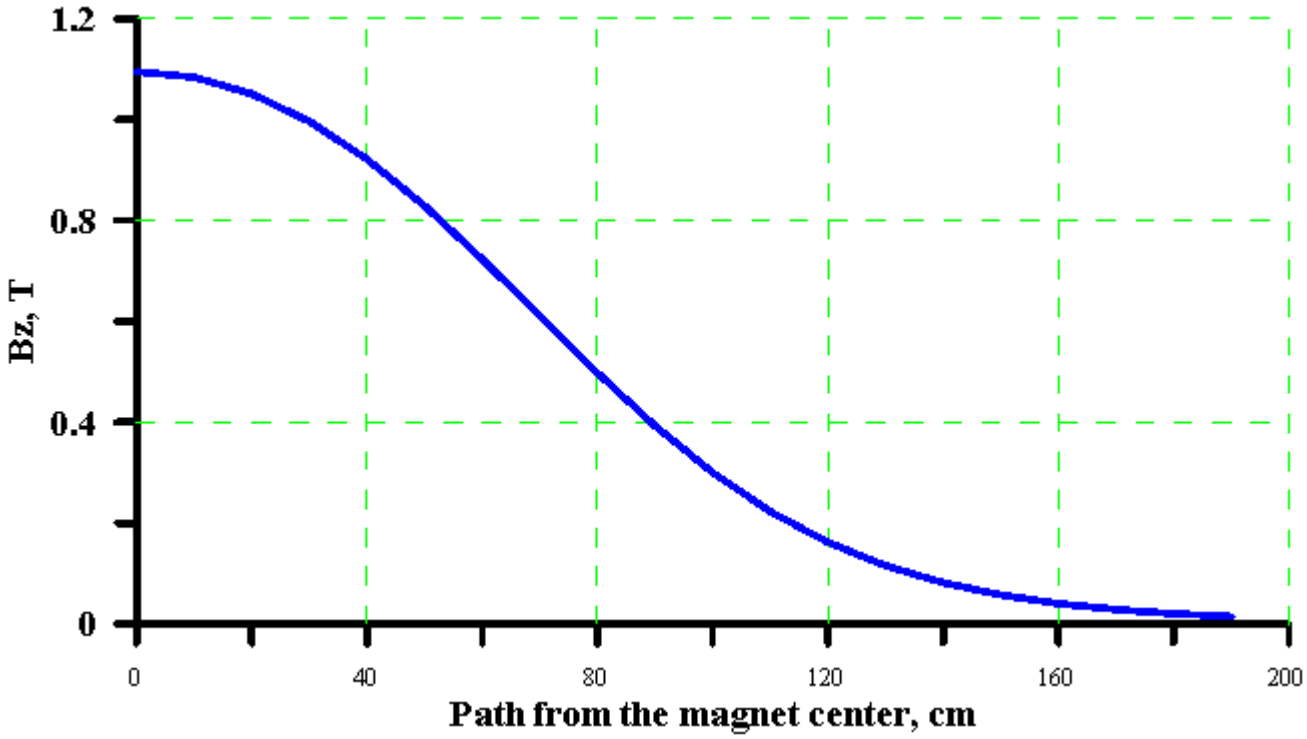

Fig. 17. Magnetic field distribution along the line from the center of the magnet detector at 686 A of the current.

Table 4 The map of the magnetic field [T] around the RICH detector. The RICH detector is placed around the grey shadows within X = 1.40÷2.10 m and Z = 1.74÷1.97 m.

Z, cm \ X, cm	110	120	130	140	150
100	1.39	1.37	0.033	0.028	0.022
110	1.38	1.37	0.021	0.019	0.016
120	1.38	1,31	0.015	0.014	0.012
130	1.16	0.87	0.012	0.010	0.009
140	1.09	0.040	0.009	0.008	0.007
150	0.0044	0.0054	0.0063	0.0061	0.0056
160	0.0051	0.0051	0.0051	0.0049	0.0046
170	0.0052	0.0048	0.0045	**0.0042**	**0.0039**
180	0.0054	0.0045	0.0040	**0.0036**	**0.0033**
190	0.0047	0.0039	0.0034	**0.0031**	**0.0029**
200	0.0035	0.0032	0.0029	**0.0027**	**0.0025**

Other results of the magnetic field calculations are listed below.

The integrals around the center of the magnet is 1.004 T*m for 686 A of the current, and is 1.018 T*m for 700 A of the current.

The vertical force on one coil toward the yoke is 2.6 MN.

The force on the poles is about 3 MN at 686A toward the center of the detector.

3.2. Mechanical calculations

The mechanical calculations were performed in ANSYS code.

The deformation of the iron yoke after applied force from attracting poles to the center of the magnet, are shown Fig. 18, Fig. 19. The forces values are 3 MN. Four bolts fixing the poles to the horizontal parts of the iron yoke are designed to keep the poles.

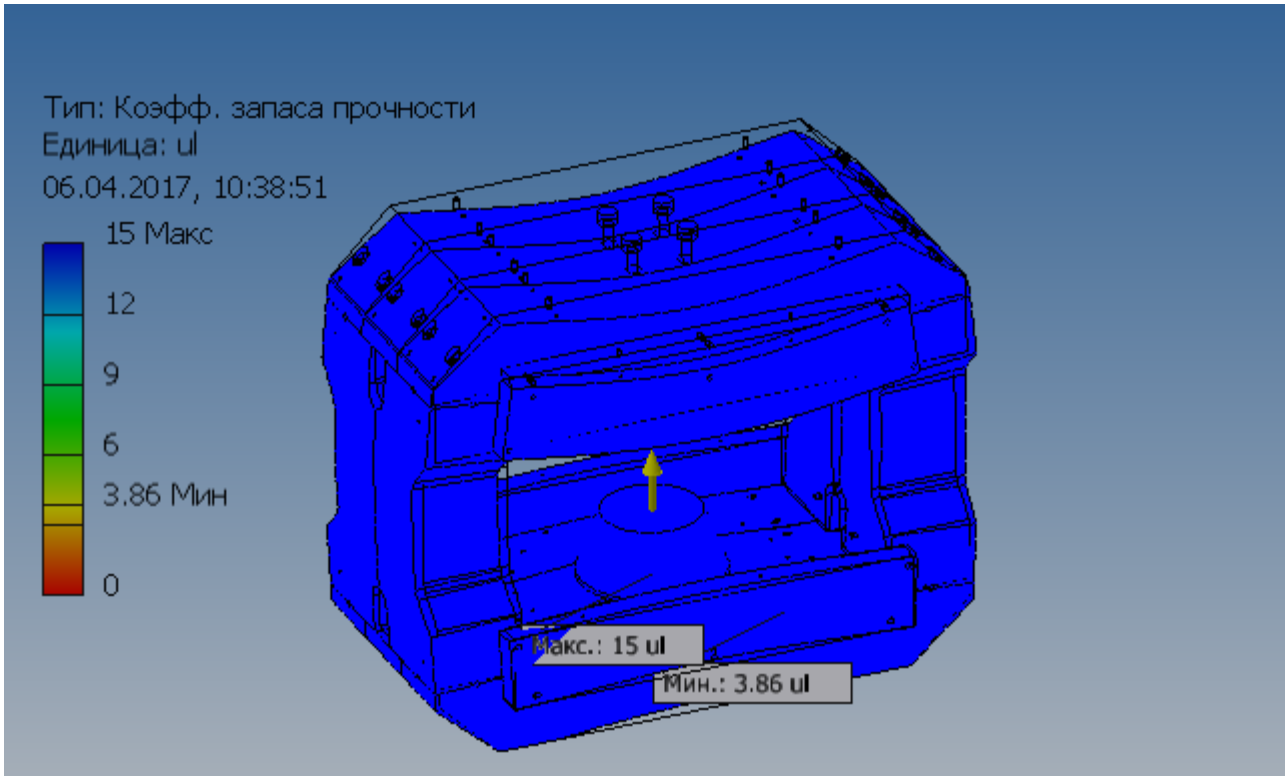

Fig. 18. The stress safety factor after applying of the attracting forces to the poles. The minimal value is 3.86 and the maximal value is 15.

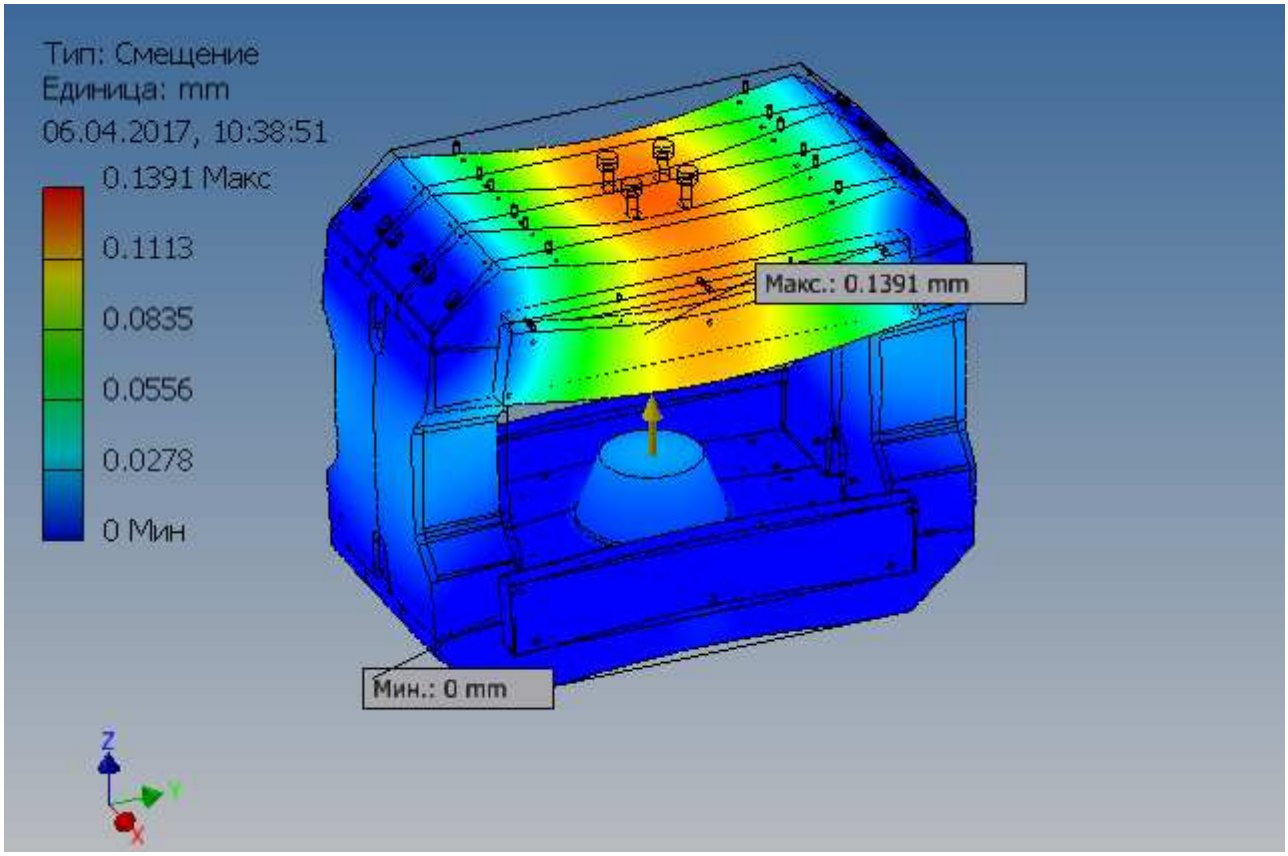

Fig. 19. Deformation of the iron after applying of the attracting forces to the poles. The maximal deformation is 0.14 mm.

Coil stresses

The cold mass of the coils consists of different materials. The internal stress will appear after

cooling down and magnetic forces application. The purpose of the calculations is to obtain stress and deformation of the CBM coil structure under the following loads:
- stress after cooling down from room temperature to 4.5 K temperature;
- stress after application of the Lorentz force, which were taken as 2.5 or 3 MN of axial direction, and of 5 MPa pressure on the inner radius of the coil. These values were taken from the magnetic field calculations.

The ANSYS code was used for these calculations. The available ANSYS package not included the magnetic field analysis, so the magnetic forces were applied as external forces on the coil. The values of the forces were taken from other ANSYS magnetic field calculations.

The criteria of acceptable stress results are:
- the stress in the stainless steel is below 600 MPa that is the yield stress at low temperatures;
- the stress in the copper is below 450 MPa that is the ultimate stress at low temperatures;
- the stress in the SC cable is below 350 MPa that is the stress of degradation of superconducting property of NbTi by ~ 5%;
- the stress in the winding structure is desired to be below 100 MPa that is the ultimate stress of epoxy compounds. Such stress beyond this value may produce epoxy cracking causing premature quenches. If such stress is exceeding the 100 MPa value but of compressive quality or not making movements of the SC cable then it may be treated as an acceptable stress.

Preamble before making ANSYS stress calculations

Before making a calculation using some code its worth to evaluate the stress in the coils with simple formulas for interpretations of the calculated results. The coil stress appears after application of the two Lorentz forces coming from radial and axial magnetic fields. Also the internal stresses from different thermal contraction of the materials should be appeared. The last stresses will be evaluated in ANSYS code. The axial magnetic field in the coils acts as pressure, it may be evaluated directly as Bz*I*L or as knowing that B^2 acts as pressure 0.4 MPa corresponding to 1 T. As the Bz ~ 3.5 T, the pressure will be ~ 5 MPa. This pressure gives hoop stress in the coils which is estimated as $\sigma = p*R/h$ (radius and radial thickness of the coils). So, $\sigma = 5*0.7/0.16 = 22$ MPa – the hoop stress without Cu and stainless steel cases. As these elements have higher Young modulus than the SC winding the code calculations of the whole model should give much less value of the hoop stress.

The radial magnetic field produces the axial force attracting the coil to the closest iron. Its value was calculated as ~ 2.5 MN. If the coil would be uniformly held in axial direction the axial stress inside the coil would be as $\sigma = F/(2\pi R*h) = 2.5/(6.28*0.8*0.16) = 3.1$ MPa – very low value. But in our design the coil will be fixed with six support struts, so the stresses from the axial force will be localized around these struts due to bending of the coil arcs in axial direction. Such bending effect may be estimated as for bending a beam having one end fixed and the other end free. This stress is evaluated according:

$\sigma = \frac{M}{J_x} * y$, where M – force momentum [F*m], Jx – momentum of inertia [m^4], y – half length of the coil axial size. For a rectangular shape beam the $Jx = a*b^3/12$, as a ~ b = 0.2 m, then Jx = $1.33*10^{-4}$ m^4. $M = F/24 * 2\pi R/12 = 4.4*10^4$ H*m. The half length y ~ 0.1 m. The result is:

$\sigma = 4.4*10^4*0.1/1.33*10^{-4} = 33$ MPa. Firstly this value should be treated as highest as the bending beam has not free end, secondly the maximal stress will be in the stainless steel case, and thirdly this value is well low.

The final stress will be with addition of the thermal contraction stresses.

The calculations presented below should interpreted upon rough estimation given in this preamble.

End of preamble

The 3D model of the coil used in the calculations was consisted of the following materials visible in Fig. 7: stainless steel case, copper case, G-10 sheets of 2 mm thickness surrounding the SC winding, the SC winding was a composite material containing ~ 50% of G-10 material. Anisotropic properties of the materials were also accounted. Some parameters of the materials are listed in the Table 5. There was a friction boundary condition between the copper and the stainless steel cases. The calculated model was represented by 1/3 length of the real model.

The first set of the calculated results is shown on the Fig. 20 - Fig. 23. These results were obtained at applied vertical force 3 MN and pressure 5 MPa on the winding. The material properties here were not optimized with respect to the contraction coefficient of epoxy inside the winding.

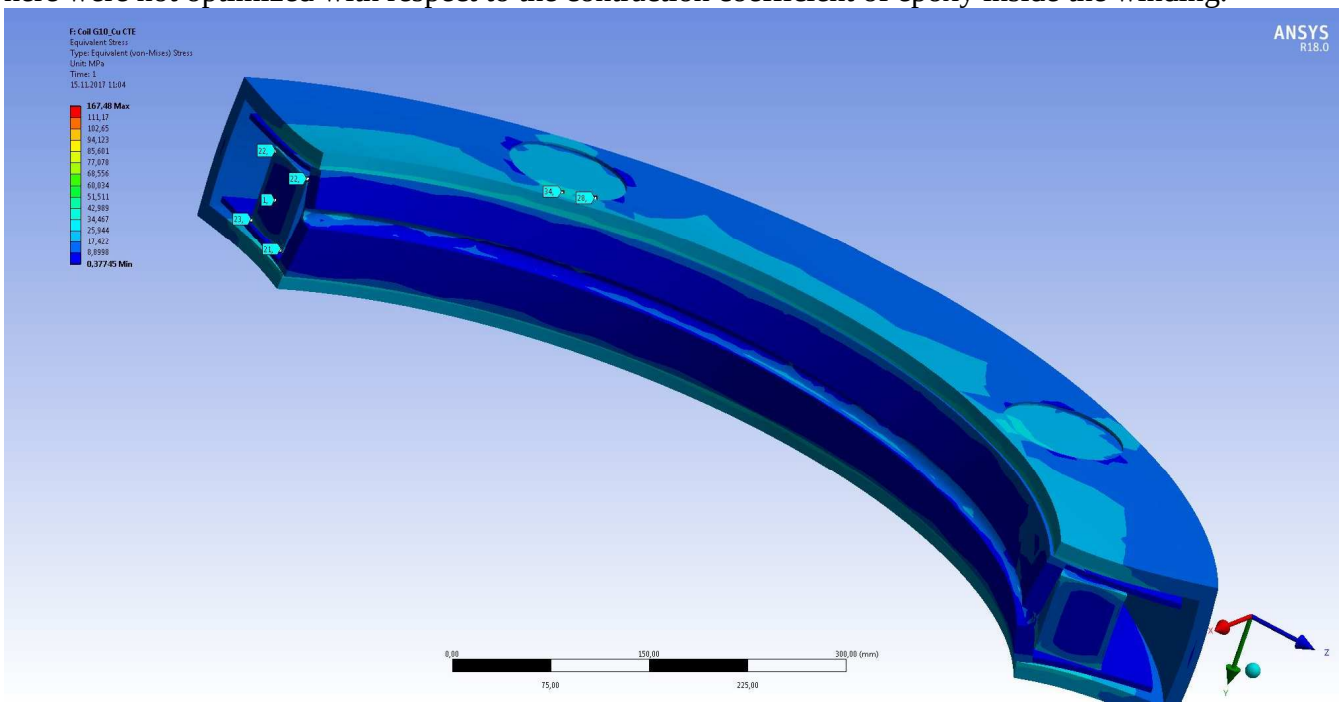

Fig. 20. The total stress in the structure after cooling. The maximal value is about 167 MPa in the stainless steel case. The mesh size here needs to be finer.

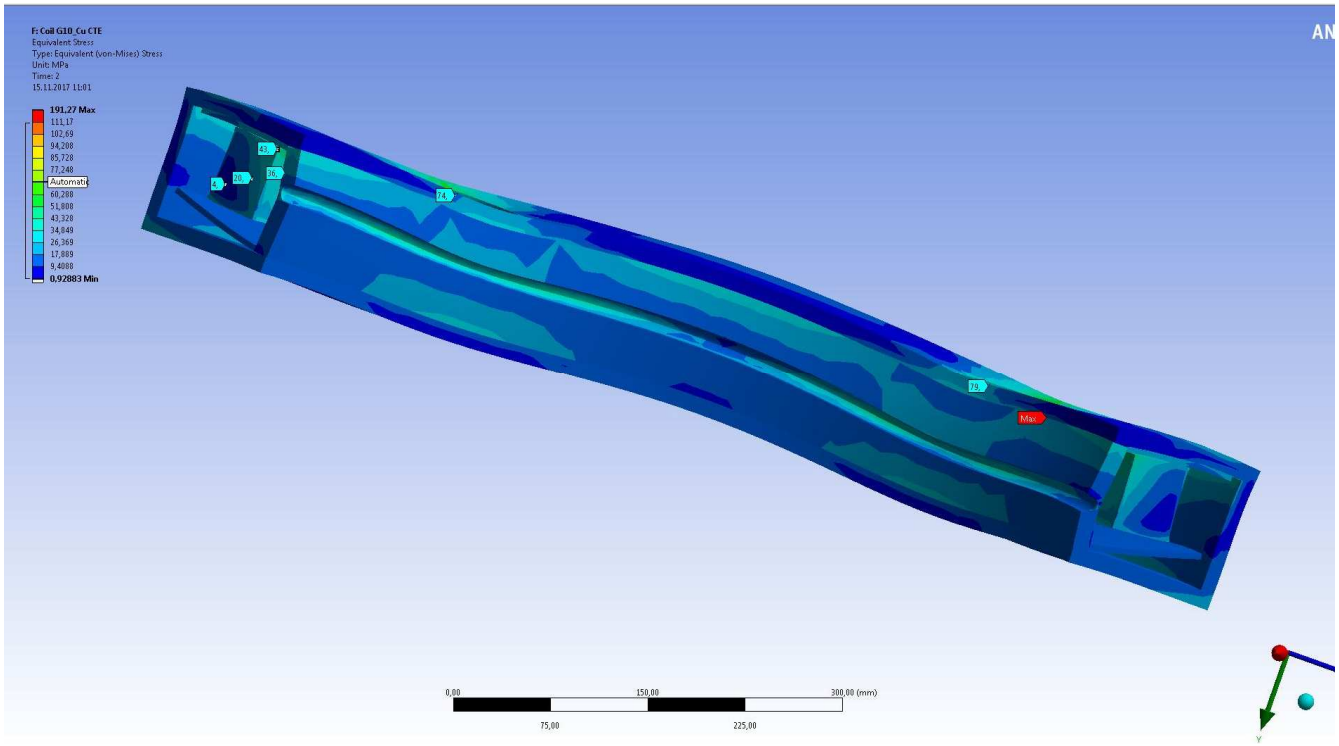

Fig. 21. The von Mises stress in the structure after cooling down + forces. The maximal value is

about 191 MPa in the stainless steel case.

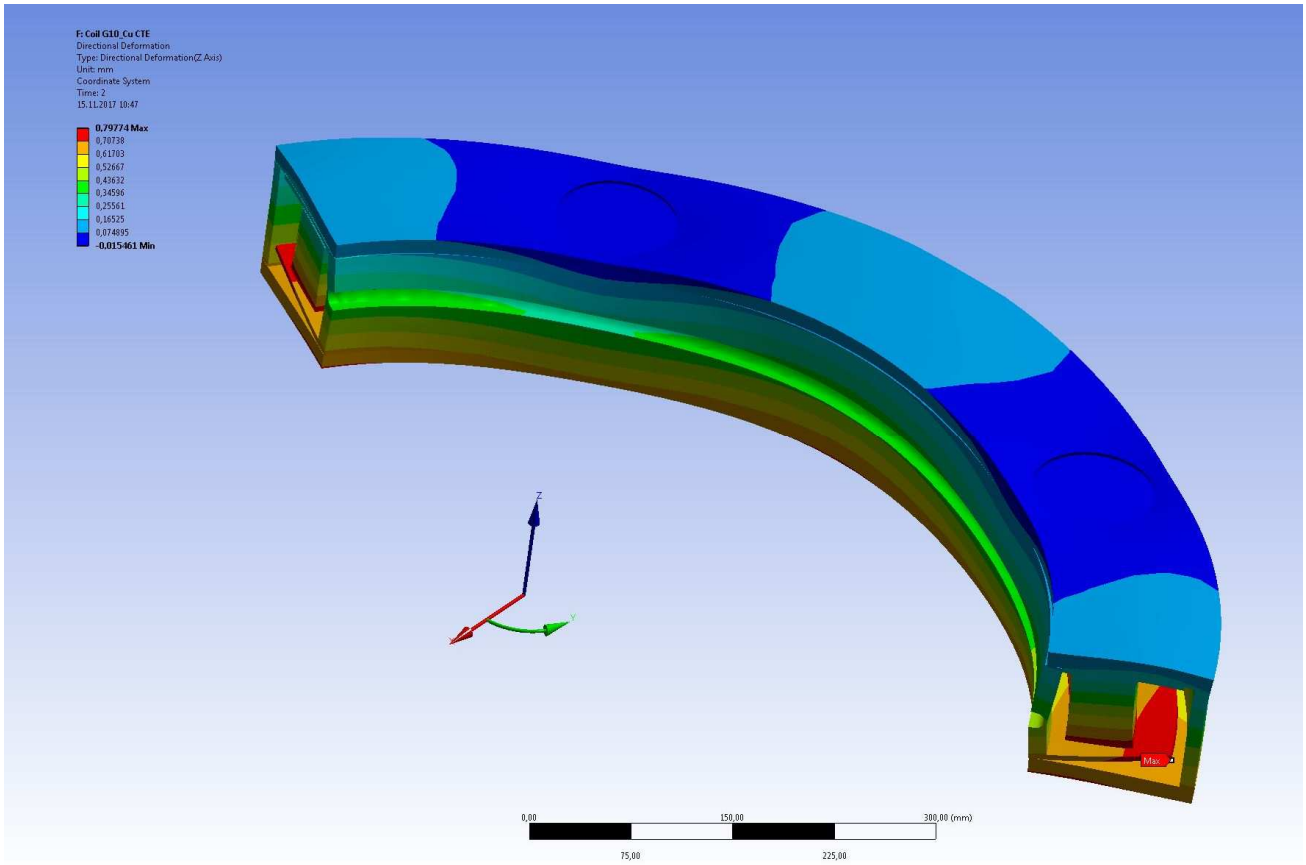

Fig. 22. The vertical deformation of in the structure after cooling and application of the forces. The maximal value is 0.9 mm.

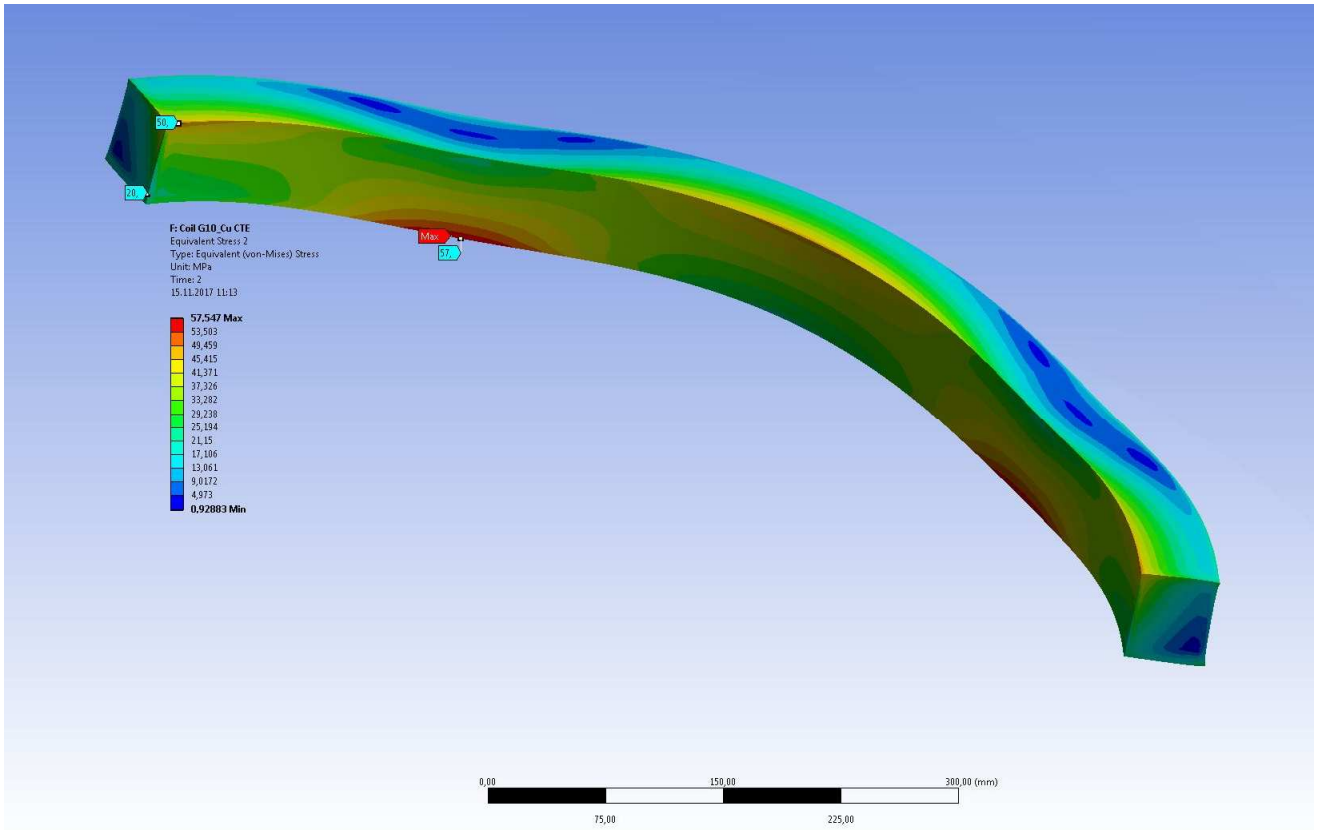

Fig. 23. The coil total stress after cooling and application of the forces. The maximal value is 58 MPa.

The second set of the calculated results is shown on the Fig. 24 - Fig. 28. These results were obtained at applied vertical force 2.5 MN and distributed pressure 5.3 MPa inside the winding. The material properties here were optimized with respect to the contraction coefficient of epoxy inside the winding. The epoxy compound contains Al_2O_3 powder decreasing the contraction coefficient.

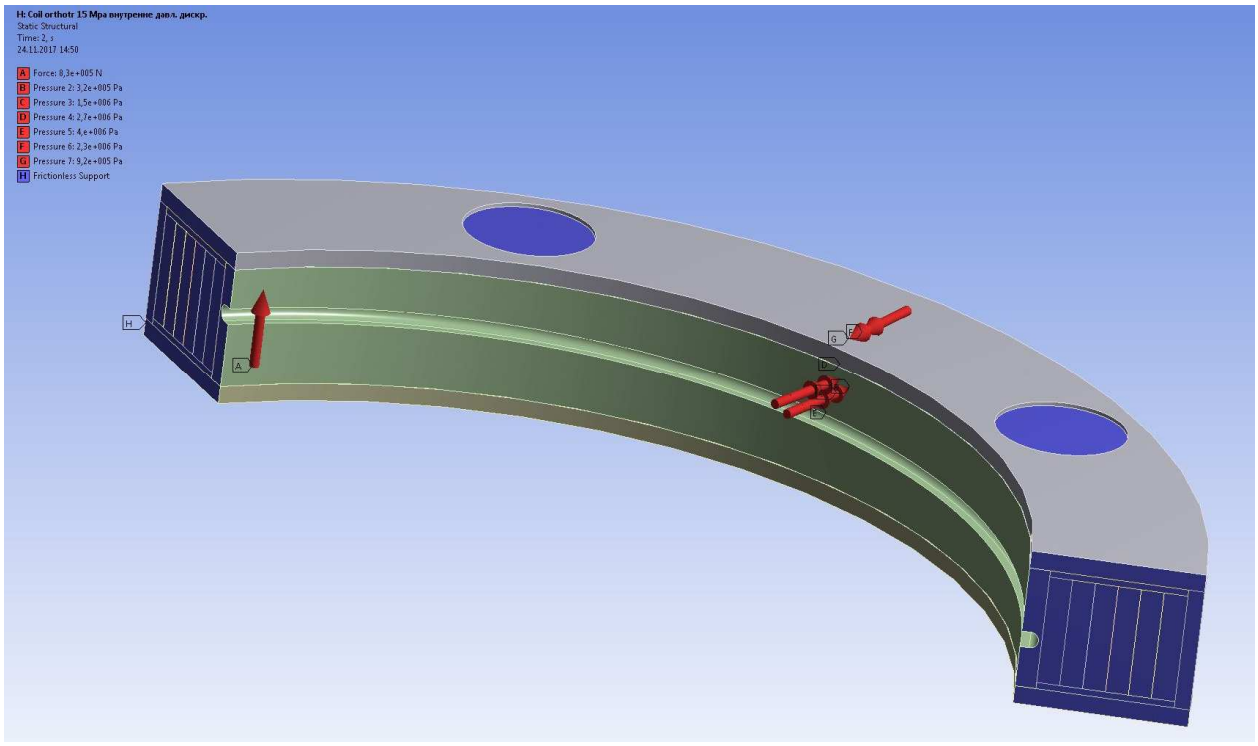

Fig. 24. The 3D model and applied pressures and force

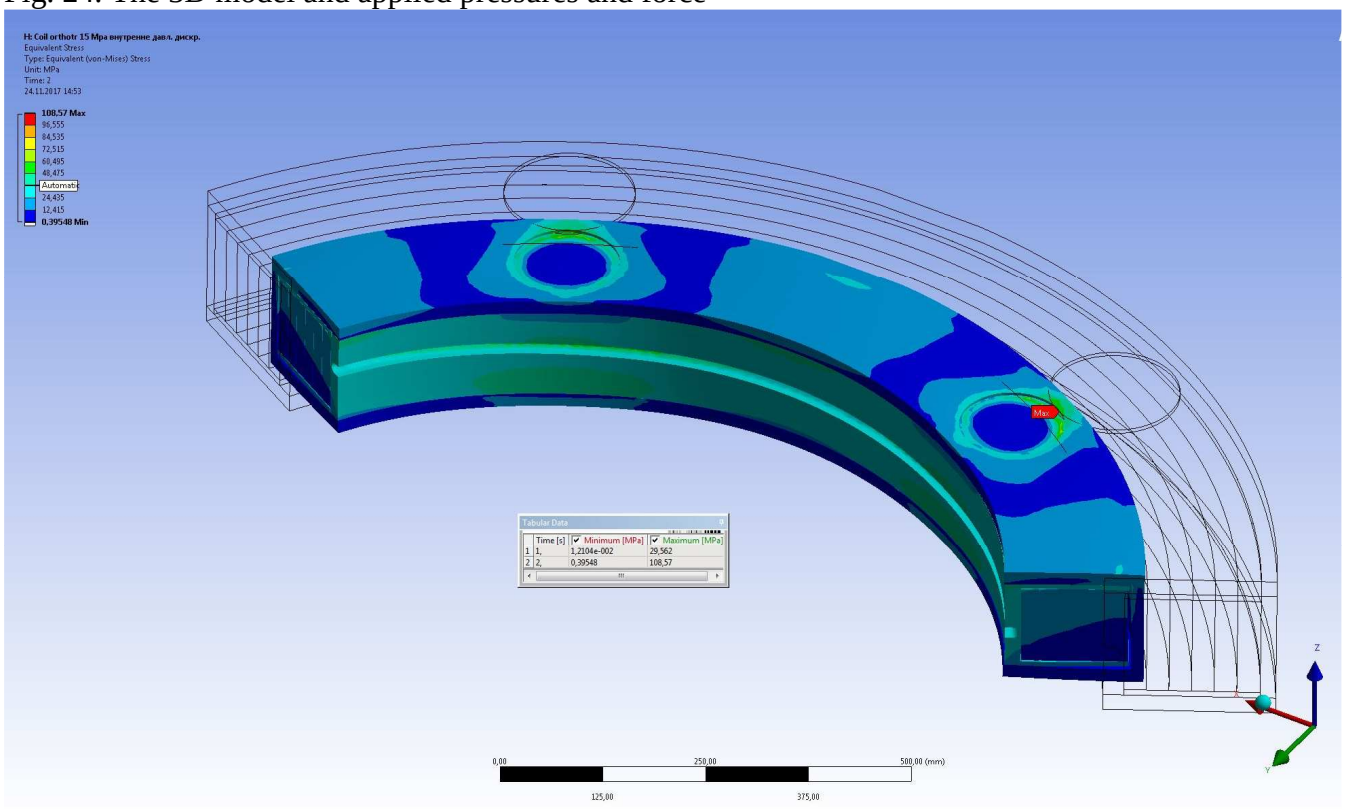

Fig. 25. The von Mises stress in the whole model. The maximal value is 108 MPa.

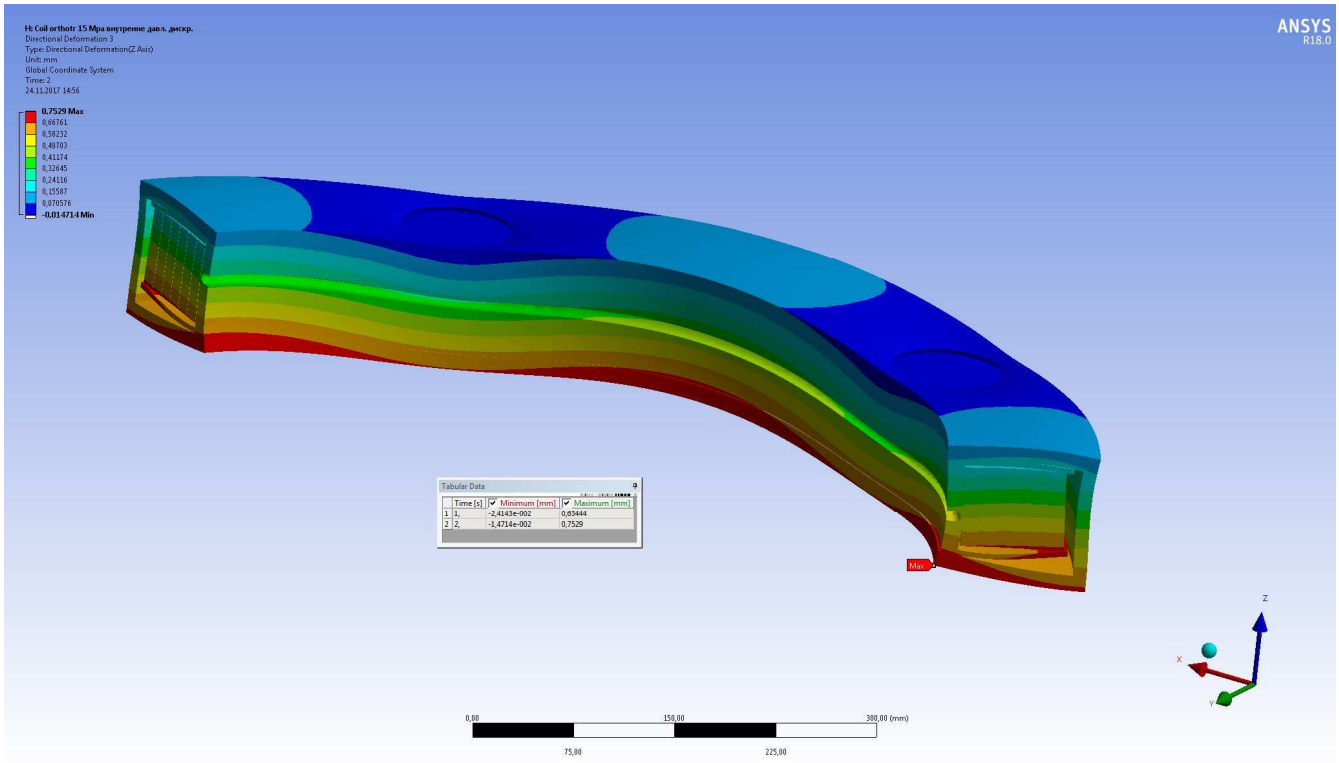

Fig. 26. The vertical deformation after cooling down and forces application. The deformation after cooling down is 0.63 mm and resulting deformation is 0.75 mm. The deformation from the axial force is 0.12 mm that is slightly less than in the TDR design.

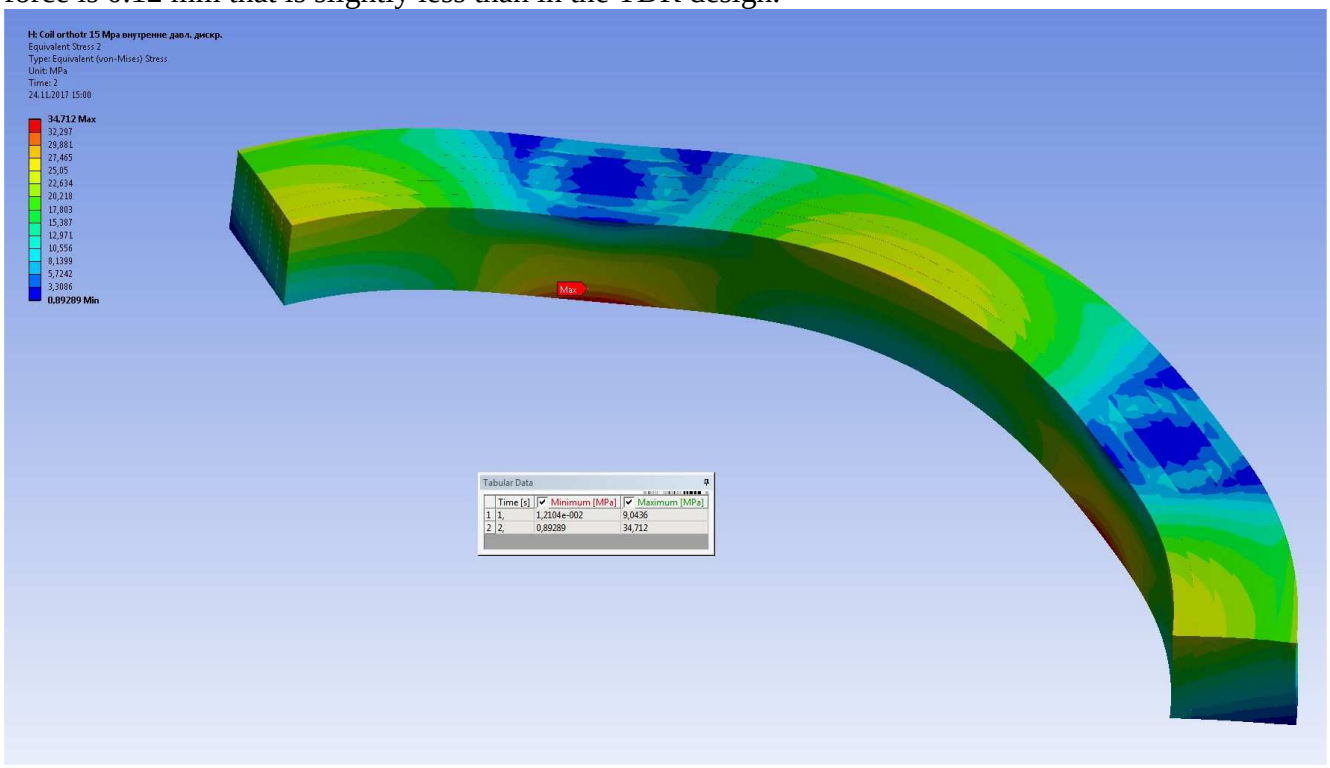

Fig. 27. The von Mises stress in the winding. The maximal value is 34 MPa. The maximal stress after cooling down is 9 MPa – the effect of epoxy compound with powder.

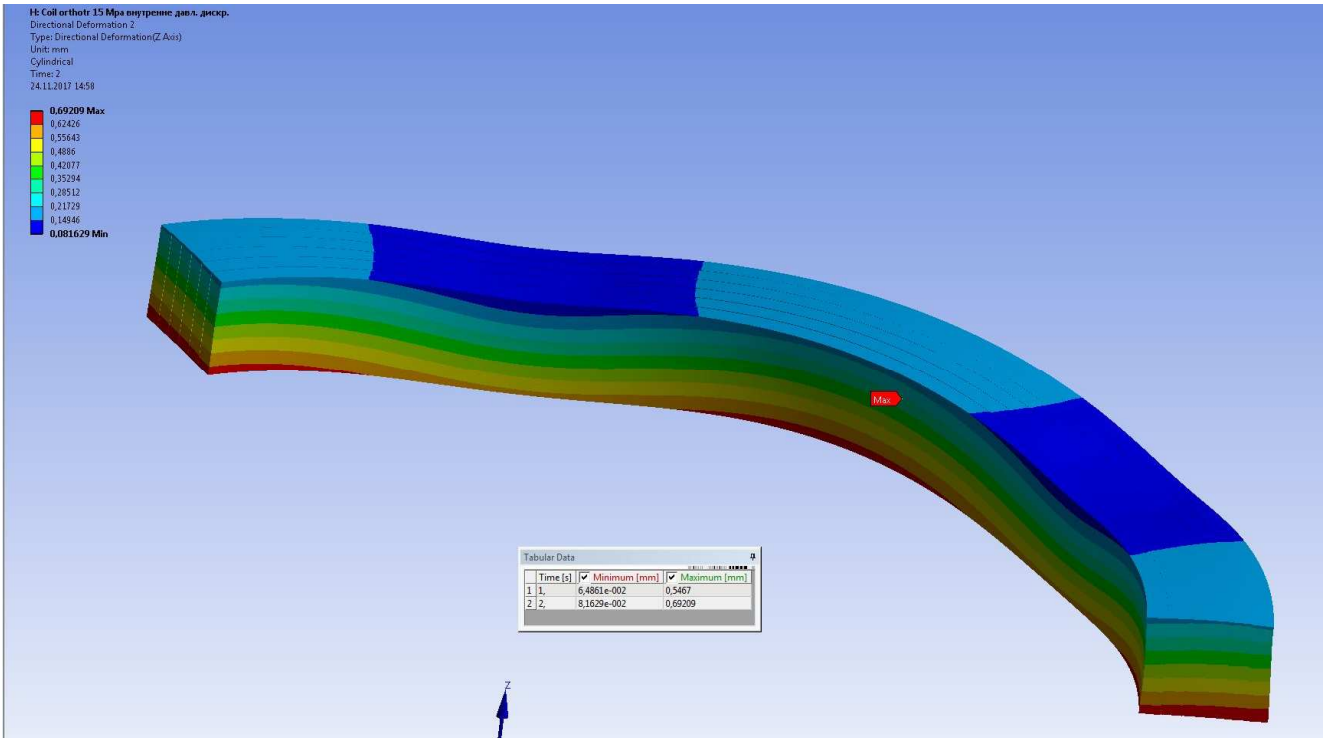

Fig. 28. The vertical deformation in the winding. The maximal value is 0.69 mm.

Table 5. The materials properties used in structural analysis.

Property	Stainless steel	GFRP material	Coils	Epoxy	Copper
Thermal expansion coefficient, K^{-1}	$1.11\ 10^{-5}$	$1.2\ 10^{-5}$	$1.2\ 10^{-5}$	$1.2\ 10^{-5}$	$1.25\ 10^{-5}$
Shear modulus in xz plain, Pa	$7.5\ 10^{10}$	$4.0\ 10^{9}$	$1.9\ 10^{10}$	$4.0\ 10^{9}$	$4.0\ 10^{10}$
Young modulus y direction, Pa	$2.0\ 10^{11}$	$1.8\ 10^{10}$	$4.1\ 10^{10}$	$9.0\ 10^{9}$	$1.2\ 10^{11}$
Thermal expansion coefficient y direction, K^{-1}	$1.11\ 10^{-5}$	$1.0\ 10^{-5}$	$1.57\ 10^{-5}$	$6.0\ 10^{-5}$	$1.25\ 10^{-5}$
Thermal expansion coefficient xz plain, K^{-1}	$1.11\ 10^{-5}$	$1.6\ 10^{-5}$	$9.2\ 10^{-6}$	$1.6\ 10^{-5}$	$1.25\ 10^{-5}$
Young modulus xz direction, Pa	$2.0\ 10^{11}$	$2.2\ 10^{10}$	$7.5\ 10^{10}$	$1.8\ 10^{10}$	$1.2\ 10^{11}$

The results of the structural analysis

The stresses in the total coil structure and inside the windings are well below stresses in all principal materials: stainless steel, copper, and NbTi superconductor. The problem of epoxy cracking is also not seen there when the stress value exceeds 100 MPa. The main principal stress inside the winding is positive and is in circumference direction, i.e. the transverse movement of the SC cable will not happen.

The stresses after cooling down due to difference of the thermal contraction coefficients give about 30% of the total stress value if epoxy will be not filled with powders. During manufacturing it is planned to impregnate the winding with epoxy composite containing up to 50% by weight of powders. Such epoxy composites have contraction coefficients very close to the contraction coefficient of metals. The considered possible powders are Al_2O_3 (continuously used in BINP) and BN having more excellent parameters, see Fig. 29. The problem that the powders will not go deep

inside the winding looks not principal because the maximal stresses are on the outer surfaces of the winding. This technology will be tested before the impregnation of the real coils as it is always done in the BINP workshop.

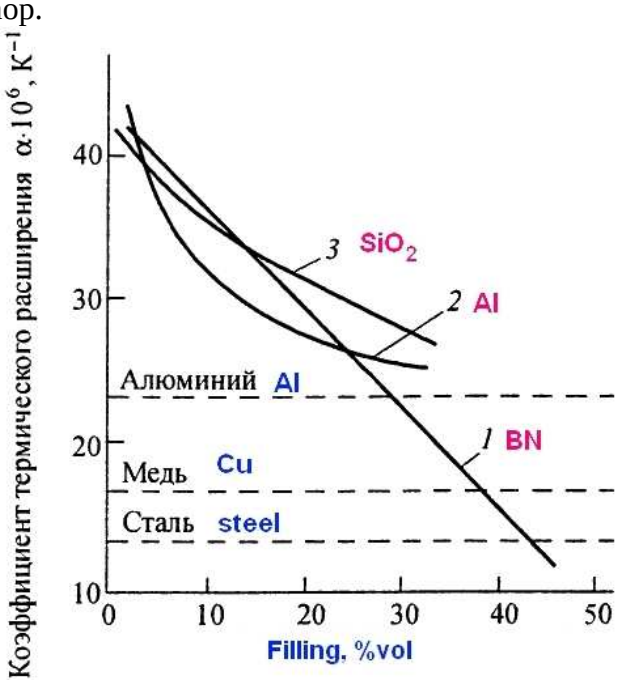

Fig. 29. Influence of filling components in epoxy on thermal expansion coefficient [Yu. Solntsev, p. 679]. The dash lines are the thermal expansion coefficients for metals for comparison.

The task when the 5 MPa pressure was applied may be considered not convincing with respect to stresses inside the winding in the first set of the results.

In the second set of the results the distributed pressures were applied to the six section of the winding. The thermal contraction coefficient was taken as for epoxy filled with powder. The results become improved.

It is planned that as far as 3D design model will be finished the ANSYS multiphysics analysis will be performed.

3.3. Heat load estimations

The results of the heat loads estimations are presented in the tables below. The view of the cold mass temperatures is shown on the Fig. 30.

Estimations of the heat loads to 4.5 K helium

The thermal radiation on the LHe coil cases was estimated as:

$Q = \varepsilon S \sigma T^4$, where ε - total emissivity was taken as 0.02, S – surface area of the stainless steel case is 4.2 m^2, T – radiation shield temperature was taken as 60 K.

The heat load from the support struts via stainless steel plates was estimated as:

Q = 12 * 0.3 = 3.6 W – for twelve struts, where 0.3 is taken from calculations presented below in Fig. 33 and multiplied by 3 as uncertainty factor.

The heat load from the Ti tie rods was estimated as:

$Q = \lambda S^* \Delta T/L$, where λ - thermal conductivity was taken as 0.15 W/(m*K), S – cross-section area is about $1.1*10^{-4}$ m^2, ΔT – temperature difference was taken as 60 K, L – length is about 0.25 m.

Joule heat in the soldered splices was estimated for soldering on 5 cm of length and resistance to be about $5*10^{-8}$ Ohm and at 686 A of current.

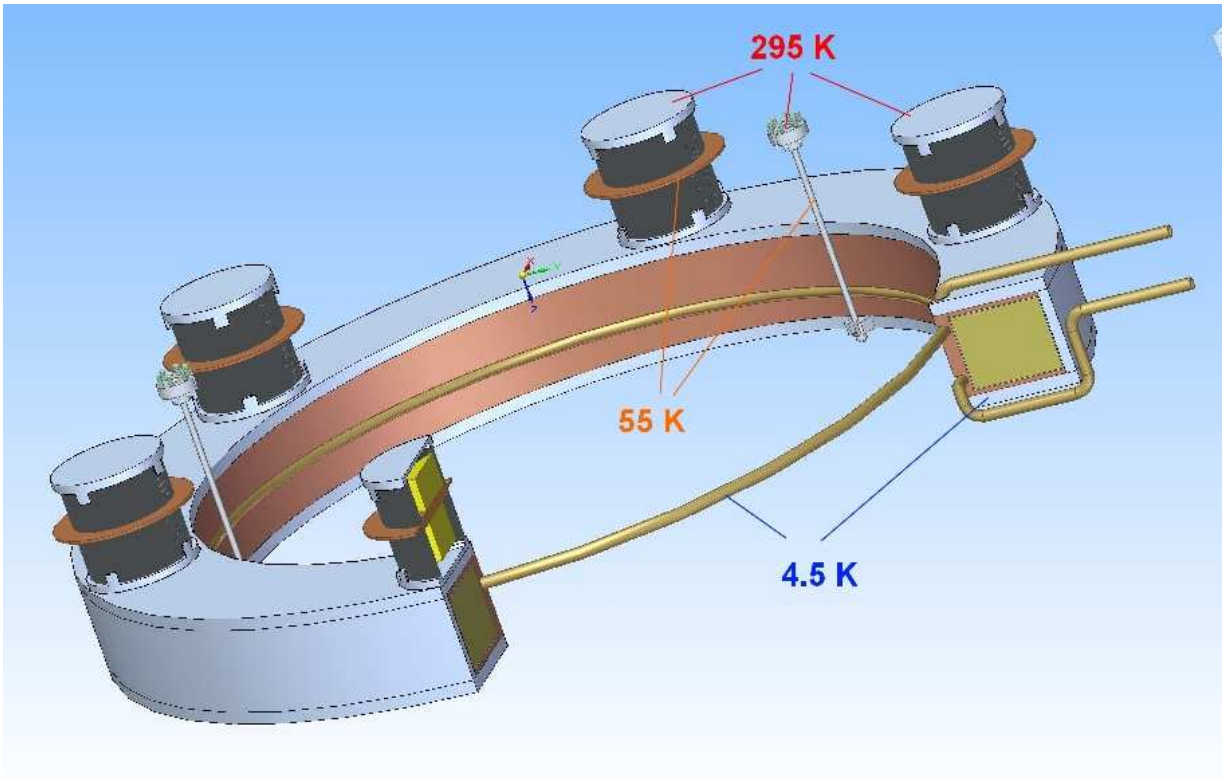

Fig. 30. View of the cold mass of the magnet connected by tie rods and support struts to the vacuum vessel. The temperatures taken into calculations are shown.

Table 6 Heat loads on 4.5 K helium from both coils and the cryostat.

Heat load sources	**Values**
Thermal radiation on the LHe case, W	0.12
Support struts, W	< 3.6 expected
Tie rods, W	0.05
Soldering connection of the cable (at least 6 short splices), W	0.12
Thermal radiation on the cryostat, W	0.015
Cryostat suspension, W	<0.1
Current leads, W	0.5
Measurements wires, W	<0.1
Heat bridges of the cryostat neck and others connections, W	<0.1
Total, W	***~ 4.71***

Hot spot by the support struts

The support struts give largest part of the magnet heat loads at 4.5 K cold mass. The superconducting winding will press the LHe case exactly opposite these struts. In the current design of the coil the superconducting winding is shielded from the hot spot by the copper case having thick walls, about 8 mm. Also, in the current design the heat in-leaks from the strut are not high, so no problems seen from the support struts.

The heat loads from the support struts are presented in the Fig. 31 - Fig. 33. The room temperature was fixed at 295 K and the thermal interception by the radiation shields was fixed at 60 K.

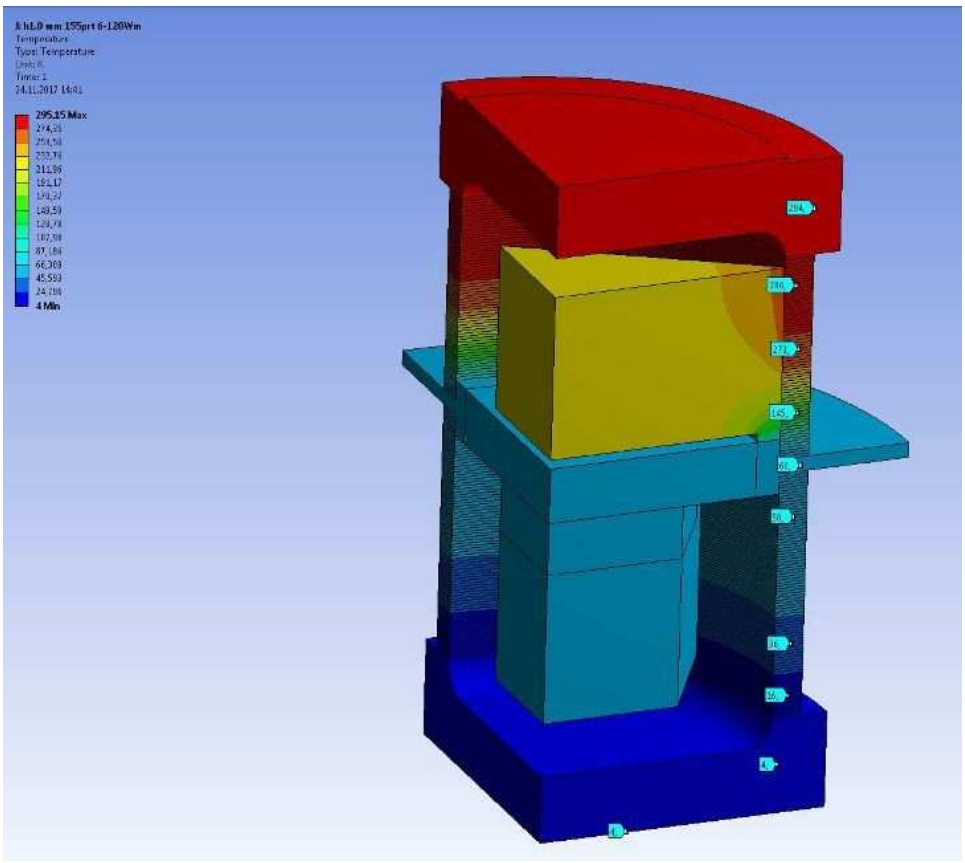

Fig. 31. Temperature distribution in the support strut then the bottom is fixed at temperature 4.5 K, the top at 295 K and the interception at 60 K.

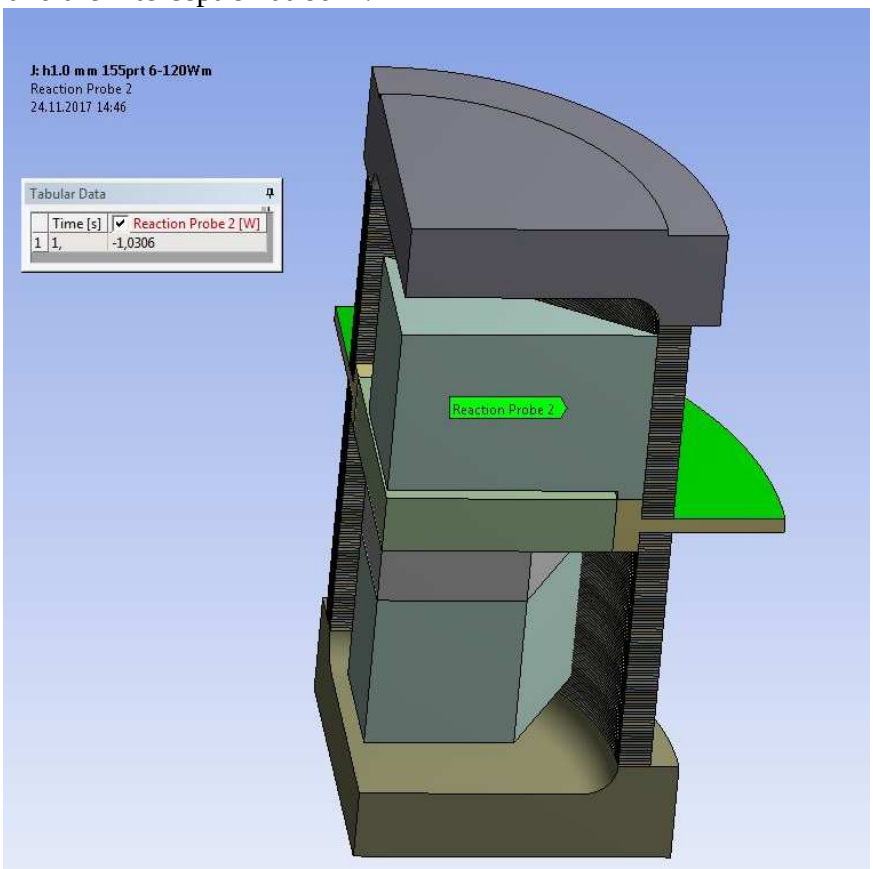

Fig. 32. Heat load on the interception at 60 K, the total value for one strut is 4.12 W.

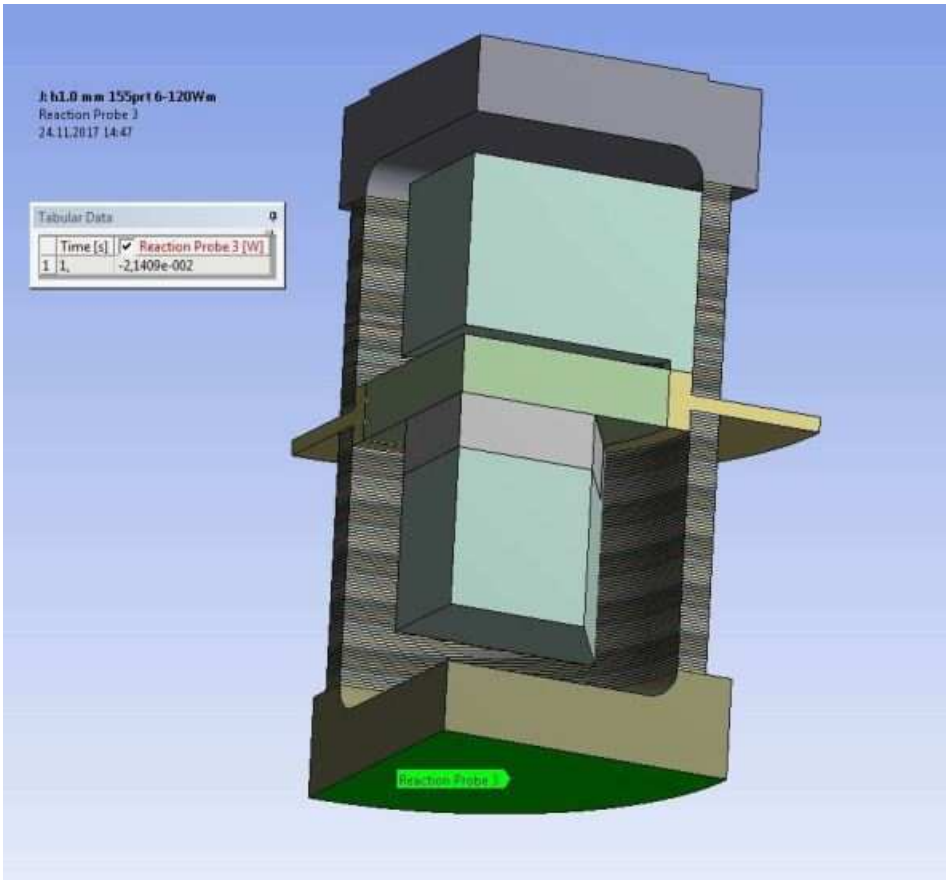

Fig. 33. Heat load on bottom of the strut at 4.5 K, the total value for one strut is < 0.1 W.

Estimations of the heat loads to 50 K helium

The thermal radiation from the vacuum vessel on the radiation shields covered by multilayer insulation may be estimated as:

$Q = q*S$, where, S – surface area of the shields is ~ 5 m^2, q – experimentally determined heat flux, its typical value is about 1 W/m^2.

The heat load from the support struts via stainless steel plates was estimated as from Fig. 32:

$Q = 12*4.12 = 49.5$ for twelve struts.

The heat load from the tie rods was estimated as:

$Q = \lambda S*\Delta T/L$, where λ - thermal conductivity was taken as 0.15 W/(m*K), S – cross-section area is about $1.1*10^{-4}$ m^2, ΔT – temperature difference was taken as 220 K, L – length is about 2*0.15 m (two cylinders).

Table 7 Heat loads on 50 K helium from both coils and the cryostat

Heat load from	**Values**
Thermal radiation on the shields from the vacuum vessel, W	10
Support struts, W	49.5
Tie rods, W	0.5
Thermal radiation on the cryostat shield, W	1.5
Cryostat suspension, W	2
Current leads, W	120*
Measurements wires, W	0.5
Heat bridges of the cryostat neck and others connections, W	1
Total, W	~ 185

*) It will be corrected after detailed design of the current leads

The estimation of heat loads from on the Branch Box, the Feed Box and on the transfer line are presented in the Table 8 and Table 9.

The thermal radiation on the surfaces at 4.5-4.6 K was estimated as:

$Q = \varepsilon S \sigma T^4$, where ε - total emissivity was taken as 0.03, S – surface area of the BB, FB and the transfer lines surfaces at 4.5 K is about 7 m^2, T – radiation shield temperature was taken as 60 K.

The heat load from the control valves was estimated on example of Weka valves of DN15 size as: $Q = N*Q_v$, where N – is the number of valves, in our case is 19, Q_v – the heat load from one valve specified by manufacturer, which is in our case about 0.8 W.

The heat load from the check valves was estimated as:

$Q = \lambda S*\Delta T/L$, where λ - thermal conductivity of stainless steel tubes and bellows was taken average as 3 W/(m*K), S – cross-section area is about 10^{-3} m^2, ΔT – temperature difference was taken as 60 K, L – length is about 0.2 m.

Table 8 Heat loads on 4.6 K helium from the Branch Box, the Feed Box and the transfer line

Heat load from	**Values**
Thermal radiation on 4.5 K surfaces from the shields on the FB and BB, W	0.15
Supports and suspensions, W	< 2
Control Valves, W	15.2
Check Valves, W	0.9
Measurement wires, W	< 0.01
Heat bridges of the cryostat neck and others connections, W	< 1
Total, W	19.26

The thermal radiation from the vacuum vessel on the radiation shields covered by multilayer insulation may be estimated as:

$Q = q*S$, where, S – surface area of the shields is ~ 7 m^2, q – experimentally determined heat flux from room temperature via multilayer insulation, its typical value is about 1 W/m^2.

The heat load from the check valves was estimated as:

$Q = \lambda S*\Delta T/L$, where λ - thermal conductivity of stainless steel tubes and bellows was taken average as 10 W/(m*K), S – cross-section area is about 10^{-3} m^2, ΔT – temperature difference was taken as 220 K, L – length is about 0.2 m.

Table 9 Heat loads on the 60 K helium (return line) from the Branch Box, the Feed Box and the transfer line

Heat load from	**Values**
Thermal radiation on the shields from the vacuum vessel, W	7
Support and suspensions, W	20
Control valves, W	38
Check valves, W	11
Measurement wires, W	< 1
Heat bridges of the cryostat neck and others connections, W	5
Total, W	82

As a conclusion, total heat load for the CBM detector:

for 4.6 K helium is Q = 24 W; for 50 K helium is Q = 267 W;

The mass rates at normal operation are $G = Q/\Delta h$:

G = 1.15 g/s for 4.6 K helium;

G = 2.54 g/s for 50 K helium which is heated from 50 to 69 K, Δh = 105 J/g. Some part of this

rate will be excluded for the current leads cooling. In further estimations it will be assumed that all of 2.54 g/s will go through the return cooling line.

3.4 Thermosyphon cooling of the coils

Thermosyphon is a cooling method based on natural convection of cooling fluid without external pumps. The superconducting coils of the CBM magnet will be cooled on thermosyphon principle in ordinary operation of the magnet, see Fig. 34. The liquid helium goes from the cryostat down to the lower coil, after this to the upper coil, and after this the helium returns to the top of the cryostat LHe vessel. There are two physical principle to force the helium go up through two coils. First, the bubble will have some velocity to go up in liquid helium due to buoyancy. Second, significant fraction of vapor inside the liquid phase will create the pressure difference between the liquid helium in the LHe vessel and the tube cooling the coils.

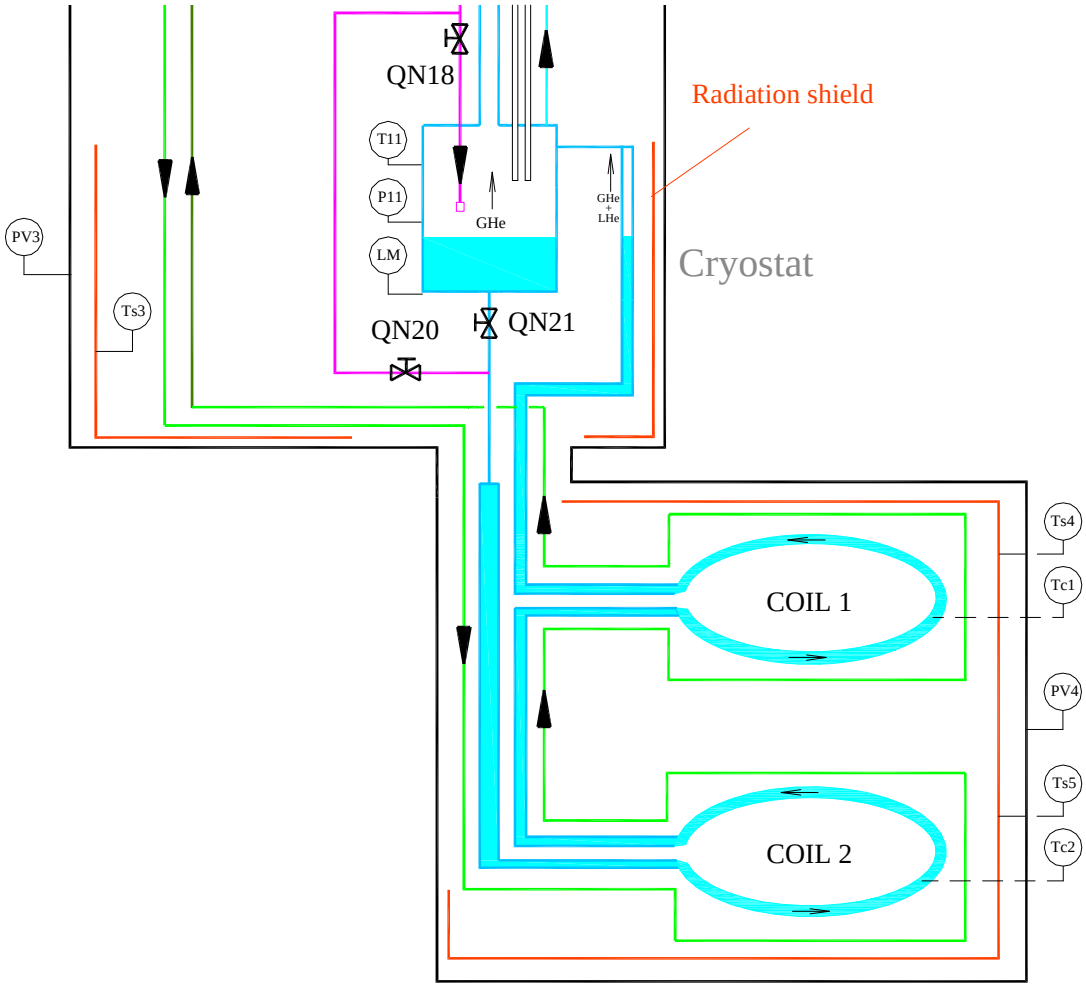

Fig. 34. The cryogenic scheme of the CBM magnet coils with the cryostat. The vertical tube between the LHe vessel and lower coil contain single phase liquid helium. The tubes in the coils are almost horizontal with inclination about 1°.

One needs to estimate the heat flux density to the cooling copper tubes of the coils to know what heat transfer regime is inside these tubes, see Fig. 35. In case if this flux density is below 10 W/m^2 then it will be single phase heat transfer in liquid helium without bubbles appeared.

For total heat in-leak to the one coil is estimated about 2 W as shown in Table 6. Take the heating power 5 W for the estimations. The copper cooling tube has following sizes inner diameter

∅16 mm and length 4.4 m. The heat flux density, q, will be:

$q = Q/(L*\pi d) = 5/(4.4*\pi*0.016) = 23$ W/m^2.

This value of the heat flux density is marked as red dot on the Fig. 35. The temperature difference between helium and copper tube is <0.03 K. It is worth to note that this value is estimated at 5 W of heat in-leaks with guaranty factors. If one take the heat in-leaks values given from direct estimations for the support bus and without the factors then q = 4.6 W/m^2. That is exactly single phase heat transfer regime.

From another hand, the value 23 W/m^2 is by 100 times less then the critical heat flux density. That can be interpreted as if the internal surface of the cooling tube would be covered by 1% of liquid helium the magnet will be cooled in boiling regime with temperature difference about 0.15 K.

This estimation concerns the condition of boiling in large volumes. The criterion of large volume is determined by the sizes of bubbles diameter with respect to the characteristic diameter of the boiling volume. Typical diameters of the helium bubbles are 0.08-0.16 mm [from paper, circa 1969].

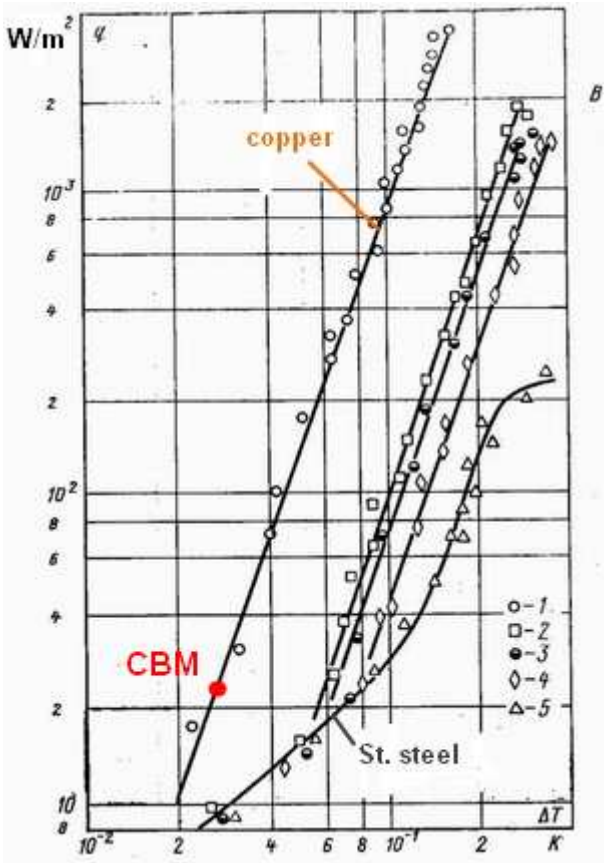

Fig. 35. The nucleate boiling of helium in large volume on different materials. The Y-axis is the heat flux density, the X-axis is the temperature difference between the helium and the surface of the materials.

The value of 5 W as heat in-leak to one coil will be left for the following estimations. The working point for the CBM magnet is shown in Fig. 36 to illustrate that this working point is where the isolated bubbles appear on the surfaces. This case may be considered as a bubble goes up in large volume without movement of the liquid helium.

Consider the important point whether such cryogenic cooling system with long horizontal tubes will be operational and stable. The stability[2] is mentioned above saying that the working point of the heat flux density is by 100 times less than the critical flux density. May the horizontal tube be

[2] The term stability is treated as possibility of a system to return to original state after application of some amount of external energy to it.

filled with gaseous helium? One of the direct answers to such questions is reference for experimental results, such as shown in Fig. 37. The red dot in this Figure is the ratio of the length of the vertical tube to the length of the cooling tube of the coils (although red dot should be higher as 1.5/4.4). It is interesting to note that in this Figure the value of the critical flux is 5 kW/m^2 than presented in Fig. 35 for boiling in large volumes.

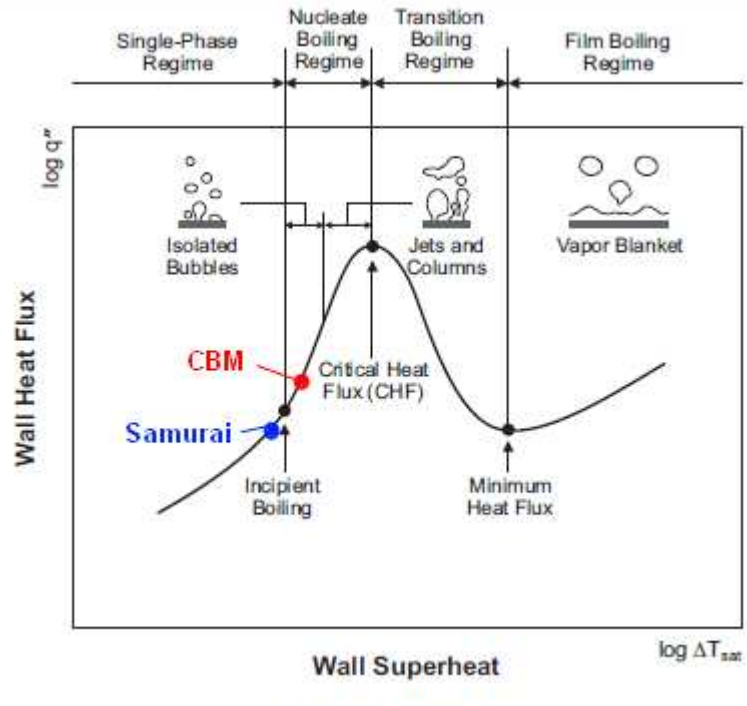

Fig. 1. Pool boiling curve.

Fig. 36. The working point of CBM magnet in basic regimes [taken from a paper].

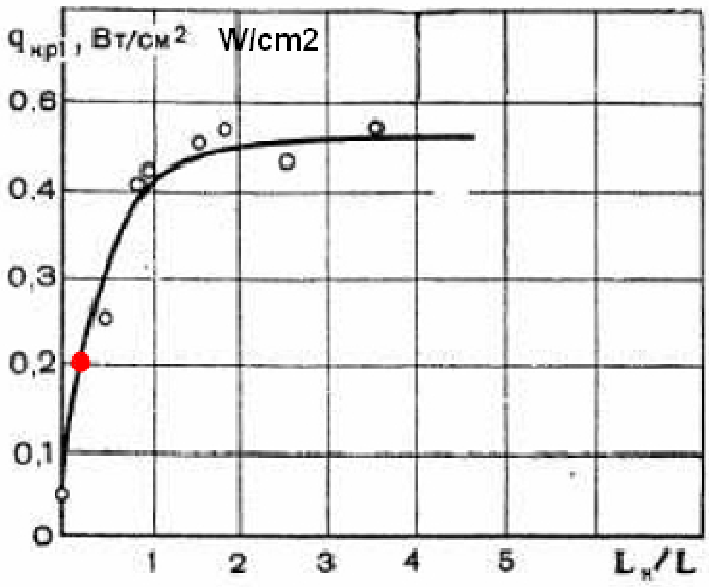

Fig. 37. Influence of vertical unheated channel on critical flux density of helium boiling in horizontal channel at natural conditions. The L_H/L is the ratio of unheated length of vertical channel to the length horizontal channel heated [V. Beliakov].

From another hand it is worth to solve several tasks about the fraction content in helium and velocities of bubbles and two-phase helium.

The velocity of the bubble going up in liquid helium can be estimated as:

$v = \frac{2}{9} \cdot \frac{g \cdot R^2 (\rho_L - \rho_V)}{\eta}$, where g – gravity constant, R – bubble radius, η - viscosity, and density difference between the liquid and gaseous helium. The parameters were taken for 4.6 K helium. So, v = 1.7 m/s. This is the velocity of bubble going up in the vertical tubes between the coils and the LHe vessel.

In the copper tubes cooling the magnet the inclination is only 1°. So, the horizontal velocity of the bubble due to buoyancy is about 0.03 m/s.

The 5 W of heat in-leak to one coils gives mass rate G about 0.25 g/s = 12.5 cm^3/s for vapor. The average time for a bubble to go through the copper cooling tube is 2.2 m/0.03 = 73 sec. Vapor volume inside the copper tube for this time will be as 12.5*73 = 900 cm^3. The volume of the cooling tube is 884 cm^3. It means that the force flow mechanism due to density difference between the vertical tubes is important.

The force flow is governed by pressure drop in the tubes.

Pressure drop along the whole LHe tubes shown in Fig. 34 can be evaluated by the following formula:

$\Delta p = \xi \frac{8G^2}{\pi^2 \rho} \cdot \frac{L}{d^5}$, where ρ - average density of two-phase helium, L and d – length and diameter of a tube, ξ - friction coefficient, G – mass flow rate.

Re = 6200.

Take ρ = 120 kg/m^3 as for liquid, ξ =0.036, G = 2.5*10^{-4} kg/s (5 W), L = 14 m, d = 0.016 m and the pressure difference will be 0.2 Pa only.

Such pressure difference will appear if the average density difference between the vertical tubes will be Δρ = Δp/(g*H), where H – height of the vertical tubes. The result is Δρ = 0.2/(9.8*3) = 0.006 kg/m^3. It means that the force flow will happen in the cooling system if the average density in the vertical tubes between the coils and the LHe vessel will be changed by 0.005%.

These estimations may be also interpreted that the real mass flow rate G will be higher than given here for evaporated helium. Some part of the liquid helium will be circulated in the loop.

The average velocity v in the forced flow can be estimated from definition of G = v*ρ*d^2*π/4. For the given above parameters v = 0.01 m/s, that is much less than the bubbles velocity in the vertical tube which is 1.7 m/s. This result means that at low mass flow in the cooling tubes the liquid helium will not return to the LHe vessel, as it should be because the cooling working point of the CBM magnet is close to single phase cooling regime.

Main conclusion is that the thermosyphon cooling of CBM magnet superconducting coils has no visible problems in realization.

3.5 Quench calculations

The quench analysis evaluates behavior of the superconducting coils during a quench to give maximal temperature in the hot spot, voltage inside the winding, etc.

Its worth to evaluate *stability parameters* of the CBM coils prior the quench estimations, they allow to see the impact the big amount of the copper stabilizer in the SC wire.

The minimal length of the normal zone propagation in a SC wire is

$L = \sqrt{\frac{2\lambda(T_c - T_o)}{\rho J_c^2}}$, where λ - thermal conductivity coefficient of the copper matrix, ρ - electrical resistivity of the copper, Jc – current density, Tc and To – critical and operation temperature of the wire.

$L = \sqrt{\frac{2 \cdot 400 \cdot 4}{10^{-10} \cdot 7.7^2 \cdot 10^{14}}} = 0.073$ m.

Minimal energy for the normal zone propagation:

$E = C\gamma A T_{av}\sqrt{\frac{2\lambda(T_c - T_o)}{\rho J_c^2}}$, where $C\gamma$ - heat capacity [J/(kg*K)], A – cross-section area of the wire, T_{av} – average temperature of the temperature rise.

$E = 2700 \cdot 10^{-5} \cdot 4 \cdot \sqrt{\frac{2 \cdot 400 \cdot 4}{10^{-10} \cdot 7.7^2 \cdot 10^{14}}}$ = 7.9 mJ. This is valuable amount of the energy to make the wire of the CBM magnet coil to be normal, as it is several orders more than in conventional superconducting magnets having wires with NbTi/Cu ratio about 1. So, one may conclude that the training of the coils during the first ramping up will take not much time, or it may not occur at all.

Uniform dissipation energy in one coil

The uniform dissipation of the stored energy in one coil is described in the TDR [1] that is according the current design of the CBM magnet. Heat exchange between the winding and the stainless steel and copper cases was not accounted. In this case we have:

- the E/M ratio is about 6.5 kJ/kg;
- the coil temperature after such uniform quench will be about 91 K;
- the resistance of one winding after such quench is about 4 Ohm;
- the characteristic time of the current decay is about 10 s (L/R);
- the estimated resistive voltage inside the winding, relating the case when a quench started inside the coils (non-uniform quench), is about 0.7 kV;
- the thickness of interlayer insulation is about 0.9 mm, including 0.2 mm of the Kapton insulation and the rest is a kind of the glass fiber insulation. The breaking voltage for the Kapton is more than 100 kV/mm, the breaking voltage for the glass fiber insulation of 10 kV/mm that is among the lowest values for G-10 materials. So, the safety factor will be least (20 + 7)/0.7 ~ 39 for the insulation breaking voltage.

An approach of the quench estimations made in BINP

Main quench calculations were described in the TDR performed by the team from Joint Institute of Dubna and the team from CIEMAT.

The current design of the CBM magnet has the minor changes in the cable parameters and it has the copper case as new element of the coil. The copper case will influence on the quench behavior. So, during the last half of the 2017 the quench estimations of the current design of the CBM coils were performed in BINP.

These estimations were performed at the following conditions:

a) the Matlab code was used for this purpose. The current-inductance dependence is presented on the Fig. 38 which was taken from the TDR works;

b) the equations for the two coupled circuits were calculated in this code which are, see Fig. 39:

$$I_1 R_1 + L_1 \frac{dI_1}{dt} + M \frac{dI_2}{dt} = 0;\ I_2 R_2 + L_2 \frac{dI_2}{dt} + M \frac{dI_1}{dt} = 0,$$

where $L_1(I_1)$ and L_2 – inductances of the CBM magnet and the copper cases. $R_1(T)$– resistance of the CBM magnet, $R_2(T)$ – resistance of the copper cases, M – mutual inductance. General considerations on whether to include the coupled circuits into calculations or not are evaluated by analytical formulas comparing the characteristic times of the main magnet - $\tau_1 = \frac{L_1}{R_1}$ and of the secondary circuit - $\tau_2 = \frac{L_2}{R_2}$. It is worth to note that the calculations with the external dump resistor give more induced current in the copper cases than without it. At the beginning I_1 =700 A, I_2 = 0 A.

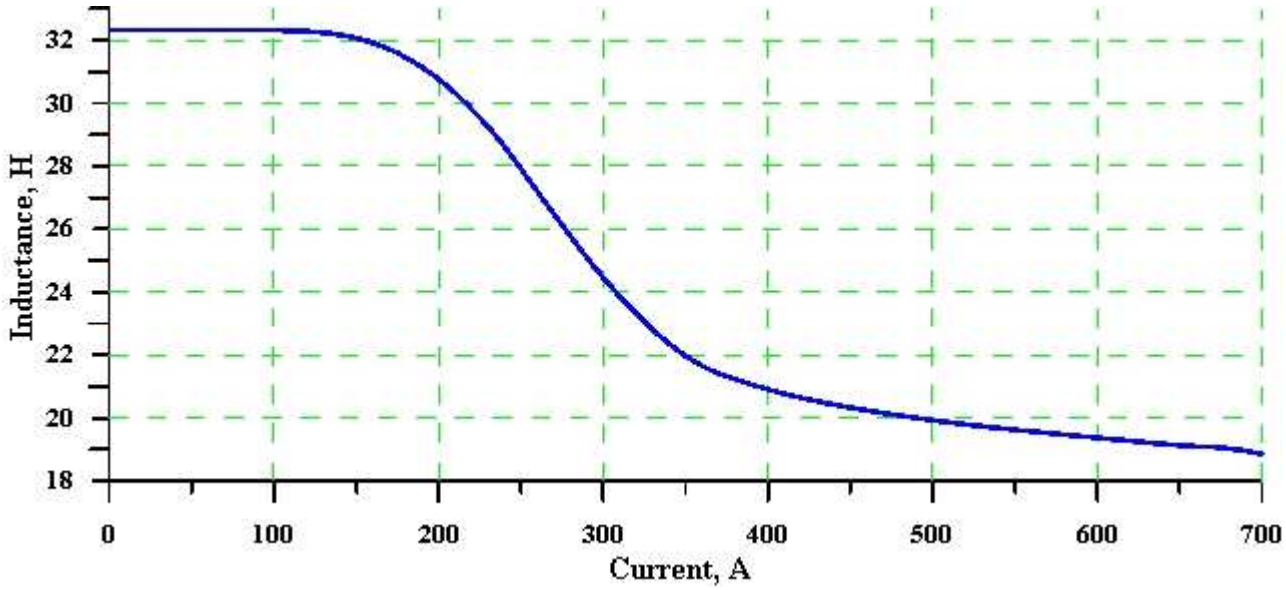

Fig. 38. The dependence of the whole CBM magnet inductance on the current.

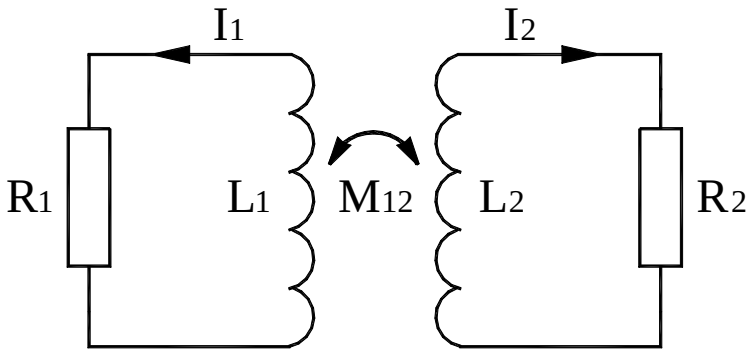

Fig. 39. Scheme of the coupled circuits.

c) the starting conditions for solving these equations were the 10 K for the one coil while the other stayed cool and the 40 K for hot wire for the hot-spot calculations. The validity of these conditions is described below.

d) while the L_1 inductance is dependent of the current the L_2 and M inductances should also has some dependence on the current due to presence of the iron yoke. Though in the calculations the fixed values of the latter inductance were used such as $L_2 = 1.09*10^{-5}$ H and $M = 1.2*10^{-2}$ H.

e) the $R_2(T)$ resistance of the copper cases was dependent on the temperature. This resistance changes its value from ~ 10^{-7} Ω to $5*10^{-6}$ Ω during a quench.

f) the cylindrical parts (poles) of the iron yoke made of technically pure iron have L-R parameters close to the copper cases. The estimated inductance of one pole with ANSYS is about $7*10^{-7}$ H. The estimated resistance at $\rho = 8.6*10^{-8}$ Ω*m at 273 K for iron is about $R = 6.4*10^{-7}$ Ω. Anyway the poles were not included in the calculations to escape more complexity. They will make benign effect on the quench behavior characteristics: on voltage, hot-spot temperature and as external energy extractors.

g) a quench-back effect due to heating of the copper cases was not accounted.

Normal zone propagation velocities

The velocity of the normal zone propagation along the wire [M. Wilson] is

$v_a = \frac{J_e}{\rho C}\sqrt{\frac{L_o \cdot T_s}{T_c - T_s}}$, where J_e – engineering current density, ρC – heat capacity [J/(m^3*K)], L_0 = $2.45*10^{-8}$ W*Ω/K^2, T_s – average temperature of heat generation, T_c – critical temperature of NbTi.

$v_a = \frac{7.7*10^7 \cdot 10^{-4}}{2700}\sqrt{\frac{2.45 \cdot 7}{9.6-7}}$ = 7.3 m/s, so it will take about 0.67 s for the normal zone to go around one turn of the coil.

The velocity of the normal zone transverse the cable was estimated in 2D model using ANSYS, as shown on the Fig. 40. The heat generation in the normal wire was set as $2.2*10^6$ W/m^3, at was assumed that in the neighbor wire it was the same heat generation at the temperature of 7 K.

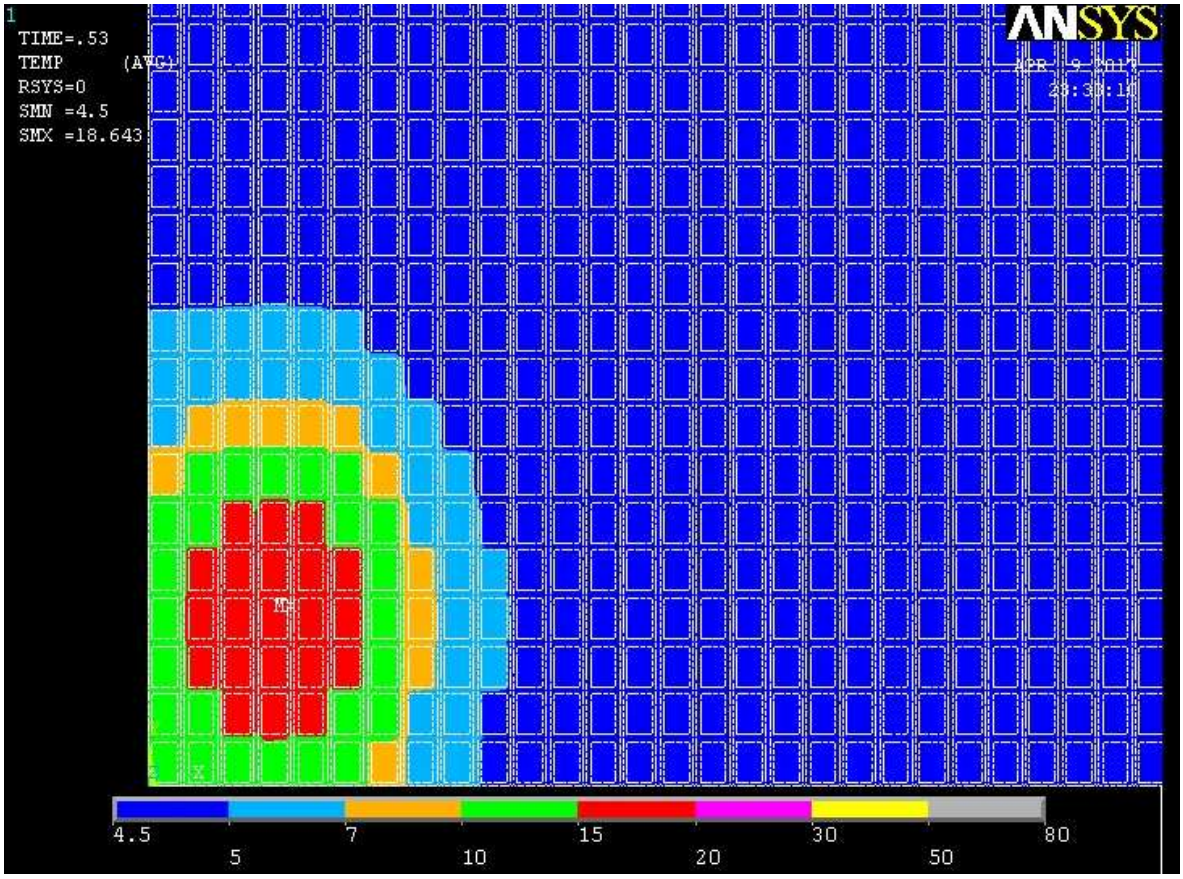

Fig. 40. Normal zone propagation in the winding in 2D calculations. Here time after start of the quench is 0.53 s, the quenched wire is in the center of the red zone and its maximal temperature is 18.6 K.

The velocity across the layers is about 0.05 m/s. This is low value, because typically such velocity has some 1-3% from the v_a value, as it mentioned in literature for convenient superconducting magnets. The reason is to high amount of the insulation between the layers of the winding. This velocity is also slightly faster for a direction along the layer. The maximal time for a normal zone going from the 1st layer to the 53rd is 0.159/0.05 = 3.2 s.

These 2D model calculations also show that after ~ 3 s the hot-spot temperature in the winding will be ~ 40 K. That temperature value was taken in the BINP quench calculations as mentioned above.

It is worth to note that if the normal zone starts to propagate in the 1st or 53rd layer, depending on the coil, the normal zone will reach the neighbor coil.

Quench estimation in ordinary conditions

The CBM magnet has an active protection system based on energy extraction on the dump resistor having 2.1 Ω. After happening of a quench the quench detection system after ~ 50 ms should switch on the powering circuit to a kind of L-R electrical circuit.

These calculations were presented in the TDR report and that results are presented on the Fig.

41. The quench was detected by 0.6 V threshold, the dump resistor was activated after 50 ms. The maximal voltage is around the current leads bus bars. The magnet and the hot spot temperatures are about 45 K and 70 K respectively.

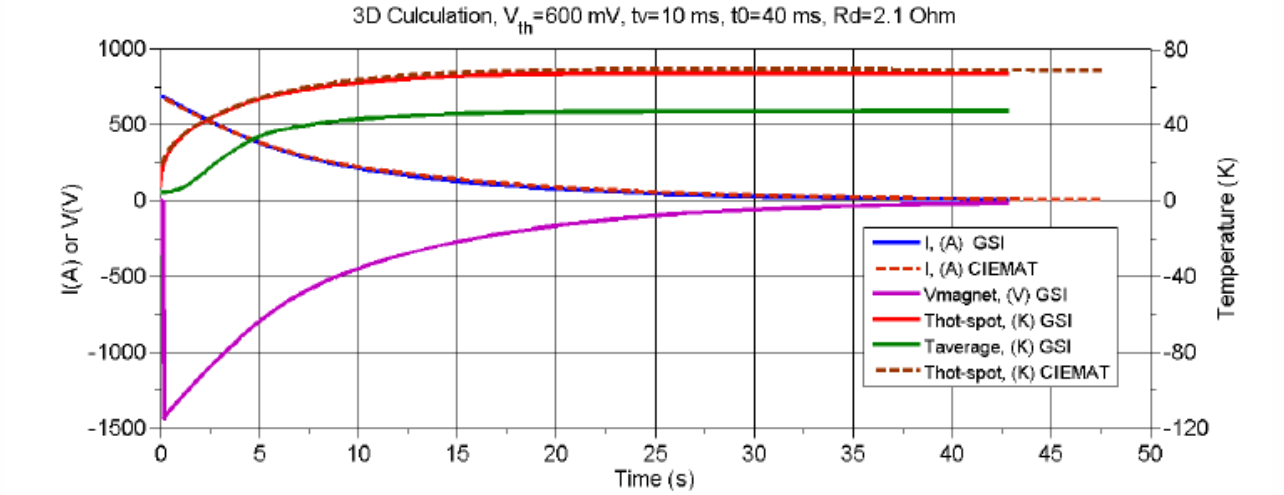

Figure 34. 3D quench calculation of the CBM dipole - magnet current, magnet voltage and the maximum (hot spot) coil temperature.

Fig. 41 The quench calculations with activated dump resistor taken from the TDR.

The BINP calculations based on the conditions described above with the dump resistor are presented on the Fig. 42 - Fig. 44. The winding temperature after such quench is about 52 K that is due to more time delay of the dump resistor activation and slightly higher current. During a quench the resistance of the copper cases changes by more than 10 times due to heating. It influences on the magnet current decay as it is seen on the Fig. 42 where the current from the copper cases “returns” to the magnet current.

The maximal temperature as in TDR as in BINP calculations are close corresponding to ~ 70 K and ~ 79 K respectively.

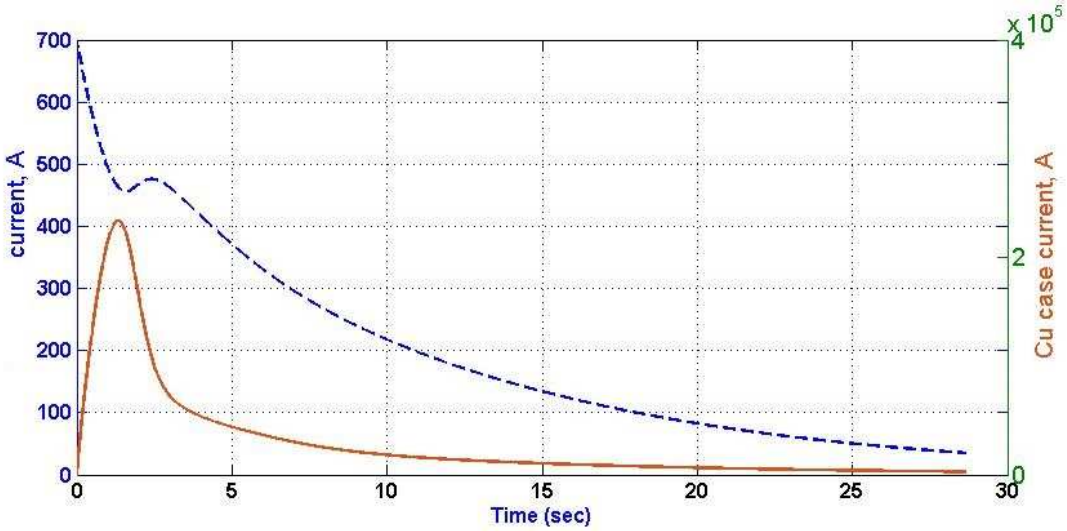

Fig. 42 The currents behavior during the quench with the dump resistor.

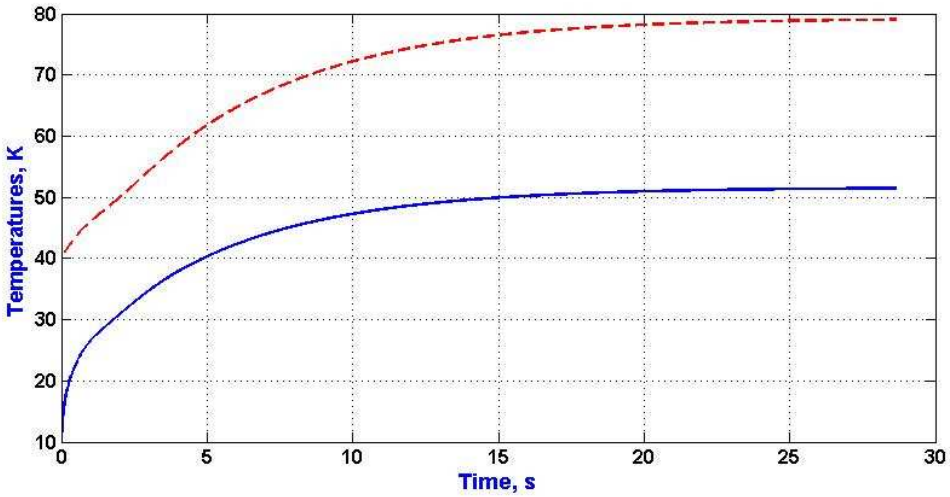

Fig. 43 The temperatures behavior during the quench with the dump resistor. The blue line is for the magnet, the red line is for the hot-spot temperature. It assumed that the dump resistor was switched on after 3 s.

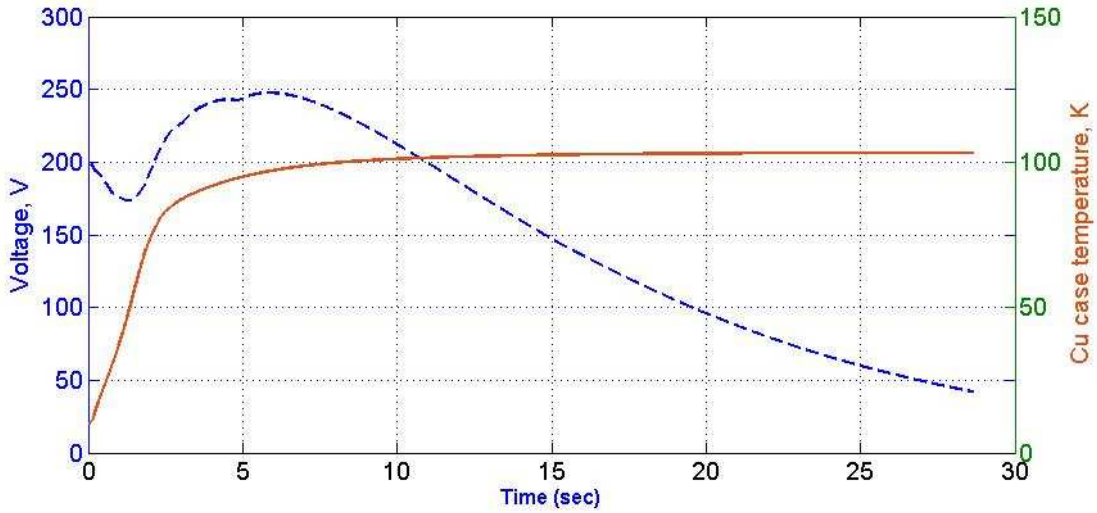

Fig. 44 The resistive voltage of the winding and temperature of the copper cases behavior during the quench with the dump resistor.

Quench estimation of short-circuited magnet and copper cases influence on it

Although it is not considered to make the quenches without the dump resistor the quench calculations at such condition were performed as in the TDR as in BINP project. The BINP calculations approach is described above. The points of interests of such calculations are the hot-spot temperature and internal voltage of the magnet. In both cases the stored energy is dissipated only in one coil of the magnet.

The results of the TDR calculations are presented on the Fig. 45. The maximal resistive voltage during this quench is about 1200 V that corresponds to the ~ 600 V of the internal voltage compensated by inductive voltage.

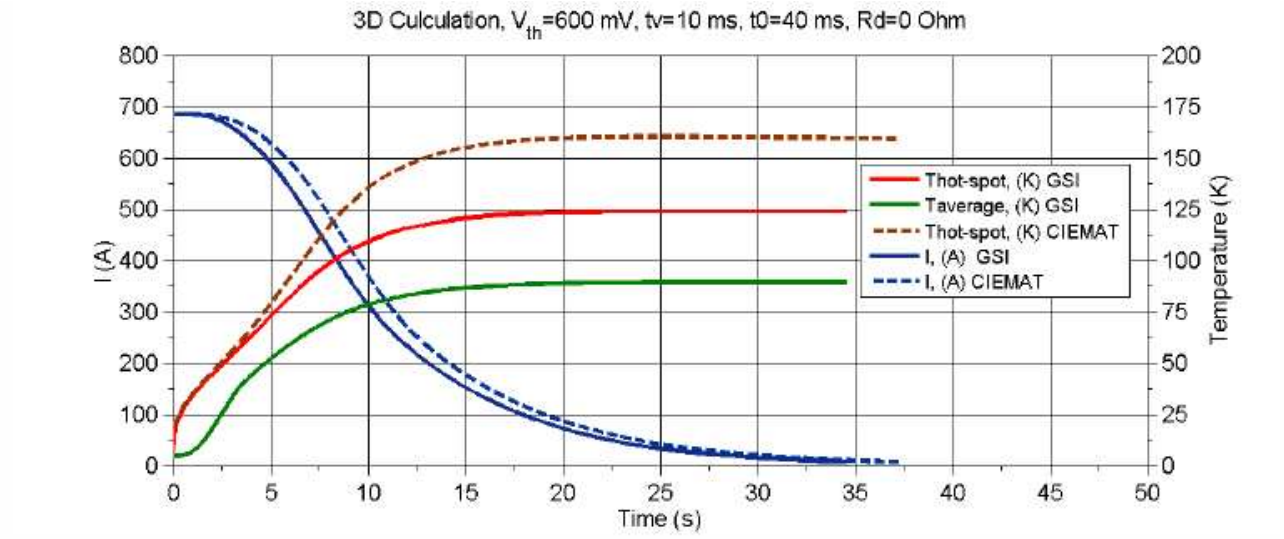

Figure 32. 3D quench calculation of the CBM dipole - the magnet current, hot-spot temperature and the average coil temperature.

Fig. 45 The results of the quench calculations extracted from the TDR.

The results of the BINP calculations are presented in Fig. 46 - Fig. 48. They are close to the TDR results if compared with Fig. 45.

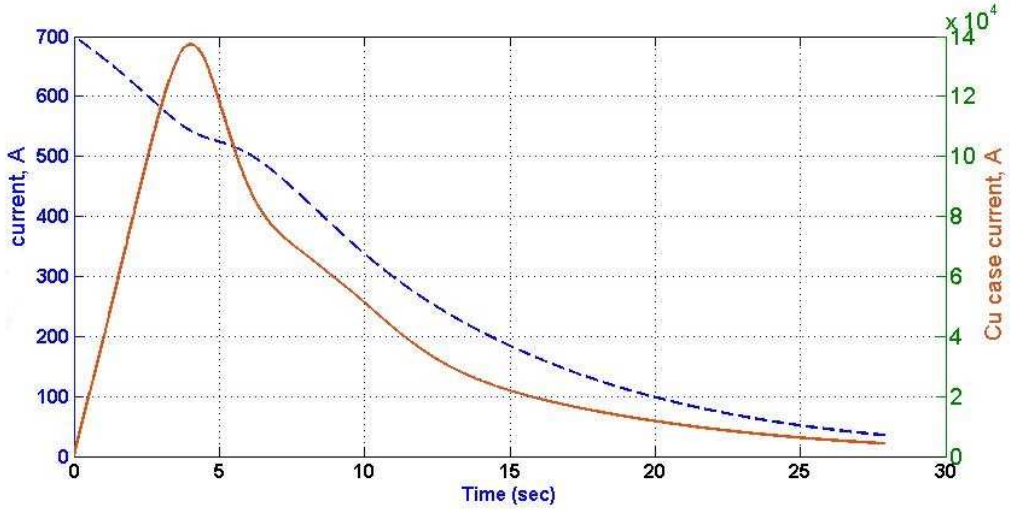

Fig. 46 The currents behavior during the quench of the short-circuited magnet.

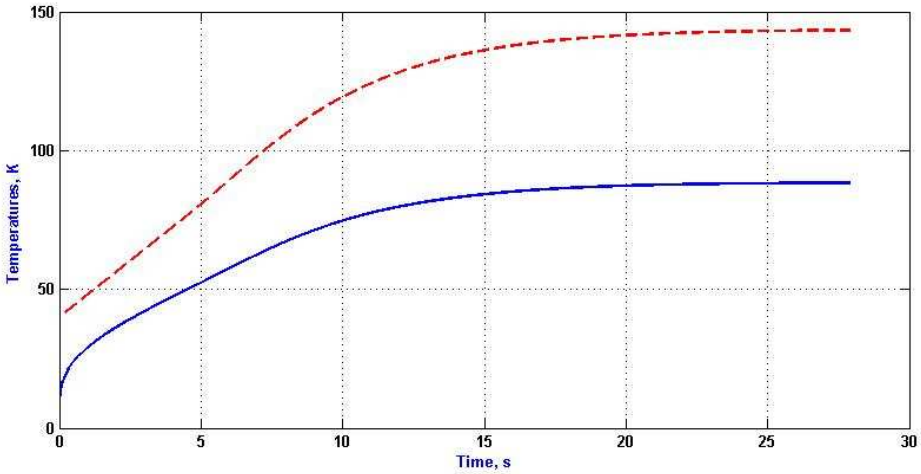

Fig. 47 The temperatures behavior during the quench of the short-circuited magnet. The blue line is for the magnet, the red line is for the hot-spot temperature.

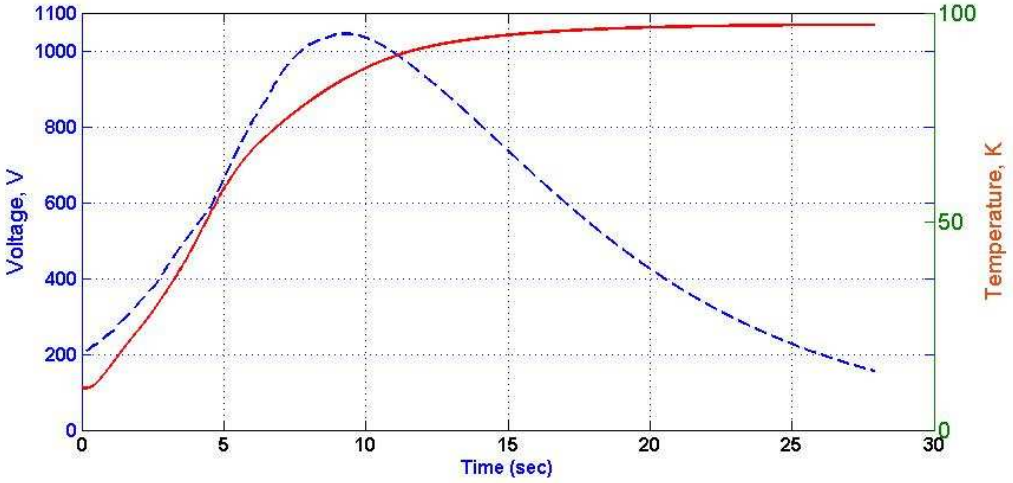

Fig. 48 The resistive voltage of the winding and temperature of the copper cases behavior during the quench of the short-circuited magnet.

The influence of the copper cases on quench behavior as the secondary protective circuit is demonstrated on the Fig. 49 - Fig. 51.

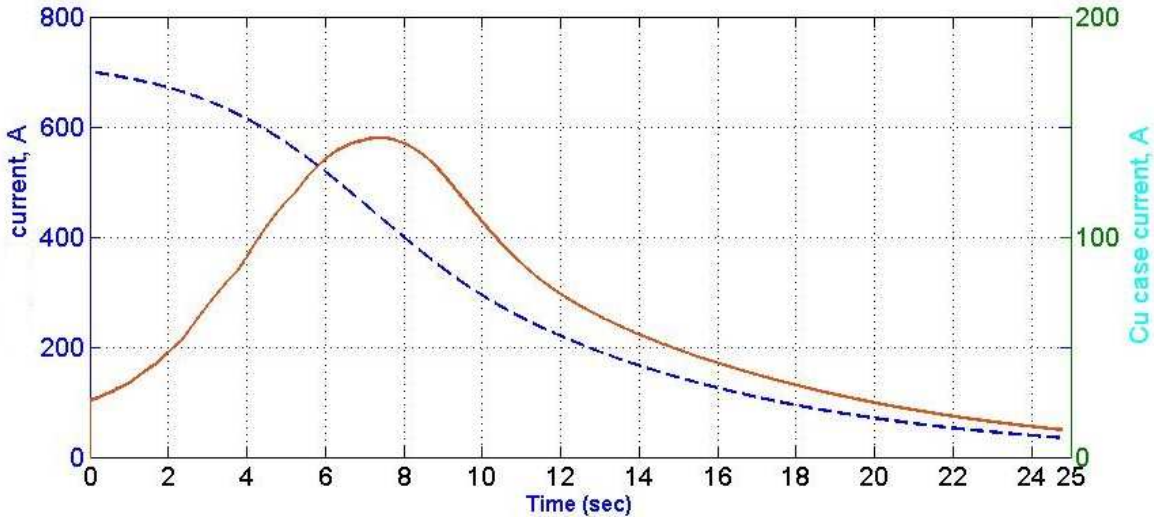

Fig. 49 The currents behavior during the quench of the short-circuited magnet and with R2 having

the resistance several orders higher than for the copper case.

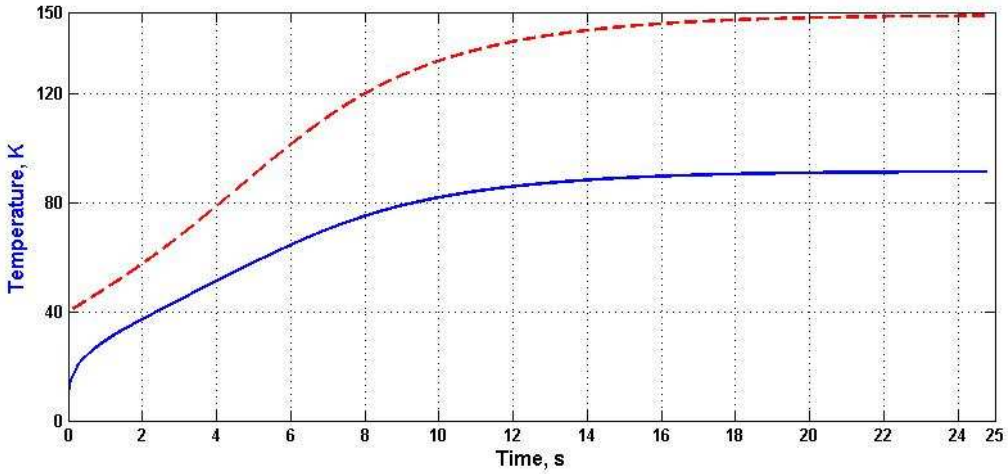

Fig. 50. The temperatures behavior during the quench of the short-circuited magnet and with high R2 value. The blue line is for the magnet, the red line is for the hot-spot temperature.

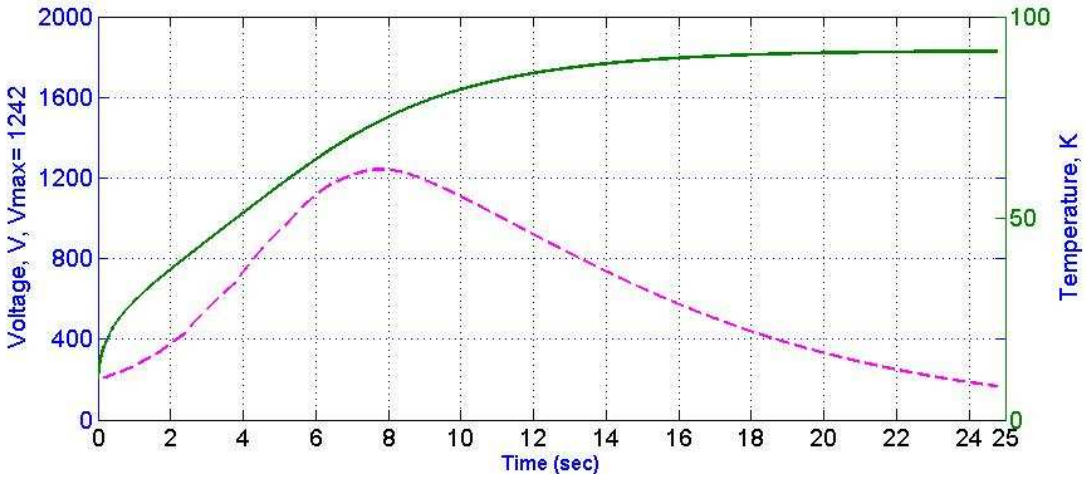

Fig. 51. The resistive voltage of the winding and the temperature of the coil winding behavior during the quench of the short-circuited magnet and with high R2 value.

Results of the quench calculation:

1. In ordinary conditions the most part of the stored energy will be extracted on the dump resistor. The average temperature in the quenched coil will be below 50 K taking into account the stainless steel case. The hot-spot temperature will be well below 80 K. The maximal voltage will be on the current leads bus bars.
2. The calculations of the short-circuited magnet shows the hot-spot temperature about 150 K and the internal voltage around 600 V. The maximal voltage will be between the coils.
3. The copper cases of the coils have some influence on the quench but not high. The resistance of the copper cases changes by ~ 14 times during a quench. The cylindrical iron poles will also affect the quench behavior but less than the copper cases.
4. In total the CBM magnet coils looks protected from quench effects. Attention should be paid to bus bars insulations especially in the cold mass zone.

3.6 Quench protection system

The proposed quench protection system is based on dissipating the stored energy of the magnet on a dump resistor after detection of a quench. The system consists of quench detection subsystem and energy extraction subsystem.

The powering circuit is shown on the Fig. 52.

Requirements for the quench protection system are:

- The amount of the stored energy to be extracted is 5.1MJ.
- Stored energy should be extracted to the external dump resistor with the value of 2 Ohm.
- The active elements of the dump resistor should not be hotter than 100° C. Cooling time should be specified;
- Quench detection circuit should provide fast detection of the normal phase appearing. The discrimination time should be about 6ms and the threshold – about 0.6V (0.6V corresponds to 6 wounds in the normal state).
- Number of the voltage tabs and the locations of their connections should be determined.
- Dump resistor should be introduced to the circuit not later than in 40 ms. That gives the demands on the energy extraction switch (current breaker).
- Dump resistor value is 2.1 Ω. Middle point should be introduced and grounded in order to minimize the voltage between coil and ground.

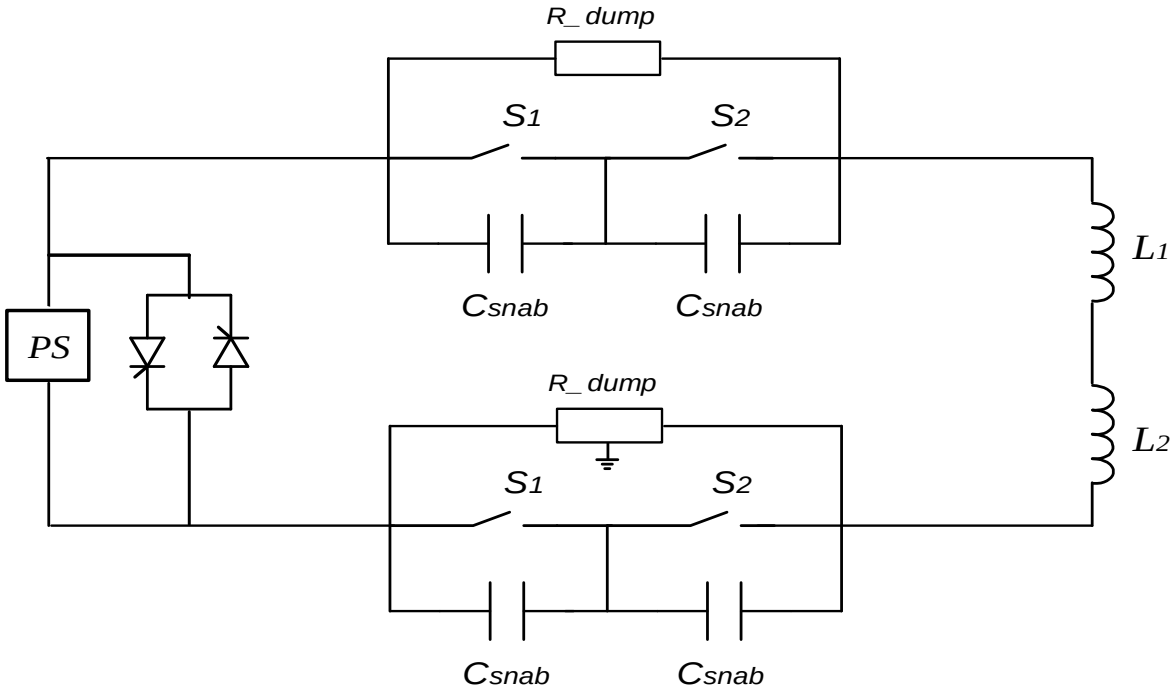

Fig. 52. Powering system of the CBM magnet.

4. Cryogenics of the CBM detector

4.1 Cryogenic diagram

The cryogenics diagram of the CBM magnet is presented on the Fig. 53. The cryogenics of the CBM detector consists of the Branch Box (BB), the Feed Box (FB), the cryostat of the CBM detector and the cryogenic transfer lines. The length of the transfer lines between the BB and the FB is about 30 m.

For the transfer line the most tubes were chosen to be DN15 STD, so OD = 21.34 mm, ID = 15.8 mm.

The parameters of the cryogenic valves are listed in the Table 10. The valves are of PN25 type – nominal pressure of 25 bar, they should have a Cu flange for a heat load interception along its stem.

The parameters of the valves are estimated at the following conditions:

- maximal heat loads for the CBM detector 60 W at 4.5 K and 3 bar, so G = 2.8 g/s = 10 kg/h; and 190 W at 50 K and 18 bar, so G = 1.8 g/s = 6.5 kg/h;
- maximal heat loads for the HADES detector 150 W at 4.3 K G = 6.9 g/s = 25 kg/h; and 400 W at 50 K and 3 bar, so G = 3.8 g/s = 13.6 kg/h.

(The mass rate G was estimated via enthalpy difference as Q/Δh.)

Valve coefficient for the control valves $K_V = \frac{G}{514}\sqrt{\frac{T_1}{\rho_g \cdot \Delta p \cdot p_1}}$, and for JT valves is: $K_V = \frac{G}{257 \cdot p_1}\sqrt{\frac{T_1}{\rho_g}}$, where G – mass flow rate [kg/h], p_1 and T_1 – upstream pressure [bar] and temperature [K], Δp – pressure difference between the valves, taken as 0.01 bar; ρ_g – gas density at normal conditions [kg/m^3].

Table 10 Cryogenic valves list.

Valve	Valve purpose, Couplings	Kv, max	Kvs	DN, mm	G_{op}, g/s	Pop, bar	Top, K	Position without electricity
QN1	Open at all operating modes	0.14		15		2.5→1.2	70	Open
QN2		0.051		15		1.3	6	
QN3		1.32		15		2	70	
QN4		0.071		15		2	4.5	
QN5		0.052		15		3	4.6	
QN6	Reduction to 3 bar	0.010		15		18→3	50	Closed
QN7		0.053		15		18	50	
QN8		0.021		15		3	4.6	
QN9		0.081		15		1.3	4.5	
QN10		0.77		15		17	70	
QN11		1.92		15		17	85	
QN12		0.11		15		1.3	5	
QN13		0.053		15		18	50	
QN14		0.076		15		17	70	
QN15		0.072		15		1.3	4.5	
QN16		0.053		15		18	50	
QN17		0.022		15		3	4.6	
QN18	JT	0.022		15		3	4.5	
QN19		0.39		15		2	300	
QN20				15		18	4.5	
QN21				20		18	4.5	

General approaches for the cryogenic system are:

- the radiation shields of all cryogenic subsystems should be cooled by return line of 55-60 K helium;
- the Branch Box may has installed vacuum pumps installed;
- vacuum behavior of the systems after a quench as in CBM and HADES detectors or warming up in one detector at operation of another should be taken into account;

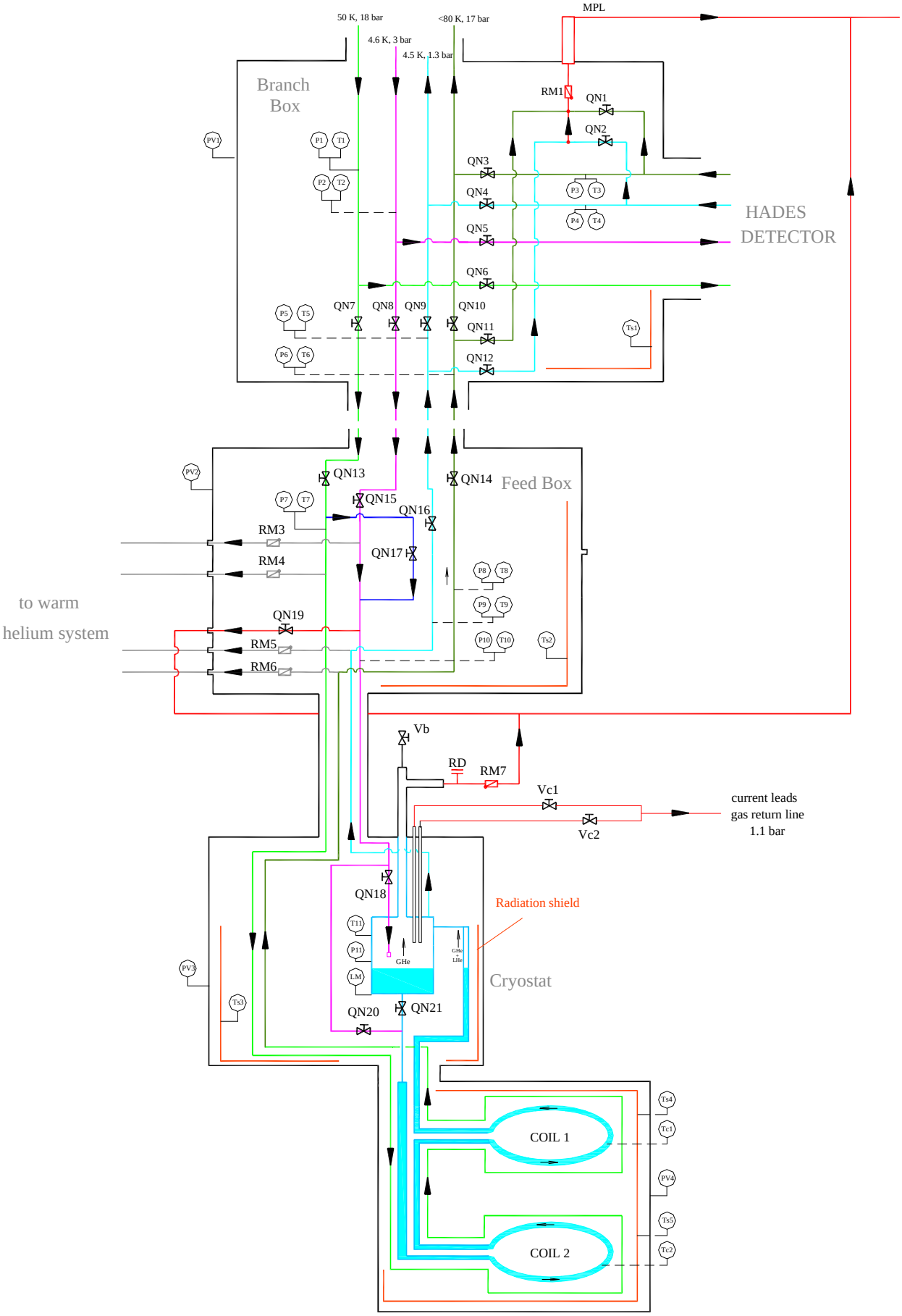

Fig. 53. General view of the CBM detector cryogenic diagram.

The designations on the diagram of the Fig. 53 are: QN – control valves, RM – check valves, P – pressure gauge, T – temperature sensor, PV – vacuum gauge.

The vacuum volume in the cryogenics should divided into independent blocks to be possible find cold leaks during assembling of the system and to exclude deterioration of vacuum during a quench of whether CBM magnet or whether HADES magnet.

4.2 Design of the Feed Box

The design of the Feed Box is shown on the Fig. 54. The cryogenic diagram of the Feed Box is shown on the Fig. 53. The Feed Box should perform all cryogenic operations of the CBM magnet such as cooling down, routine operation at 4.5 K, warming up and quench recovery.

The control valves will give a major part of heat in-leaks, the interception at 60 K temperature should be foreseen at procurement stage of work.

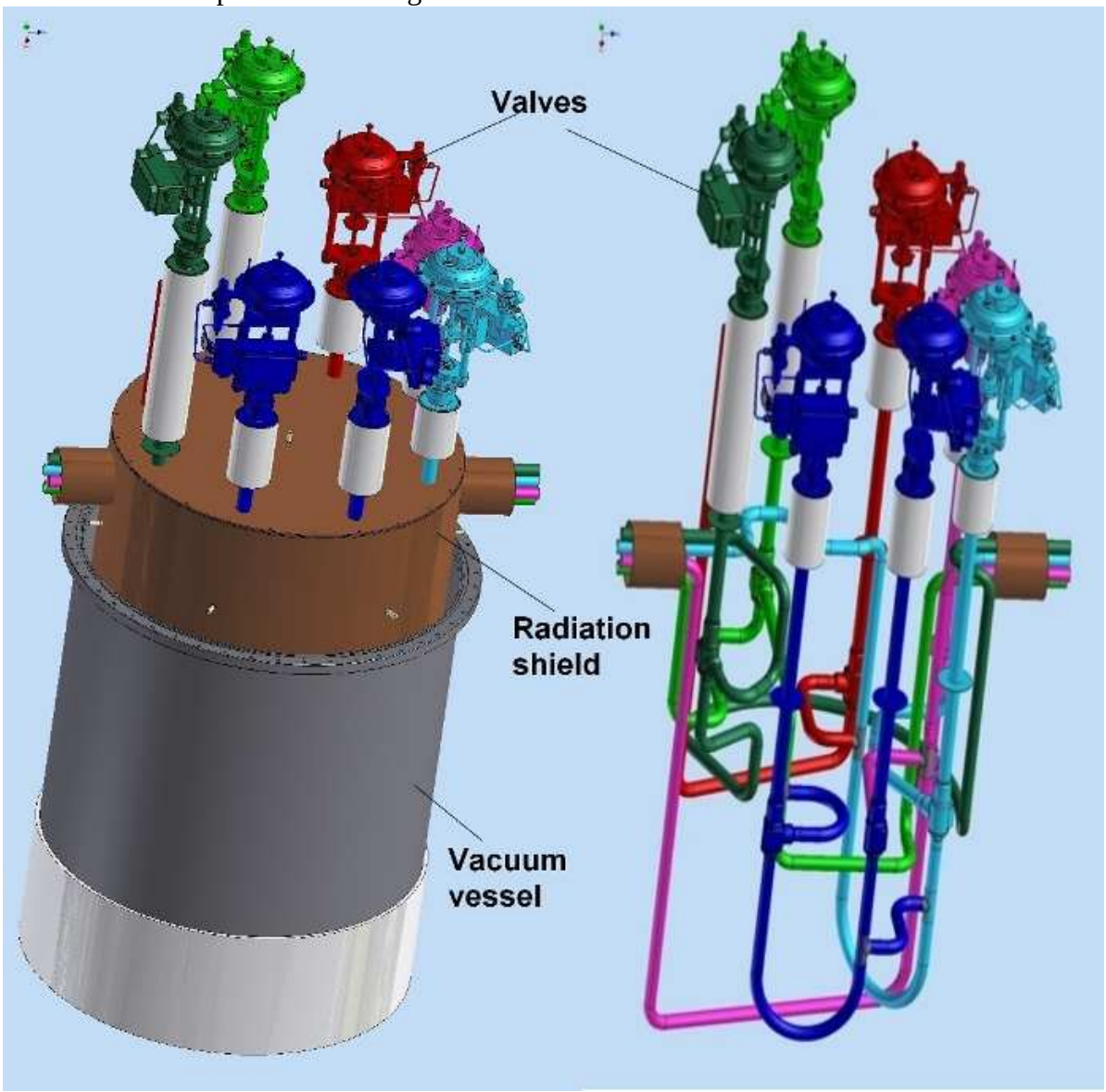

Fig. 54. The design of the Feed Box.

Items for discussion:

It is demanded to have warm helium purge system and warm helium line for warming up the magnet. It is not clear why the purging can't be performed during installation of the system when the helium lines can be vacuum pumped. After this the cryogenic system can be purged by helium from the cryoplant.

4.3 Design of the Branch Box and the transfer line

The destination of the Branch Box is to supply He gases the CBM and the HADES detectors. All cryogenic operations of these detectors should be performed independently. So, the scheme and the placement of the cryogenic valves in the Branch Box should have symmetry, as it is shown on the cryogenic diagram, Fig. 53. The helium goes from the local cryoplant and after the Branch Box it may go ever to CBM detector ever to the HADES. The return lines of the Branch Box will have sensors of temperature and pressure for controlling parameters of helium. In case of improper parameters of helium the return gas will go to the multipurpose line.

The design of the Branch Box is shown on the Fig. 55.

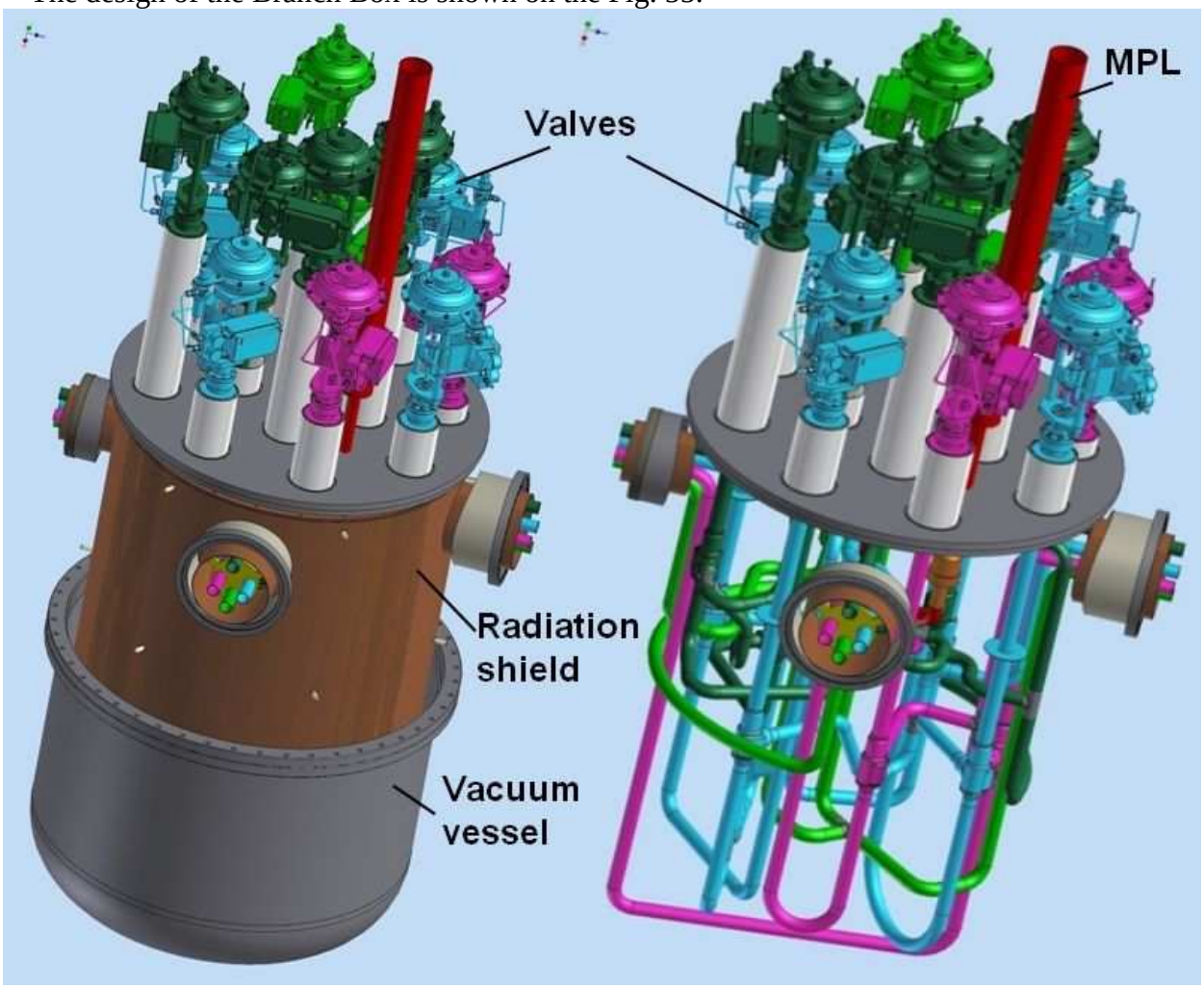

Fig. 55. The design of the Branch Box. MPL – multipurpose line.

The vacuum volume of the CBM and the HADES cryogenics should be separated around the vacuum vessel of the Branch Box, as stated above. The vacuum ports and measurements flanges should be foreseen.

The common design of the transfer line is shown on the Fig. 56. Details of the thermal contraction compensators are not shown. The design of the separator may be changed to have specific separator for the 50 K tubes and specific separator for the 4.6 K tubes.

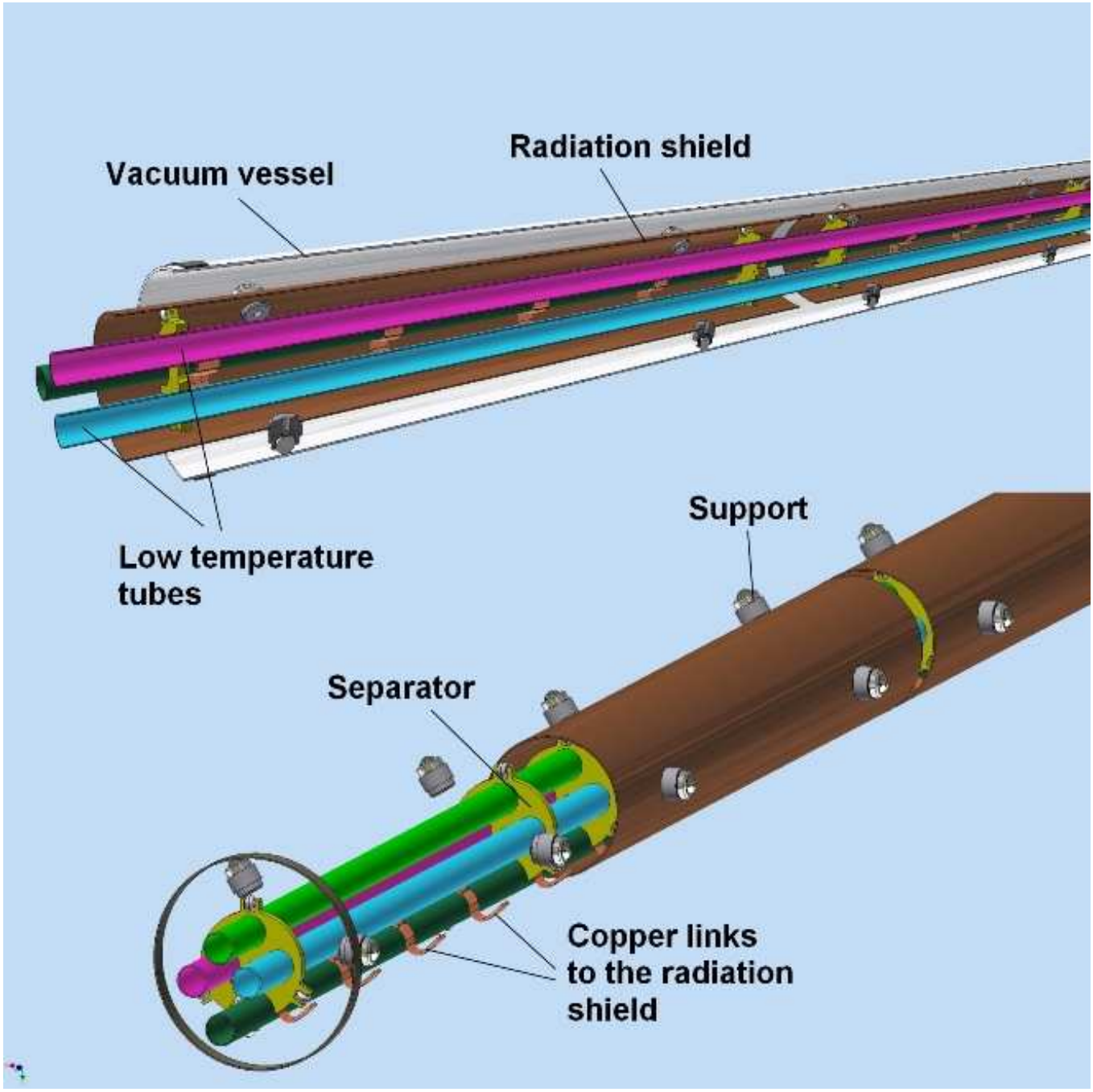

Fig. 56. The design of the transfer line.

4.4 Estimations of pressure drops and heat transfer

These estimations will determine a diameter of a pipe and a mass flow rate for the transfer pipes from the Branch Box to the cryostat and will evaluate the needed mass flow rate for the heat transfer. The pressure drop along the transfer line should be much less than 0.1 bar at ordinary operation of the CBM magnet.

Pressure drop of isothermal gas along a pipe can be evaluated by the following formula:

$\Delta p = \xi \frac{v^2 \rho}{2} \cdot \frac{L}{d}$, where ρ - density, v – velocity, L and d – length and diameter of a pipe, ξ - friction coefficient. Addition pressure drop appears due to acceleration of gas heated along a pipe – not considered here.

With a mass flow rate G = v*ρ*d^2*π/4 it will be more convenient:

$$\Delta p = \xi \frac{8G^2}{\pi^2 \rho} \cdot \frac{L}{d^5}.$$

Reynolds number $Re = \frac{4G}{\pi d \eta}$ determines the flow mode, where η - viscosity [Pa*s].

At turbulent flow, when Re = $2.3*10^3 \div 10^5$, the friction coefficient is calculated as $\xi = \frac{0.316}{Re^{0.25}}$.

The input parameters of the pipe are inner diameter ID = 15.8 mm and the length of the pipe L = 120 m. The length of the pipe includes the length itself and additional length from the valves, and bellows parts. The parameters of helium at various temperature and pressure are listed in the Table 11 that will be used in the following estimations.

For the 4.6 K helium lines at G = $1.7*10^{-3}$ kg/s we have:

$$Re = \frac{4G}{\pi d \eta} = \frac{4 \cdot 1.7 \cdot 10^{-3}}{\pi \cdot 0.0158 \cdot 3.4 \cdot 10^{-6}} = 40000 \text{ – turbulent flow.}$$

Friction coefficient $\xi = \frac{0.316}{Re^{0.25}} = 0.022.$

Pressure drop: $\Delta p = \xi \frac{8G^2}{\pi^2 \rho} \cdot \frac{L}{d^5} = 0.022 \cdot \frac{8 \cdot 2.89 \cdot 10^{-6}}{\pi^2 \cdot 128} \cdot \frac{120}{0.0158^5} = 49$ Pa = 0.00049 bar.

In the ordinary operation the pressure drop along the transfer lines is very low.

For the 50 K helium lines at G = $1.8*10^{-3}$ kg/s we have:

$$Re = \frac{4G}{\pi d \eta} = \frac{4 \cdot 1.8 \cdot 10^{-3}}{\pi \cdot 0.0158 \cdot 7.4 \cdot 10^{-6}} = 20000 \text{ – turbulent flow.}$$

Friction coefficient $\xi = \frac{0.316}{Re^{0.25}} = 0.027.$

Pressure drop: $\Delta p = \xi \frac{8G^2}{\pi^2 \rho} \cdot \frac{L}{d^5} = 0.027 \cdot \frac{8 \cdot 3.24 \cdot 10^{-6}}{\pi^2 \cdot 14} \cdot \frac{120}{0.0158^5} = 617$ Pa = 0.006 bar

In the ordinary operation the pressure drop along the transfer lines is also very low.

Heat transfer between helium and tubes for cooling

The return helium at 50-70 K of temperature should cool the heat in leaks presented in the Table 7 and Table 9. The temperature differences should be estimated between the helium and the cooling tubes of radiation shields in all components of the CBM magnet cryogenics.

The heat transfer between the helium and the pipe wall is estimated as:

Q = αS*ΔT, where α - heat transfer coefficient, S – heat transfer surface, ΔT – temperature difference between helium and a pipe wall.

The heat transfer coefficient is estimated as $\alpha = \frac{\lambda \cdot Nu}{d}$, where λ - thermo conductivity coefficient of helium, Nu – Nusselt number, d – inner diameter of a tube.

The reduced heat transfer coefficient may be taken into account if tube wall is thick and has low thermal conductivity (w – wall parameters):

$\frac{1}{\alpha_r} = \frac{1}{\alpha} + \frac{h_w}{\lambda_w}$, where h_w – wall thickness.

For turbulent flow Nusselt number is estimated as: $Nu = 0.023*Re^{0.8}Pr^{0.33}$, where $Pr = \frac{\eta c_p}{\lambda}$ - Prandtl number, where c_p – heat capacity.

For 60 K helium Nu = 56, so $\alpha = \frac{0.055 \cdot 56}{0.0158} = 195$ W/(m^2*K).

Heat load for one coil from support struts and the radiation shield is about Q = 25 W. The cooling tube going around the radiation shield has cooling surface S = πd*L = 3.14*0.0158*5 = 0.25 m^2. So, the temperature difference between helium and tube wall will be:

$\Delta T = Q/\alpha S = 25/(195*0.25) = 0.5$ K.

The cooling helium will be heated, its temperature can be estimated as:

$Q = G*c_p*\Delta T_h$, then $\Delta T_h = Q/(G* c_p) = 25/(1.8*5.3) = 2.6$ K. So, helium entering the lower coil at 50 K will go to the upper coil at temperature 52.6 K that is acceptable.

Table 11. Parameters of helium at given T and p.

T, K	**p, MPa**	**ρ, kg/m^3**	**λ ,W/(m*K)**	**10^{-6} μ, Pa*s**	**h, kJ/(kg)**	**Pr**
4.6	0.1	13.6 (20 at 1.3)	0.009	1.3	33.5	1.15
4.6	0.2	121.5	0.02	3.2	11.8	
4.6	0.3	127.8	0.02	3.4	11.9	
4.5	0.1	14.2	0.009	1.25	32.7	1.15
4.5	0.2	124.2	0.019	3.2	11.2	
4.5	0.3	129.8	0.02	3.4	11.4	
50	1.0	9.5	0.048	6.5	266.1	
50	1.5	14.0	0.049	6.6	275.3	
50	2.0	18.4	0.05	6.7	275.8	
60	1.0	7.9	0.054	7.3	318.5	
60	1.5	11.7	0.055	7.35	328.3	
60	2.0	15.4	0.055	7.4	329.1	0.69
70	0.1	0.7	0.058	7.83	369.0	
70	1.0	6.8	0.059	7.0	371.0	
70	1.5	10.0	0.060	8.0	380.9	
70	2.0	13.3	0.061	8.1	381.9	
80	1.0	6.0	0.065	8.7	423.2	
80	1.5	8.8	0.065	8.7	433.4	
80	2.0	11.7	0.066	8.8	434.5	
100	0.1	0.48	0.074	9.8	534.3	0.67
100	0.2	0.96	0.074	9.8	534.5	
100	1.5	7.1	0.075	10.0	537.8	
100	2.0	9.4	0.076	10.0	539.1	
140	0.1	0.34	0.093	11.9	742.1	
140	0.2	0.69	0.093	11.9	743.3	
140	1.5	5.1	0.094	12.1	746.0	
140	2.0	6.7	0.094	12.1	747.5	
200	0.1	0.24	0.118	15.1	1053.7	0.67
200	0.2	0.48	0.118	15.1	1054.0	
200	1.5	3.57	0.119	15.3	1057.8	
200	2.0	4.75	0.120	15.3	1059.3	
240	0.1	0.2	0.134	17.1	1261.4	
240	0.2	0.4	0.134	17.1	1261.7	
240	1.5	3.0	0.135	17.2	1265.5	
240	2.0	4.0	0.135	17.2	1267.0	
273	0.1	0.175	0.146	18.6	1423.2	
273	0.2	0.35	0.146	18.7	1423.6	

4.5 Operation modes of the CBM magnet cryogenics

The cryogenic system of the CBM magnet should work at the following operating conditions:
- cooling down the system during two weeks;
- ordinary operation of cooled magnet at 4.5 K;
- warming up of the magnet for demanded time;
- quench recovery.

Cooling down of the system

The biggest gold mass of the system is the superconducting magnet having about 3.6 tonnes and the internal energy is about 320 MJ. The rest cold components of the cryogenic system will be cooled down much faster and may be not considered here. Three stages of the cooling down will be proposed:
- first stage – the magnet is cooled to ~ 200 K;
- second stage – the magnet is cooled to ~ 80 K;
- third stage – the magnet is cooled to 4.5 K – operating conditions.

First stage – cooling down to ~ 200 K

Before cooling down, the system should have vacuum in the range $10^{-2} \div 10^{-3}$ Pa. The vacuum pump will be attached by the cryostat where it will have effective pumping capacity not more than 500 l/s.

For cooling a magnet from room temperature to ~ 200 K one needs to take off about 50% of the internal energy. In our case it will be 160 MJ and the cooling time is 48 hours. So, the desired cooling capacity is 930 W.

It is assumed in the TDR that the cooling rate should be about 2 K/hour, the high cooling rate may lead to high mechanical stress inside the superconducting structure. From another hand, if a magnet is cooled uniformly this rate may be higher. If firstly the radiation shields of the coils will be cooled down to about 200 K the heat transfer via radiation and support struts conduction will take place. The effect of these factors can be estimated as follows.

The cooling by the radiation shields is

$Q = \varepsilon S \sigma (T^4 - 200^4)$ where ε - total emissivity was taken as 0.06, S – surface area of the two LHe cases is 8.5 m^2, T – magnet temperature.

The results are Q = 85 W for T = 260 K, and Q = 21 W for T = 220 K.

The cooling by the support struts via G-10 elements is estimated as:

$Q = \lambda S^* \Delta T/L$, where λ - thermal conductivity was taken as 0.8 W/(m*K), S – cross-section area of one support is 9.1^*10^{-3} m^2, ΔT – temperature difference was taken as 100 K, L – length is about 0.16 m.

The result is Q = 55 W for ΔT = 100 K on the length of the support struts.

So, the cooling down the shields only will give cooling capacity from ~150 W at the beginning to about 50 W in the first stage.

BINP proposes to control the cooling process by measuring the temperature difference in the winding structure in order to be less than 10 K during the cooling down process. This is direct way for controlling the safe conditions during the cooling down process. The cooling diagram is shown on the Fig. 57.

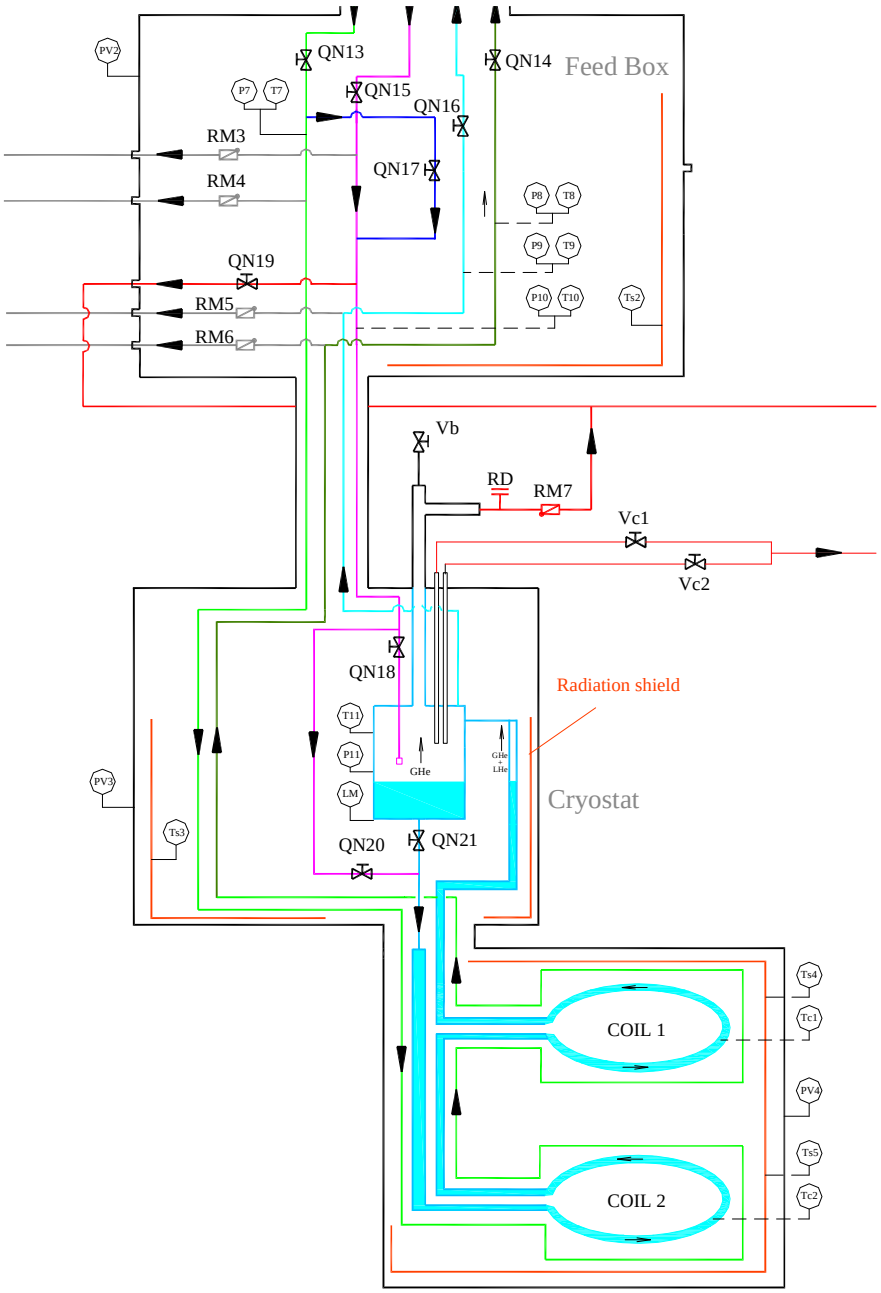

Fig. 57. The diagram of the cooling down procedure of the first and the second stages. The arrows show the helium running helium. The closed valves are QN15, QN16, QN18, and QN21. The open valves are QN17, QN20, RM7.

The coils are cooled by helium from 50 K line. The flow is divided between shields and coils by the QN13 valve. The mass flow rate of 0.9 g/s value or lower is enough in this stage.

The cooling helium has large cooling capacity due to high heat transfer coefficient, big cooling surface ~ 1.5 m^2 for every coil, even taking into account reduced heat transfer coefficient due to presence of G-10 around the coil.

The cooling is controlled by thermal sensors which are shown on the Fig. 57. If the temperature difference became more than 10 K the helium flow may be decreased by closing the QN13 valve. Temperature difference in solid body is dissipated with characteristic time as:

$t = \frac{C_v \cdot \langle L \rangle^2}{\lambda \cdot \pi^2}$, where C_v – volumetric heat capacity, λ - thermal conductivity, L – characteristic length of temperature difference. In the first stage of cooling down this time is about one hour.

Second stage – the magnet is cooled to ~ 80 K

The cooling diagram in this stage is the same. In the controlling process one needs to increase the mass flow if the cooling down rate becomes too slow due to decreasing of temperature difference between the coil and the cooling helium. The extracted energy in this stage is about 40% from original 160 MJ.

Third stage – the magnet is cooled to 4.5 K

In this stage the line of 4.6 K helium will be used. In is assumed that the line itself already has a temperature not high than 60 K as it was surrounded by operating 50 K lines. The cooling starts with closing QN17 valve and opening QN15 valve.

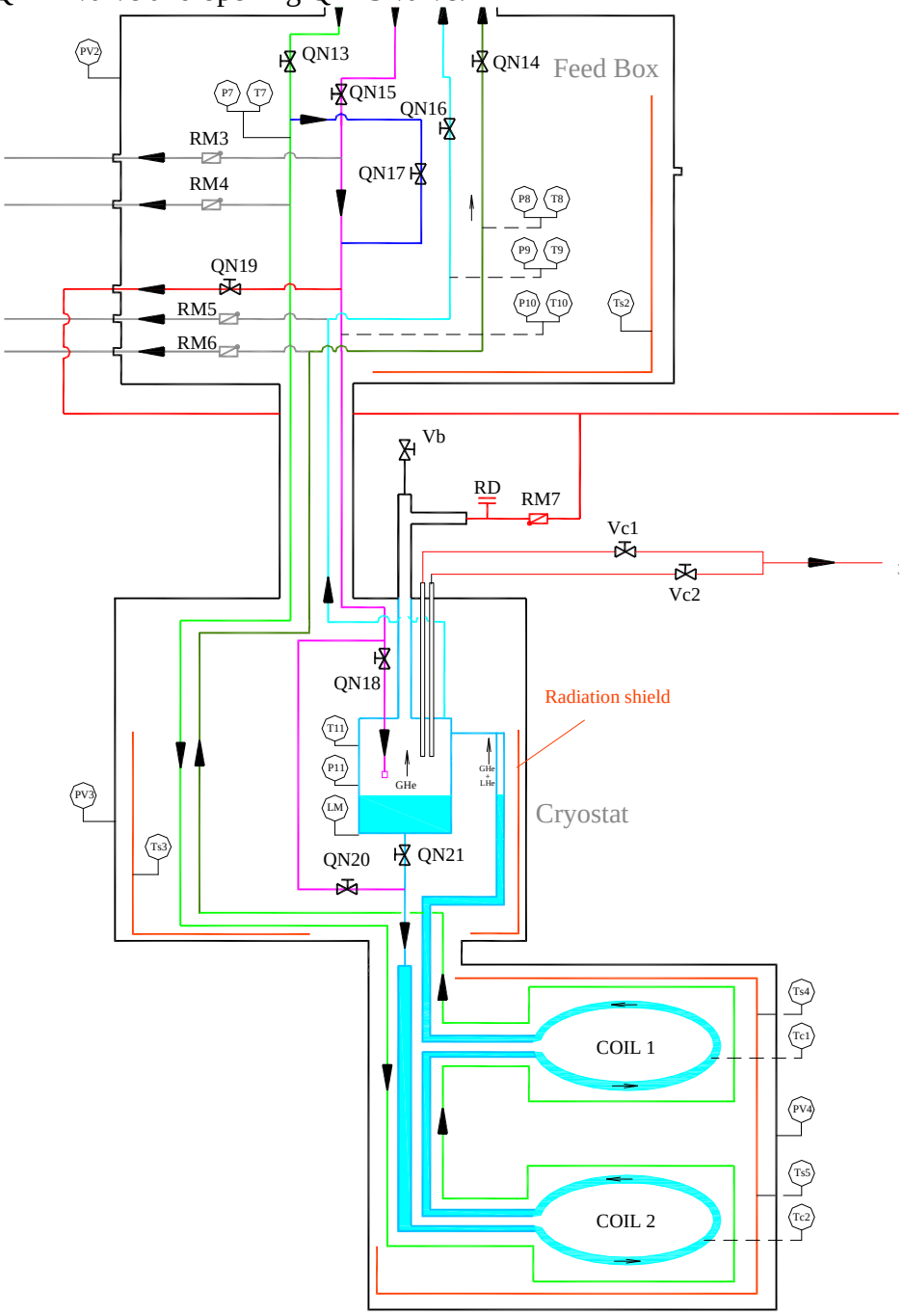

Fig. 58. The diagram of the cooling down procedure of the third stage. The closed valves are QN17, QN20, RM7. The open valves are QN15, QN16, QN18, and QN21.

At the end of the cooling when liquid helium starts accumulating on the lower coil one may close QN20 valve and open QN18 and QN21 valves, then liquid helium will fill the cryostat. The moment of liquid helium accumulation in the low coil may be detected by pressure drop in the

cryostat on P11 manometer.

On should find a moment when to close RM7 valve and open QN16 valve.

Total cooling down time will be about 8 days.

Ordinary operation of the cooled magnet at 4.5 K

In the ordinary operation of the cryogenic system the helium flows will be as shown on the Fig. 53. Some part of gaseous helium will go through the current leads; its flow will be controlled by a heater installed in the cryostat.

The liquid helium level will be measured by installed LHe level meter.

One of the possible scenarios of LHe level controlling is to operate at insufficient flow of helium by controlling of QN15 valve, i.e. 1.5 g/s instead of demanded 1.7 g/s of flow rate. When the LHe level becomes too low then the QN18 will be opened to supply 1.8 g/s rate until demanded level of helium in the cryostat.

Warming up of the magnet for demanded time

For accelerated warming up the 300 K line of helium is installed to the Feed Box. This process will be conducted on the same principle as in the cooling down in the first and the second stages. The supply of 50 K helium should be shut. After increasing the lowest temperature in the cryogenic system beyond 27-28 K the vacuum pressure will be increased rapidly.

As a proposal, a number of heaters may be installed on the cold mass of the magnet to give power 200-400 W. Additional power will come from heat transfer between the radiation shields and the magnet due to radiation and gases of vacuum volume. This power will be greater than from the proposed heaters.

Quench recovery

If quench had occurred then the QN15 and QN16 valves should be closed. The rising pressure in the cryostat will open RM7 valve to the multipurpose line. Liquid helium in the cryostat will not go down to the coils. The highest pressure in the system will be not more than 3 bar due to little amount of stored liquid helium in the system.

In the worse case of quench, when the stored energy is fully dissipated in one coil – this coil after a quench will be slowly cooled from ~ 90 K to ~ 50 K due to heat transfer between the winding and the heavy LHe case. After this the cooling down procedure will go as in the third stage of cooling down the magnet.

4.6 Safety analysis

Very high pressure may be in the cryostat in case of a quench in the magnet or any break of insulating vacuum when air or even helium can leak inside the vacuum volume. This pressure can be estimated as follows. It is assumed that the cryostat is equipped with relief valve allowing helium to go into the multipurpose line.

Formula for pressure buildup in the cryostat:

$\Delta p = \xi \frac{8G^2}{\pi^2 \rho \cdot Y^2} \cdot \frac{L}{d^5}$, where Y – expansion correction coefficient, about 0.8; the rest parameters are the same as for the pressure drop.

The mass rate G is determined by external heat flow to the helium in the LHe case. Typical heat transfer coefficient is about 10^3 W/(m^2*K) that can be found in literature. It may be reduced by a factor of 2 because heat transfer going through G-10 insulation (quench case) or thick wall of stainless steel (vacuum break). So, the heat flux to helium can be q = 5000 W/m^2 at temperature difference about 10 K – film boiling. The heat transfer surface is about 1.5 m^2 in one coil case. So, total heating power can be about Q = 5000*3 = 15 kW. The mass rate is determined as G = Q/Δh,

where Δh – latent heat, about 21 J/g. The length of the pipe is about 3 m, diameter was chosen 0.03 m. G = 0.714 kg/s.

$\Delta p = 0.03 \frac{8 \cdot 0.714^2}{\pi^2 14 \cdot 0.64} \cdot \frac{3}{0.03^5}$ = 1.7*10^5 Pa = **1.7 bar**. This is maximal overpressure in the cryostat during a quench at condition that helium goes out through the cryostat neck to the multipurpose line.

It is worth to note that LHe volume in both coils will be not more 30 l, i.e. total mass is 30*124 = 3.7 kg. It means that at given mass rate all liquid helium will go out after 5 s. This time is comparable with the current decay during a quench; it means that helium will start to go out at lower pressure.

The estimated mass flow rate is by a factor of 400 larger than the rate supplied from the cryoplant. The control valves may be closed during several seconds, no problems here seen.

Thermal oscillation may happen in the cryogenic system at various stages of operation. The simple thermal oscillations criteria can be used in designing the system, see Fig. 59.

Characteristic radius is calculated as: $R^*_c = r_0 \cdot \left(\frac{a}{\nu \cdot L} \right)^{1/2}$, where r_0 - tube radius, a - acoustic velocity, m/s, ν - kinematic viscosity, L - length of the pie.

$a = (\gamma \cdot R \cdot \overline{T})^{1/2} = (1.67 \cdot 2078 \cdot 20)^{1/2} = 263.4$ m/s for helium.

$\nu = \eta / \rho$

Another parameter is $\alpha = \frac{T_h}{T_c}$ - ration of warm end of a pipe to cold end of the pipe.

The stability region is at low values of given parameters $R^*_c < 8$ and $\alpha < 6$.

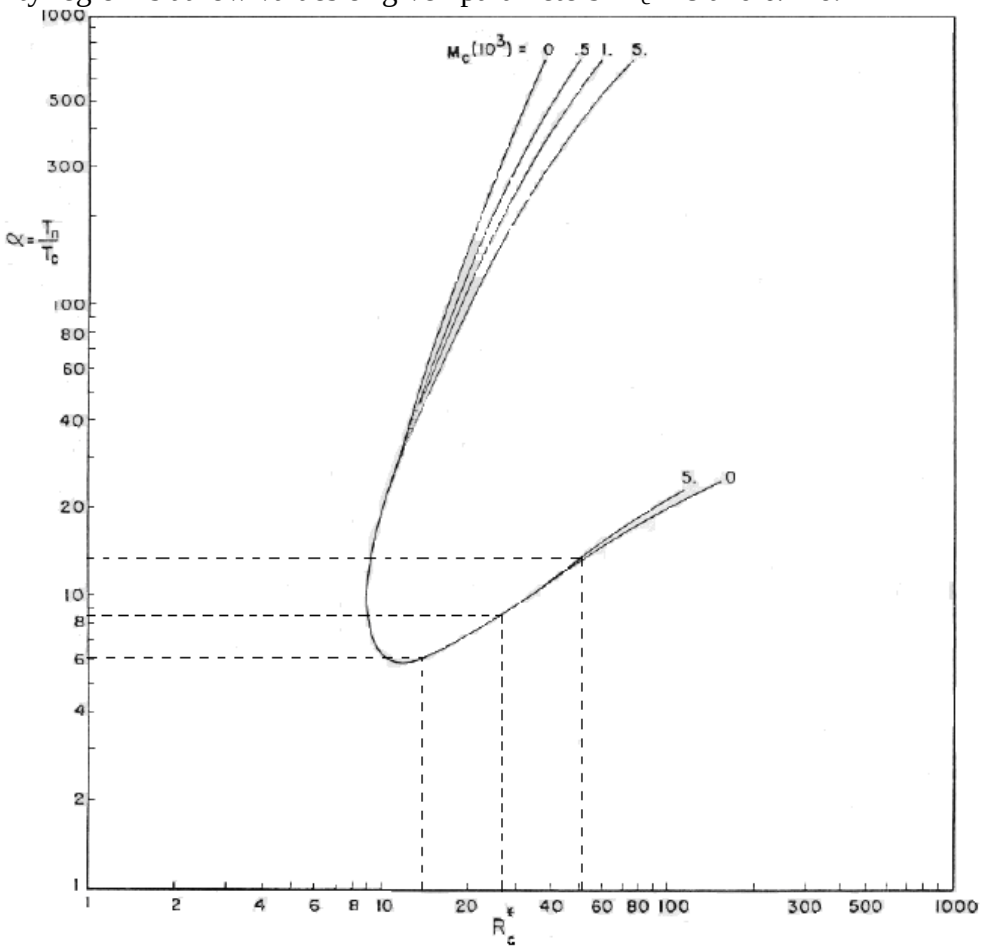

Fig. 59. The graph for the thermal oscillations criteria taken from [J.A. Liburdy].

This criteria show that thermal oscillations will mostly occur during cooling down of the cryogenic system.

5. BINP tests of the CBM magnet (FAT)

The BINP does not have such cryogenic station to provide helium with parameters as of the CBM magnet. Currently it proposed to cool the CBM magnet with liquid helium directly into the cryostat and the radiation shields will be cooled by liquid nitrogen. In this case heat loads to the magnet will be increased.

Quench heaters for quench demonstration should be installed.

6. References

1. Collaboration Contract CBM-Magnet BINP Annex3 - Technical specifications, 2016.
2. Technical design report
3. M. Wilson, Superconducting magnets
4. Y. Iwasa, Case studies in superconductivity
5. Thermodynamical properties of helium, Sychev V.V. et al, 1984.
6. J.A. Liburdy, J.L. Wofford «Acoustic oscillation phenomena in low-velocity steady flow with heating», Advances in Cryogenic Engineering, 1980, Vol. 25, p. 528.
7. M.A. Green “Quench back in thin superconducting solenoid magnets”. Cryogenics, 1984, Vol. 24, n. 1, p. 3, *and* M.A. Green “The role of quench back in quench protection of a superconducting solenoid”. Cryogenics, 1984, Vol. 24, n. 12, p. 659.
8. Cryogenic data handbook, 1980.
9. J. Weisend Handbook of cryogenic engineering, 1998.
10. Yu. Solntsev, “Materials for low and cryogenic temperatures”, S.-Peterburg, 2008 (in Russian).
11. V.P. Beliakov “Cryogenic technique and technology”, Moscow, 1982 (in Russian).

7. Discussion of the experts recommendations of May 2017

Recommendation 1
It is presented above.
No comments.

Recommendation 2
It is presented above.
No comments.

Recommendation 3
The effect of helium bath cooling is discussed here.

1. The liquid helium being in close contact with a superconducting winding works as stabilizer. The volumetric heat capacity of liquid helium is >10 times higher than volumetric heat capacity of solid materials at 4.5 K temperatures. In our case the SC winding is not in close contact with helium as it is surrounded by isolation of thickness more than 2 mm. Such thickness delays thermal diffusion from SC cable to liquid helium (TDR design) for > 15 ms. At the same time the characteristic time of the thermal diffusion along the SC cable via copper stabilizer is ~ 2 ms on the L = 0.073 m – maximal length of normal zone propagation.

The calculations were done by well known formula for thermal diffusion across a specific length: $\tau = \frac{Cp \cdot \rho \cdot L^2}{\pi^2 \cdot \lambda}$ - it contains thermal properties and specific length.

Conclusion: copper stabilizer of the SC cable will have more stabilizing effect from local disturbances than heat transfer to liquid helium due to large thickness of insulation.

2. A movement of SC winding may happen during energizing. Suppose that the movement happened between the copper and the stainless steel cases. Energy release in this case is estimated as E = F*x, where F – force of 2.5 MN value towards the struts, x – movement distance, the friction coefficient is 1. Assume x = 0.1 mm. E = 250 J for the whole winding. This energy will heat the wall of the copper case having thickness ~ 5 mm (real thickness is 8 mm), volume $5*10^{-3}$ m^3. The temperature of the cooper wall will be 13 K.

The safe amount of energy is ~ 20 J then the temperature of the copper wall will be ~ 6 K.

Conclusion: rigidity of the coil structure is important. The movement by 10 μm of the considered task looks to be safe.

3. Ultimate decision is to impregnate the wall insulator having thickness 2 mm with high heat capacity powder such as Gd_2SO_4. It is available in BINP now. This powder has extreme value of thermal capacity at low temperatures that is about 1000 time more than the heat capacity of solids. This insulator is a separate element of the winding placed between the copper case and the winding. It is attached to the wall of the copper case before the start of the winding procedure.

Recommendation 4
There is no technical benefit seen by using of two independent cooling circuits. The presented cooling circuit has large safety margin with respect to the critical flux density on the cooling tubes. Two independent circuits demand two cryostats, two current leads, etc. It will give more helium consumption and more operational complexity.

Recommendation 5
It is presented above.

No comments.

Recommendation 6

It is presented above.

No comments.

Recommendation 7

It is presented above.

The CBM magnet coils are protected with external dump resistor and without it when the whole energy dissipated in one coil only. Sometimes, actively protected magnets (with dump resistors or quench heaters) are not analyzed in case of failure of such protection methods. For example: Samurai magnet which looks as not surviving a quench after failing its quench heaters. The CBM magnet is passively protected as presented above.

Recommendation 8

The current leads are being developed. The design with HTS insertions will avoid the demand to keep the current leads operational without cooling during 1 min.